DESIGN OF A NANOPLATFORM FOR TREATING PANCREATIC CANCER

by

HARSHI CHATHURANGI MANAWADU

B. Sc. (Hons), University of Colombo, Sri Lanka, 2009

AN ABSTRACT OF A DISSERTATION

submitted in partial fulfillment of the requirements for the degree

DOCTOR OF PHILOSOPHY

Department of Chemistry
College of Arts and Sciences

KANSAS STATE UNIVERSITY
Manhattan, Kansas

2014

Abstract

Pancreatic cancer is the fourth leading cause of cancer-related deaths in the USA. Asymptomatic early cancer stages and late diagnosis leads to very low survival rates of pancreatic cancers, compared to other cancers. Treatment options for advanced pancreatic cancer are limited to chemotherapy and/or radiation therapy, as surgical removal of the cancerous tissue becomes impossible at later stages. Therefore, there's a critical need for innovative and improved chemotherapeutic treatment of (late) pancreatic cancers. It is mandatory for successful treatment strategies to overcome the drug resistance associated with pancreatic cancers. Nanotechnology based drug formulations have been providing promising alternatives in cancer treatment due to their selective targeting and accumulation in tumor vasculature, which can be used for efficient delivery of chemotherapeutic agents to tumors and metastases.

The research of my thesis is following the principle approach to high therapeutic efficacy that has been first described by Dr. Helmut Ringsdorf in 1975. However, I have extended the use of the Ringsdorf model from polymeric to nanoparticle-based drug carriers by exploring an iron / iron oxide nanoparticle based drug delivery system.

A series of drug delivery systems have been synthesized by varying the total numbers and the ratio of the tumor homing peptide sequence CGKRK and the chemotherapeutic drug doxorubicin at the surfaces of Fe/Fe_3O_4-nanoparticles. The cytotoxicity of these nanoformulations was tested against murine pancreatic cancer cell lines (Pan02) to assess their therapeutic capabilities for effective treatments of pancreatic cancers. Healthy mouse fibroblast cells (STO) were also tested for comparison, because an effective chemotherapeutic drug has to be selective towards cancer cells.

Optimal Experimental Design methodology was applied to identify the nanoformulation with the highest therapeutic activity. A statistical analysis method known as response surface methodology was carried out to evaluate the *in-vitro* cytotoxicity data, and to determine whether the chosen experimental parameters truly express the optimized conditions of the nanoparticle based drug delivery system. The overall goal was to optimize the therapeutic efficacy in nanoparticle-based pancreatic cancer treatment. Based on the statistical data, the most effective iron/iron oxide nanoparticle-based drug delivery system has been identified. Its Fe/Fe_3O_4 core has a diameter of 20 nm. The surface of this nanoparticle is loaded with the homing sequence CGKRK (139-142 peptide molecules per nanoparticle surface) and the chemotherapeutic agent doxorubicin (156-159 molecules per surface), This nanoplatform is a promising candidate for the nanoparticle-based chemotherapy of pancreatic cancer.

DESIGN OF A NANOPLATFORM FOR TREATING PANCREATIC CANCER

by

HARSHI CHATHURANGI MANAWADU

B. Sc. (Hons), University of Colombo, Sri Lanka, 2009

A DISSERTATION

submitted in partial fulfillment of the requirements for the degree

DOCTOR OF PHILOSOPHY

Department of Chemistry
College of Arts and Sciences

KANSAS STATE UNIVERSITY
Manhattan, Kansas

2014

Approved by:

Major Professor
Dr. Stefan H. Bossmann

Copyright

Abstract

Pancreatic cancer is the fourth leading cause of cancer-related deaths in the USA. Asymptomatic early cancer stages and late diagnosis leads to very low survival rates of pancreatic cancers, compared to other cancers. Treatment options for advanced pancreatic cancer are limited to chemotherapy and/or radiation therapy, as surgical removal of the cancerous tissue becomes impossible at later stages. Therefore, there's a critical need for innovative and improved chemotherapeutic treatment of (late) pancreatic cancers. It is mandatory for successful treatment strategies to overcome the drug resistance associated with pancreatic cancers. Nanotechnology based drug formulations have been providing promising alternatives in cancer treatment due to their selective targeting and accumulation in tumor vasculature, which can be used for efficient delivery of chemotherapeutic agents to tumors and metastases.

The research of my thesis is following the principle approach to high therapeutic efficacy that has been first described by Dr. Helmut Ringsdorf in 1975. However, I have extended the use of the Ringsdorf model from polymeric to nanoparticle-based drug carriers by exploring an iron / iron oxide nanoparticle based drug delivery system.

A series of drug delivery systems have been synthesized by varying the total numbers and the ratio of the tumor homing peptide sequence CGKRK and the chemotherapeutic drug doxorubicin at the surfaces of Fe/Fe_3O_4-nanoparticles. The cytotoxicity of these nanoformulations was tested against murine pancreatic cancer cell lines (Pan02) to assess their therapeutic capabilities for effective treatments of pancreatic cancers. Healthy mouse fibroblast cells (STO) were also tested for comparison, because an effective chemotherapeutic drug has to be selective towards cancer cells.

Optimal Experimental Design methodology was applied to identify the nanoformulation with the highest therapeutic activity. A statistical analysis method known as response surface methodology was carried out to evaluate the *in-vitro* cytotoxicity data, and to determine whether the chosen experimental parameters truly express the optimized conditions of the nanoparticle based drug delivery system. The overall goal was to optimize the therapeutic efficacy in nanoparticle-based pancreatic cancer treatment. Based on the statistical data, the most effective iron/iron oxide nanoparticle-based drug delivery system has been identified. Its Fe/Fe_3O_4 core has a diameter of 20 nm. The surface of this nanoparticle is loaded with the homing sequence CGKRK (139-142 peptide molecules per nanoparticle surface) and the chemotherapeutic agent doxorubicin (159 molecules per surface), This nanoplatform is a promising candidate for the nanoparticle-based chemotherapy of pancreatic cancer.

Table of Contents

List of Figures

List of Tables

Acknowledgements

It would not have been possible to complete my doctoral studies without the help and support of many people around me, and I take this opportunity to thank each one of you for making my desire to pursue a PhD in chemistry a success.

First and foremost I would like to express my heartiest gratitude to my major professor Dr. Stefan H. Bossmann for his guidance and support during my studies. This thesis would not have been possible without his advice, encouragements and the trust he kept on me throughout the years. He is truly a great mentor and a role model for all of his students.

I would also like to acknowledge the members of my PhD committee: Dr. Duy H. Hua, Dr. Christer B. Aakeröy, Dr. Deryl L. Troyer, and outside chairperson Dr. Weiqun Wang for their support and dedication.

I am very grateful to Kathrine Bossmann for all the support gave me in every possible way and taking care of us all the time. A big thank you goes to all the past and present members of the Bossmann group for their tremendous support and friendship.

I would like to acknowledge all the faculty members specially Dr. Duy Hua, Dr. Christer Aakeröy, Dr. Dan Higgins, for allowing me to use their instrumentation and staff members in the Department of Chemistry, Dr. Leila Maurmann for helping with NMR characterization, Mr. Jim Hodgson, Mr. Ron Jackson and Mr. Tobe Eggers for all the technical support.

I am extending my gratitude to Ms. Nadeesha Perera and Dr. Dallas Johnson in the Department of Statistics for helping me with the statistical analysis of my research work.

A special thank you goes to Ms. Tharanga Kumudini, Ms. Sahani Weerasekara, Ms. Medha Gunaratna, Ms. Buddhika Galkaduwa helping me with IR, Mass and ICP instrumentation, and also to Ms. Marla Pyle in the Troyer's lab at Department of Anatomy and Physiology for all the support given to me during the cell experiments.

Words are hardly enough to express my heartfelt gratitude to my beloved parents and my sister for their unconditional love, support and courage given to me throughout my life to mold in to the person who I am today. I know you are proud of me and it is all because of you.

Last but not least I am very grateful to my husband Anushka been there with me for the past four years providing me strength, courage and inspiration whenever needed. I am forever in debt to you for everything you have given to me.

Dedication

Dedicated to *Amma*, *Thaththa* and *Aiya* for their unconditional love

Chapter 1 - Introduction

1.1 Pancreatic Cancers

Cancer is a disease caused by uncontrolled division of abnormal cells in the body. Cells bearing damaged DNA are known as abnormal cells which do not under go apoptosis hence led to the formation of new set of abnormal cells by cell division. During the propagation it also has the ability of invading nearby tissues as well as distant areas within the body by transporting the malignant cells through blood stream or lymphatic vessels.[1] Spreading of the cancer within the body is known as metastasis. The causes of cancer are not yet understood properly and various genetic factors as well as life style factors such as use of tobacco, alcohol, dietary habits, certain infections are known to increase the risk of cancers. According to the world health organization 7.6 million deaths were occurred worldwide due to cancers and 21 million deaths are expected in year 2030.[2] Among the various types of cancers lung, stomach, liver and breast cancers causes most deaths worldwide. In the USA, cancer is the second largest cause of death and about six hundred thousand deaths were expected in year 2013.[3] Fore mentioned cancer statistics strongly urges the need of effective diagnostic techniques and anticancer treatments to minimize deaths due to the cancers.

Conventional cancer treatment methods include chemotherapy, radiation therapy, transplantation and surgery where chemotherapeutic treatments are the widely used as early treatment method. With the ongoing research works through out the world novel treatment approaches are also introduced such as targeted therapy, photodynamic therapy, hyperthermia etc.[3] Combination of conventional and novel approaches are currently in use for effective treatments of cancers by medical practitioners.

My research work is aimed towards development of a drug delivery system for effective treatment of pancreatic cancer. Pancreatic cancer is the fourth leading cause of cancer-related deaths in USA.[4] Some of the main risk factors associated with pancreatic cancer are smoking, diabetes and obesity. It is a well-known fact that early stages of pancreatic cancer are asymptomatic. Diagnosis at very late stages led to very low survival rates due to the cancer compared to other cancers.

Due to the advancements in diagnosis and treatments, cancer survival rates have been improving from decades to decade while pancreatic cancer still has very low survival rates as shown in figure 1.1.[5] Therefore, the disease is still considered largely incurable. According to the American Cancer Society, for all stages of pancreatic cancer combined, the one-year relative survival rate is 20%, and the five-year rate is 4%. These low survival rates are attributable to the fact that fewer than 20% of patients' tumors are confined to the pancreas at the time of diagnosis; in most cases, the malignancy has already progressed to the point where surgical removal is impossible.

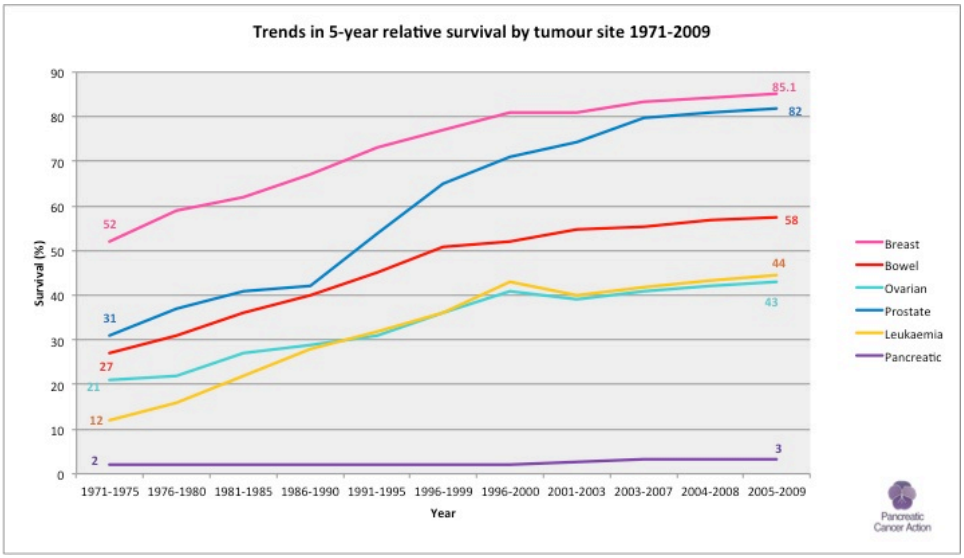

Figure 1.1 Relative five year survival rates of tumors[5]

Therefore, chemotherapy and radiation therapy have become the best available methods for pancreatic cancer treatments. But pancreatic cancer cells show high resistance towards chemotherapeutic and radiation agents due to the enhanced tumor stromal components and disordered vasculature of tissues in tumor microenvironment, which causes very low drug encapsulation within the tumor compartments and make them less effective towards therapy.[4,6,7] During my research work a multifunctional drug delivery system was developed that is capable of targeting and delivering the therapeutic agents selectively to the pancreatic cancer cells with high efficacy.

1.2 Drug Delivery

Drug delivery is a specific method for introducing pharmaceutical components to the human body. Once the drugs have reached their target, their therapeutic effects have to be activated in order to cure or overcome the medical condition that is being treated.[8] In early medical practices drinking plant decoctions and chewing plant materials were the primary ways of delivering the drugs to the body.[9] But most of these methods are lacking the basic requirements that have to be addressed in drug delivery. Consistency and uniformity of the therapeutic agents are most important to lead to predictable results in therapy. This led to the discovery of conventional drug delivery systems that are currently in use, such as pills, tablets lotions etc., which are using different routes.[8] Regardless of the drug or its mode of delivery, once it is inside the human body it undergoes a series of events before it reaches its final site of action, which may greatly reduces it concentration and, eventually, its effectiveness.[10] Therefore, continuing research and development are taking place in order to design effective drug delivery systems.

According to the literature, in order to obtain maximum benefits for a specific drug, it should be selectively delivered to its target site at a rate and concentration that permit optimal activity and efficacy with a minimum side/toxic effects.[11] Notari *et al* has reported certain parameters that need to be considered during the formulation of a specific drug delivery system. They are,

- "Pharmacokinetics properties of the drug: such as rate of absorption, rate and mechanism of drug elimination, biological half-life and bioavailability for the human body.
- Pharmacological properties of the drug: minimum effective therapeutic concentration, influence of drug peaking and desirability of steady state kinetics.
- Toxicological properties of the drug release system: minimum toxic concentration and frequency and type of toxicological effects.[11]

There are two main classes of drug delivery systems, which are "controlled drug release systems" and "targeted drug delivery systems", which depend on the drug releasing site and its site of action.[9] 1) Controlled release systems are capable of releasing the drugs at predetermined rate to the blood circulation from specific sites, where it is not essentially the target site of the drug. 2) Targeted drug delivery systems release the drug at the site of action once it is selectively delivered it to exactly this site.[11] In general it is advantageous to develop targeted delivery systems, which achieve the delivery of high concentrations of active drug components to the site of action.

1.2.1 The Ringsdorf Model for Targeted Drug Delivery Systems

Synthetic or natural macromolecules have been widely studied and used as polymeric drugs since the 1950s.[12] Some of the characteristics of polymers that make them an ideal candidates as drug delivery modalities are biocompatibility, low toxicity, and high solubility in physiological medium, and finally, easy excretion from the body. Chemical properties of polymers facilitate the attachment of therapeutic agents via simple bond formations, which have contributed to their wide applications in targeted drug delivery.[13] Considering these characteristics, Prof. Dr. Helmut Ringsdorf has suggested a generalized model in 1975 that can be used for the construction of polymeric drugs with high efficiency.[10]

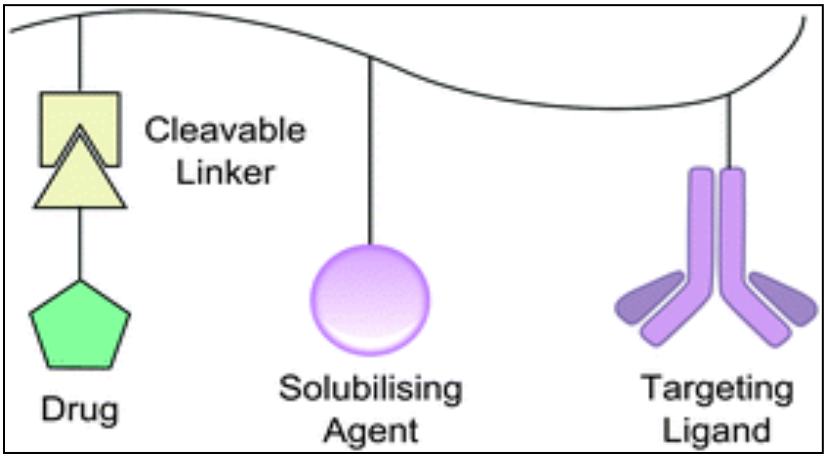

Figure 1.2 Schematic representation of the Ringsdorf model

The Ringsdorf model considers of five main components, which are the 1) the polymeric backbone, 2) the spacer/cleavable linker, 3) the drug, 4) the targeting moiety and 5) the solubilizing agent.[11] Each group has their own significance and contributes to the maximum efficacy of the system as one unit. Usually, the polymer can be inert or biodegradable, and a cleavable linker specifically attaches the drug to it. One of the most significant advantages of the system is the proper selection of spacer/linker, which facilitates the rate of release of the active

drug by hydrolysis or enzymatic cleavage at the site of action. The second most important feature is the ability of changing the body distribution and cell uptake mechanisms of the polymeric delivery vehicle by attaching a targeting ligand, which is usually specific for a particular cell type of a group of cells with related biological features.[13] Finally, the solubilizer enhances the solubility of the system in aqueous media, depending on the pharmacological requirements and applications.[11] Regardless of its simplicity, the Ringsdorf model has been a historic milestone in the development of polymeric drug delivery systems and has been widely studied and applied by many research groups since then.[11]

Drug delivery systems that has been developed and used in the research work is basically followed the original Ringsdorf model with structural modifications in order to make the system more effective towards pancreatic cancer treatments. Since the late twentieth century nanotechnology based applications have been extensively studied and nanoformulations have shown promising results in drug delivery.[14] Therefore metal nanoparticles are incorporated in to the system as an alternative to the polymeric backbone to study their efficacy as drug delivery components. Other important theranostic components are attached to the surface of the nanoparticles by chemical modifications to maintain the consistency of the system as each of these components play their own role in drug delivery mechanisms. Magnetic iron/iron oxide (Fe/Fe_3O_4) nanoparticles are selectively used as the nanomaterial, as monodispersed magnetic iron/iron oxide (Fe/Fe_3O_4) are successfully synthesized and used in cancer treatment methods in the our lab. In addition to that iron oxide nanoparticles provide straightforward surface modification, which facilitate the drug conjugation around the nanoparticles and shows high solubility in physiological media.[14] Biological significances, and advantageous of using nano materials and specially the role of iron nanoparticles are discussed in the chapter 03.

1.3 Ligand Targeted Anticancer Therapy

Chemotherapy is the use of chemical agents for the treatment of cancers and it is one of the most widely used methods due to the fact that they are succeeded in improving the cancer survival rate over the past 25 years.[15] Despite their activity against cancer cells they do act on healthy cells causing severe side effects because cancer cells resembles many common features with normal cells. For example both cancer cells and hair follicles, gastrointestinal cells show high proliferation rates and chemotherapeutic drugs such as paclitaxel, doxorubicin can interact with all these cells. As a result selective toxicity of the chemotherapeutic drugs becomes limited towards cancer cells. Various approaches are investigating in order to develop the selective toxicity of the chemotherapeutic drugs which includes two main methods, (i) introduction of new chemotherapeutic drugs and (ii) use of antibodies or ligands that specifically bound onto the receptors present on the cancer cells.[16] Potential of using targeting ligands is taken in to consideration in the Ringsdorf as well since it increase the targeting activity of the drug system.

Ligand mediated targeting is the delivery of chemotherapeutic drugs in to the cancer cells or to tumor vasculature selectively by associating them with molecules that binds to the antigens or receptors over expressed or uniquely expressed by cancerous cells compared to the normal healthy tissues.[15] These targeting ligands can be incorporated with the drug carrier systems, polymers or liposomes as well. The choice of good targeting ligand or antibody depends on several factors such as receptor expression, internalization methods, and immune responses to the antibodies or binding affinities towards the ligands etc.[16] There should be high antigen or receptor density on the targeted cells for effective targeting activity and receptor mediated internalization of the drug or the drug system facilities the high drug accumulation within the tumor vasculature.

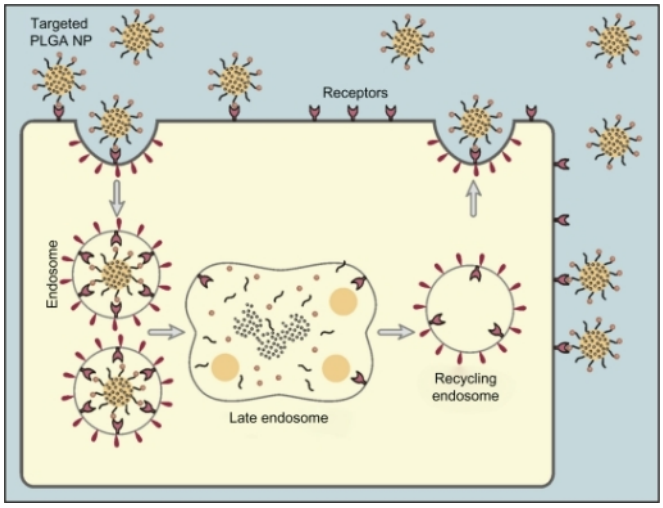

Figure 1.3 Ligand mediated targeted therapy[17]

During the tumor propagation, blood vessels around them grow along with the tumor by angiogenesis, formation of blood vessels from the existing vessels in order to supply the nutrient and oxygen demands. Therefore, tumor blood vessels have become important therapeutic target, which inhibits the tumor growth by inhibiting the angiogenesis.[18] Tumor blood vessels also express high amounts of various cell surface and extracellular matrix proteins, compared to normal cells. Among the vast number of ligands that are used for the targeting purposes peptide sequences show several advantages over others as they can be achieved in smaller sizes compared to antigens and large-scale synthesis using chemical methods with high specificity. Moreover, various types of peptide ligand receptors such as integrin receptors, thrombin receptors are found on the tumor cell surfaces that is the key for peptide mediated targeting of the cancers.[19] Tumor targeting peptide ligands are successfully incorporated into drug delivery vehicles, such as small chemotherapeutic drugs, liposomes and inorganic nanoparticles due to their high specificity and efficacy with minimum side effects.[20] With the fore mentioned advantages of using peptide sequences as targeting moieties motivates us to use short peptide

sequence CGKRK as the targeting ligand in the constructed drug delivery platform.

1.4 Fe/Fe_3O_4 Nanoparticle Based Drug Delivery System

Considering the factors mentioned in the original Ringsdorf model, I have carried out the design of a ligand mediated drug delivery platform using Fe/Fe_3O_4 nanoparticles as drug carrier. This was the first step of my thesis research. The schematic representation of the nanoplatform is shown in the diagram below.

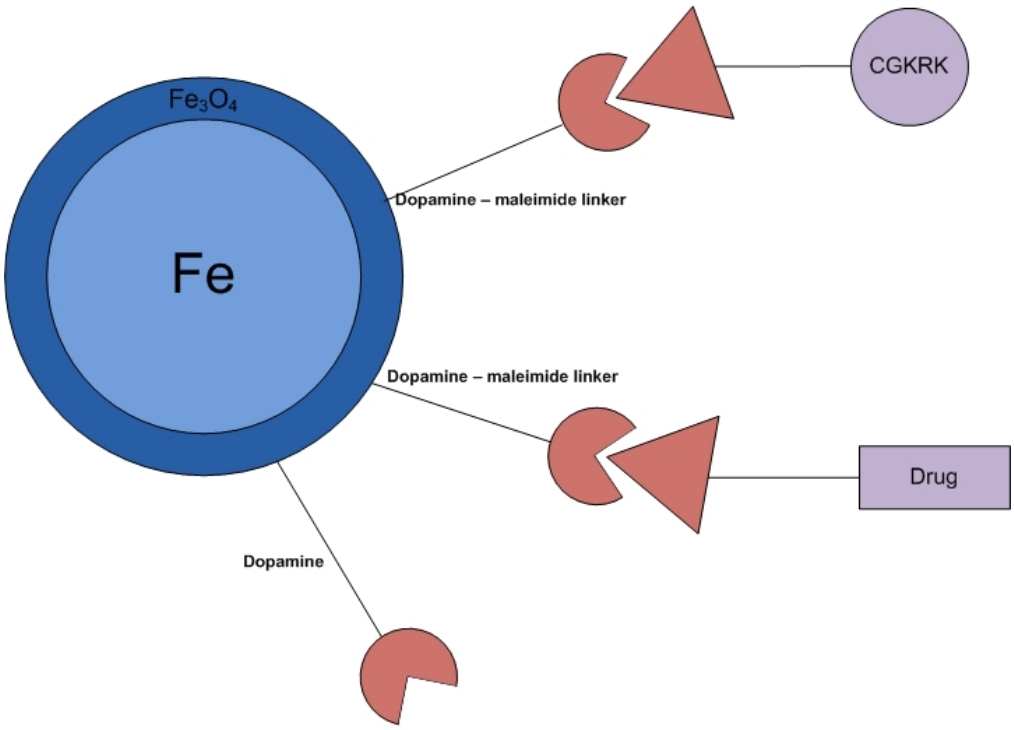

Figure 1.4 Schematic representation of the nanoparticle based drug delivery system

This system consists of all five components mentioned in the original Ringsdorf model with structural variations in order to maximize its therapeutic specificity and efficacy. Fe/Fe_3O_4 nanoparticles are used as the backbone of the system. Fe/Fe_3O_4 nanoparticles are synthesized from thermal decomposition of iron pentacarbonyl ($Fe(CO)_5$) as the iron source.[21] Selective air

oxidation of the outer layer of the Fe(0) nanoparticles causes the formation of thin adherent Fe_3O_4 layer around the core Fe(0) nanoparticles. The basic synthetic strategy for the synthesis of Fe(0) nanoparticles are shown below.

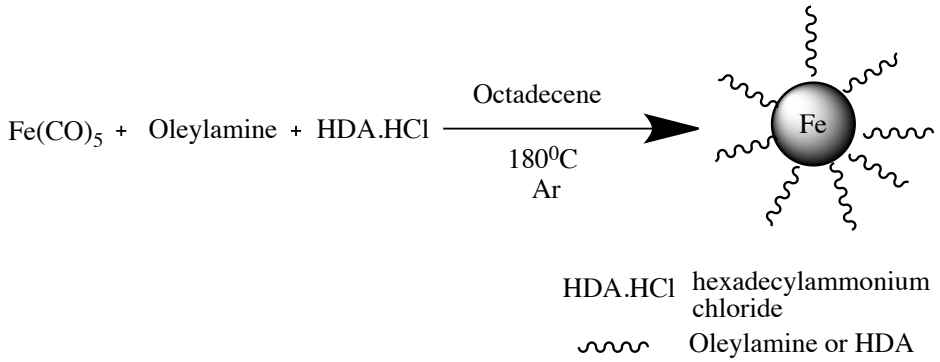

Figure 1.5 Preparation of Fe(0) nanoparticles

1.4.1 Surface Functionalization of the Fe/Fe_3O_4 Nanoparticles

There are several important factors that need to be considered during the use of metal nanoparticles for applications. Most importantly, they should have good (bio)chemical stability and dispersibility in physiological media, which must not alter their properties while they are transported to the active site. They should also possess long circulation times within the blood stream with minimum non specific binding with other proteins present in the blood. Finally, they should be well excreted from the body via the renal system with minimum toxicity effects. In order to meet these requirements nanoparticles are conjugated or coated with various organic/inorganic ligands, polymeric materials or protein molecules.[22] For example, when magnetic iron oxide nanoparticles are used in biomedical applications they are coated or functionalized with polymers (polyethylene glycol, dextran or chitosan), organic ligands (foliate, citrate or dopamine) and inorganic materials, such as SiO_2.[22] The outer ligand coating shields the magnetic iron core from the surrounding environment and it also can enhance the incorporation

of other therapeutic agents to the nanoparticles.

Dopamine, a catecholamine, is widely used for the surface functionalization of magnetic nanoparticles due to the formation of a stable, robust anchor on the surfaces of Fe_3O_4 or Fe_2O_3 nanoparticles by forming a five membered metallocycle with Fe (III) irons. It also facilitates the functionalization with other ligands of interest via the primary amine group present at the terminal.[23] The hydrophilic nature of dopamine also makes the nanoparticles become more biocompatible in aqueous or physiological media. Therefore, dopamine is used as the solubilizing agent, as well as for the construction of spacer/cleavable linkers in the construction of functional nanoparticle-based systems.[24] The spacer or cleavable linker can be constructed by introducing the maleimide moiety, which is reacting with the primary aliphatic amine of dopamine.[25] Furthermore, this modified maleimide moiety acts as a versatile synthetic platform due to its dienophilic nature, making Diels-Alder reactions feasible,[26] and its ability of forming stable C-S bonds with thiol groups and C-N bonds with primary amines of the biologically important molecules via Michael addition reactions.[27] pH mediated hydrolysis of the dopamine-maleimide ligands enhances the release of active drug components once they are selectively delivered to the tumor cells. Detailed structural and chemical significances of the use of dopamine and maleimides will be discussed in the chapter 03.

A short peptide sequence with terminal cysteine amino acid, CGKRK (Cys-Gly-Lys-Arg-Lys) is used as the targeting ligand in the constructed drug delivery system. CGKRK was first discovered by phage display and found to bind both neovascular endothelial cells and tumor cells with high affinity. The specific receptor for the CGKRK is found to be heparan sulfate, a sulfated polysaccharide mainly located in endothelial and tumor cells.[19] Previous research work showed that the CGKRK peptide can be used for effective tumor targeting. Furthermore, intravenously

injected CGKRK recognizes the blood vessels in most tumors, but not in normal tissues. [28]

1.4.2 Doxorubicin – Chemotherapeutic Drug

Doxorubicin is used as the chemotherapeutic agent in the constructed drug delivery system according to the Ringsdorf model. Doxorubicin is an anthracycline antibiotic widely used as chemotherapeutic agent in treatment of various cancers including breast, lung, ovaries, multiple myeloma, bladder and many others.[29] It is also used to treat noncancerous disease conditions as well. Like most of the anthracyline drugs, doxorubicin interacts with DNA by intercalation and inhibition of the DNA replication mechanisms. Specifically it is a topoisomerase II inhibitor, where it prevents the relaxing of supercoiled DNA, thereby inhibiting DNA transcription and replication.[30]

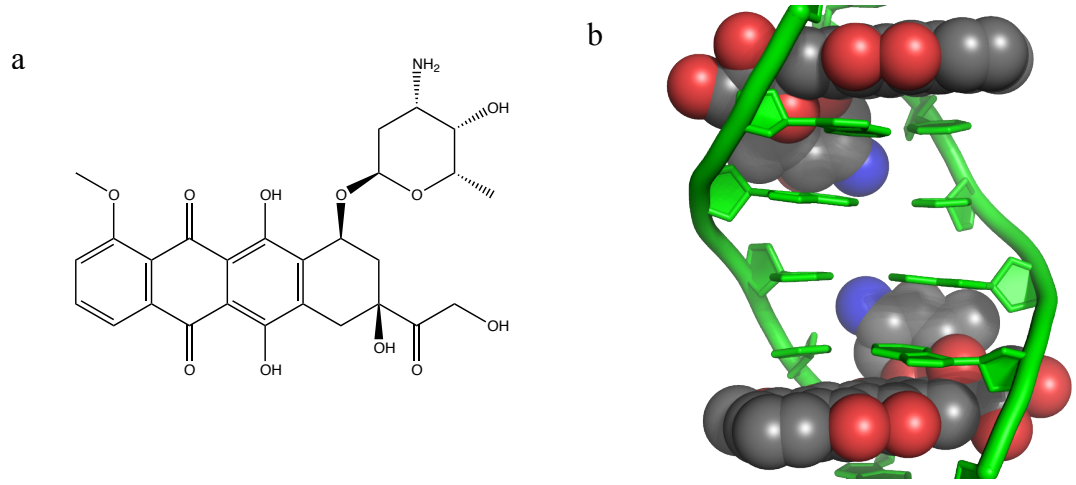

Figure 1.6 (a) structure of doxorubicin (b) doxorubicin intercalation in to the DNA double helix[31]

It is also reported that doxorubicin induced apoptosis in cancer cells by formation of reactive oxygen species (ROS) by means of redox activity even though the exact mechanism of ROS mediated doxorubicin induced apoptosis remains uncertain.[32]

Doxorubicin is given to the patents intravenously as its hydrochloride salt due to the hydrophobic nature of the drug itself. A liposomal formulation of the drug is also available to minimize the side effects associated with the drug. Acute toxicity effects of doxorubicin include nausea, vomiting, hair loss and suppression of bone marrow. In addition to that doxorubicin shows dose-dependent severe cardiotoxicity, renal and hepatic toxicity on the cancer patients with prolonged use, it has been recently found that it also causes toxicity effects on the central nervous system (CNS).[33] It is believed that toxic effects on the heart is basically due to the formation of the reactive oxygen species generated form the redox reactions of doxorubicin within the cells, while brain toxicity may be due to the high level of cytokines generated by chemotherapeutic drugs and tumors itself.[28] Hoffman et al further reported that cytokines are signaling molecules activated upon infection due to inflammatory activities within the body, where they also play a role in dopamine and serotonin metabolism in the CNS. High levels of cytokines present in the CNS cause adverse effects on the brain, resulting in fatigue, lack of appetite, sleep disturbance and concentration as well.

Due to this forementioned factors, it is vital that chemotherapeutic agents, especially when doxorubicin is used, need to be selectively delivered to the tumor compartments to minimize the adverse side effects. Incorporation or attachment of the drugs with drug delivery vehicles, which selectively deliver the drugs into the tumor vasculature by releasing them within the tumor environment, greatly reduces the adverse side effects associated with chemotherapeutic agents. In the constructed model, the drug is covalently bound to the nanoparticles via dopamine-maleimide ligands. The release of doxorubicin is achieved by the lower pH values present in the lysomosal/late endosomal compartments within the cancer cells.[34] Therefore, the release of free doxorubicin during the time of blood circulation is minimal due to

the high pH values present under these physiological conditions.

1.5 Optimization of the Therapeutic Activity of the Nanoparticle Based Drug Delivery System

Once the system is constructed, the second part of the research work was to perform cell-based assays to determine the therapeutic efficacy of the nanoparticle-based systems. Using the toxicity data, the optimized composition of the system with proper ratios of doxorubicin to CGKRK and the optimum concentration of the drug delivery system was determined by using a statistical analysis method. The multivariate statistical technique, which is known as "response surface methodology" is used as tool to carry out these optimization processes. Experimental design methodology was used to plan the experiments. Then the experimental data (cell experiments) was analyzed using mathematical models. Based on these data, the optimized conditions for basically any particular process can be identified. Experimental design methodology is especially suited in optimizing systems that depend on several variables, and where no clear mathematical hypothesis exists, which can verified or falsified. Furthermore, experimental design methodology is the method, which requires the fewest experiments to optimize a system. A detailed introduction and discussion of the statistical analysis method is provided in the next chapter.

References

1. http://www.cancer.org/cancer/cancerbasics/what-is-cancer
2. http://www.who.int/mediacentre/factsheets/fs297/en/
3. http://www.cancer.gov/statistics
4. Lee, G.Y.; Qian, W.P.; Wang, L.; Wang, Y.A.; Staley, C.A.; Satpathy, M.; Nie, S.; Mao, H.; Yang, L., Theranostic Nanoparticles with Controlled Release of Gemcitabine for Targeted Therapy and MRI of Pancreatic Cancer. *ACS Nano* 2013, 7, 2078–2089
5. http://pancreaticcanceraction.org/pancreatic-cancer/about/research-funding/
6. Yang, L.; Mao, H.; Cao, Z.; Wang, Y.A.; Peng, X.; Wang, X.; Sajja, HK.; Wang, L.; Duan, H.; Ni, C.; Staley, CA.; Wood, WC.; Gao, X.; Nie, S., Molecular Imaging of Pancreatic Cancer in an Animal Model using Targeted Multifunctional Nanoparticles. *Gastroenterology* 2009,136(5), 1514-25
7. Kumagai, M.; Sarma, T.K.; Cabral, H.; Kaida, S.; Sekino, M.; Herlambang, N.; Osada, K.; Kano, M.R.; Nishiyama, N.; Kataoka, K., Enhanced in vivo Magnetic Resonance Imaging of Tumors by PEGylated Iron-Oxide–Gold Core–Shell Nanoparticles with Prolonged Blood Circulation Properties. Macromol. Rapid Commun. 2010, 31, 1521–1528
8. http://en.wikipedia.org/wiki/Drug_delivery
9. Paolino, D.; Sinha, P.; Fresta, M.; Ferrari, M., Drug delivery systems. In: Webster, J.G. (Ed.), The Encyclopedia of Medical Devices and Instrumentation, John Wiley & Sons, 2006 pp 437–495
10. Ringsdorf, H., Structure and properties of pharmacologically active polymers. *J. polym. sci., C Polym. symp.,* 1975, 51, 135–153
11. San Roman, J.; Gallardo, A.; Levenfeld, B., New Polymers for Biomedical Applications: Synthesis and Characterization of Acrylic Systems with Pharmacological Activity, *Macromol. Symp.* 1994, 84, 145-15
12. http://www.scribd.com/doc/15042616/dextran

13. Hoste, K.; Winne, K.D.; Schacht, E., Polymeric Prodrugs. *Int J Pharm.* 2004, 277, 119–131.

14. Faraji A.H.; Wipf, P., Nanoparticles in Cellular Drug Delivery. *Bioorg Med Chem* 2009, 17(8), 2950–2962

15. Brannon-Peppas, L.; Blanchette, J.O.; Nanoparticle and Targeted Systems for Cancer Therapy. *Advanced Drug Delivery Reviews* 2004, 56, 1649 – 1659

16. Allen, T.M., Ligand-Targeted Therapeutics in Anticancer Therapy. *Nature Reviews Cancer* 2002, 2, 750-763

17. Dinarvand, R.; Sepehri, N.; Manoochehri, S.; Rouhani, H.; Atyabi, F., Polylactide-co-glycolide Nanoparticles for Controlled Delivery of Anticancer Agents. *Int J Nanomed.* 2011, 6, 877–895

18. Agemy, L.; Friedmann-Morvinski, D.; Kotamraju, V.R., Targeted Nanoparticle Enhanced Proapoptotic Peptide as Potential Therapy for Glioblastoma. *Proc. Natl Acad. Sci. USA*. 2011, 108, 17450–17455

19. Hu, Q.; Gao, X.; Kang, T., CGKRK-Modified Nanoparticles for Dual-Targeting Drug Delivery to Tumor Cells and Angiogenic Blood Vessels. *Biomaterials* 2013, 34(37), 9496-9508

20. Zhang, X.X.; Eden, H.S.; Chen, X., Peptides in Cancer Nanomedicine: Drug Carriers, Targeting Ligands and Protease Substrates. *J. Control Release* 2012, 159, 2-13

21. Lacroix, L.M.; Frey, H. N.; Ho, D.; Sun, X.; Cheng, K.; Sun, S., Stable Single-Crystalline Body Centered Cubic Fe Nanoparticles. *Nano Lett.* 2011, 11, 1641–1645

22. Shan J.; Khin Y.W.; Shuhua Li.; Choon P. T.; Yuangang Z.;Ming-Yong H., Surface-Functionalized Nanoparticles for Biosensing and Imaging-Guided Therapeutics. *Nanoscale* 2013, 5, 3127-3148

23. Shultz, M.J.; Reveles, J.U.; Khanna, S.N.; Carpenter, E.E., Reactive Nature of Dopamine as a Surface Functionalization Agent in Iron Oxide Nanoparticles. *J. AM. CHEM. SOC.* 2007, 129, 2482-2487

24. Rajh, T.; Chen, L. X.; Lukas, K.; Liu, T.; Thurnauer, M. C.; Tiede, D. M., Surface Restructuring of Nanoparticles: An Efficient Route for Ligand-Metal Oxide Crosstalk. *J. Phys. Chem. B* **2002**, *106*, 10543

25. Geiseler, B.; Fruk, L., Bifunctional Catechol Based Linkers for Modification of TiO_2 Surfaces. *J. Mater. Chem.* **2012**, 22, 735-741

26. Zhang, F.; Lees, E.; Amin, F.; Rivera-Gil, P.; Yang, F.; Mulvaney, P.; Parak, W. J., Polymer-Coated Nanoparticles: A Universal Tool for Biolabelling Experiments, *Small* **2011**, *7*, 3113-3115.

27. Mather, B. D.; Viswanathan, K.; Miller, K.M.; Long T.M., Michael Addition Reactions in Macromolecular Design for Emerging Technologies. *Prog. Polym. Sci.* **2006**, 31, 487–531

28. Hoffman, J. A.; Giraudo, E.; Singh, M.; Zhang, L. L.; Inoue, M.; Porkka, K.; Hanahan, D.; Ruoslahti, E. Progressive Vascular Changes in a Transgenic Mouse Model of Squamous Cell Carcinoma *Cancer Cell* 2003, 4, 383-91

29. http://www.cancer.org/treatment/treatmentsandsideeffects/guidetocancerdrugs/doxorubicin

30. Bodley, A.; Liu, L.F.; Israel, M.; Seshadri, R.; Koseki, Y.; Giuliani, F.C.; Kirschenbaum, S.; Silber, R.; Potmesil, M., DNA Topoisomerase II-Mediated Interaction of Doxorubicin and Daunorubicin Congeners with DNA. *Cancer Res* 1989, 49, 5969-5978

31. http://upload.wikimedia.org/wikipedia/commons/e/ee/Doxorubicin%E2%80%93DNA_complex_1D12.png

32. Wang, S.; Konorev, E.A.; Kotamraju, S.; Joseph, J.; Kalivendi, S.; Kalyanaraman, B., Doxorubicin Induces Apoptosis in Normal and Tumor Cells via Distinctly Different Mechanisms. Intermediacy of H_2O_2- and p53-Dependent Pathways. *J Biol Chem.* 2004, 279(24), 25535-25543

33. Aluise, C.D.; Sultana, R.; Tangpong, J.; Vore, M.; St Clair, D.; Moscow, J.A.; Butterfield, D.A., Chemo Brain (Chemo Fog) as a Potential Side Effect of Doxorubicin Administration: Role of Cytokine-Induced, Oxidative/Nitrosative Stress in Cognitive Dysfunction. *Adv Exp Med Biol.* 2010, 678, 147-156

34. Cho, K.; Wang, X.; Nie, S.; Chen, S.; Shin, D.M., Therapeutic Nanoparticles for Drug Delivery in Cancer. *Clin Cancer Res* **2008**, 14(5), 1310-1316

Chapter 2 - Optimization

One of the key objectives in any system, regardless of its nature, is the ability of getting the maximum in production or maximum benefits from it during the desired application. In order to maximize its benefits the given system is adjusted by changing the critical parameters of the system. This is known as the process of optimization.[1] In general, this is achieved by changing the variables one at a time while keeping the others constant and observing the responses in order to obtain optimal conditions. This method is known as one-variable-at-a-time.[2] This is the most commonly used method in many scientific studies. However, this method has several disadvantages, such as it does not account for the interactive effects of the variables on the response, and the required number of experiments is high, which ultimately increases the time and costs of the system.[1] Therefore, more versatile optimization procedures are constructed using multivariate statistical techniques, which can be used to study interactive effects on the responses in a given system.[2] Multivariate designs can be used to study critical variables simultaneously, which can be implemented fast and, therefore, more cost effective than applying univariate methods.[3] Multivariate statistical analysis methods are widely in use for the optimization of particular system when a set of responses is influenced by more than one variable.[1] The multivariate system that is used the most is the selection of suitable experimental parameters in systems, for which no straightforward mechanistic paradigm exists. For these systems, the key variables that need to be studied and the experimental domain, in which the optimization has to take place, have to be designed.[4]

Optimization techniques are widely used in analytical chemistry for the optimization of separation, extractions etc., more than in any other chemistry disciplines. With the continuously growing importance, quality and demand of synthetic chemistry, specifically in drug delivery,

the synthetic procedures or clinical applications should be optimized in order to enhance their capacity of producing effective therapeutic drugs in an inexpensive manner. To date, application of optimal experimental design techniques in drug synthesis and drug delivery were rarely carried out. Their availability in literature is very limited.

2.1 Response Surface Methodology

Response surface methodology (RSM) was originally developed and described by Box and Wilson in 1951.[5] By definition "RSM consists of a group of mathematical and statistical techniques that are based on fit of empirical models to the experimental data obtained in a relation to experimental design".[1] The relationship between the response and the variables is given by,

$$y = f(x_1, x_2, x_3 \dots \dots x_n) + \varepsilon \qquad (1)$$

, where y is the response, f is the function of response by independent variables $x_1, x_2, x_3 \dots x_n$ with n number of variables and ε is statistical error associated with the experiments. Optimization studies using RSM can be separate into three main stages, which are

1. Determination of independent variables and their levels
2. Selection of experimental design and prediction, verification of model equation
3. Evaluation of response plots and determination of optimal conditions

Detailed explanations of the steps are adapted from two journal articles, "Response surface methodology (RSM) as a tool for optimization in analytical chemistry" by Bezerra and co-workers (*M.A. Bezerra, R.E. Santelli, E.P. Oliveira, L.S. Villar, L.A. Escaleira, Talanta 76 (2008) 965–977.*) and "Modeling and optimization I: Usability of response surface methodology" by Bas and co-workers (*D. Bas, I.H. Boyaci, J. Food Eng. 78 (2007) 836*).

2.1.1 Determination of Independent Variables and Their Levels

The main objective is to identify the experimental domain and independent variables, which are involved in any given system. The experimental domain is working domain of interest, defined by minimum and maximum limits of the variables that are studied. On the other hand, independent variables are experimental factors that can be changed independently of each other, such as temperature, reactant concentration, reaction time etc. In a given biological or chemical process, the experimental response is affected by numerous variables, and it is practically impossible to study the effects of all parameters. Therefore, it is vital to select the parameters that have significant effects on the system. Preliminary screening studies have to be carried out to identify important variables, as well as their interactive effects on the responses of the system. This is usually achieved by applying factorial design. After the identification of independent parameters, the next step is to determine the directions that need to be changed to obtain the maximum response, and the levels of parameters that need to be studied. Levels of variables simply mean the values of the variables, for which the experiments are carried out. For example, temperature limits can be set to 150^0C ± 10. Correct determination of these values truly affects the success of the optimization.

Units and the range of independent variables differ from one another in a given experimental domain thus statistical analysis cannot be performed. Therefore, independent variables must be normalized into a set of coordinates applying a scale of dimensionless values, which are proportional to their localization in the experimental region. This process is known as codification. The commonly used equation for transforming real values (z_i) into their coded values (x_i) is,

$$x_i = \left(\frac{z_i - z_i^o}{\Delta z_i}\right)\beta_d \qquad (2)$$

, where Δz_i is the distance between the real value in the central point and real value in the highest or lowest level of a variable, β_d is the major coded limit value in the matrix for each variable and z_i^o is the real value at the center point. In general, coded values are ranging from -1 to 1.

2.1.2 Selection of Experimental Design and Prediction, Verification of Model Equation

As mentioned in the introduction, the most critical step in the optimization is the selection of a suitable experimental design depending on the complexity of the system. The simplest model is a linear function for first order models, where data does not present any curvature. When curvatures are represented in the responses, quadratic response surfaces, such as three level factorial, central composite, Box-Behnken, or Doehlert design must be used. After the proper selection of the model, a model equation is defined to predict the interaction between different experimental variables. A second order model will possess the following model equation,

$$y = \beta_o + \sum_{i=1}^{k} \beta_i x_i + \sum_{1 \le i \le j}^{k} \beta_{ij} x_i x_j + \varepsilon \quad (3)$$

, where β_o is the constant term, k is the number of variables, β_i represents the coefficients of the linear parameters, β_{ij} represents the coefficients of the interaction parameters, x_i and x_j represents the variables and ε is the residual associated to the experiments.

In order to determine the responses at their critical points, quadratic terms are incorporated into the equation (3). So it can be represent as,

$$y = \beta_o + \sum_{i=1}^{k} \beta_i x_i + \sum_{i=1}^{k} \beta_{ii} x_i^2 + \sum_{1 \le i \le j}^{k} \beta_{ij} x_i x_j + \varepsilon \quad (4)$$

, where β_{ii} represents the coefficients of the quadratic parameters.

In order to estimate the β parameters, the matrix notation of the model can be constructed as,

$$y = x\beta + \varepsilon \tag{5}$$

$$\underbrace{\begin{pmatrix} y_1 \\ y_2 \\ . \\ . \\ . \\ y_n \end{pmatrix}}_{y} = \underbrace{\begin{pmatrix} 1 & x_{11} & x_{12} & \cdot & \cdot & x_{1k} \\ 1 & x_{21} & x_{22} & \cdot & \cdot & x_{2k} \\ . & . & . & . & . & . \\ . & . & . & . & . & . \\ . & . & . & . & . & . \\ 1 & x_{n-1} & x_{n-2} & \cdot & . & . \end{pmatrix}}_{x} \underbrace{\begin{pmatrix} \beta_0 \\ \beta_1 \\ . \\ . \\ . \\ \beta_k \end{pmatrix}}_{\beta} + \underbrace{\begin{pmatrix} \varepsilon_1 \\ \varepsilon_2 \\ . \\ . \\ . \\ \varepsilon_n \end{pmatrix}}_{\varepsilon} \tag{6}$$

, where y is the response vector, x is the matrix of the chosen experiment design, β is the vector constituted by the parameters and ε is the residual value. Equation (5) is solved by a statistical method known as method of least square (MLS).[5] MLS is a multiple regression analysis method, which uses to fit a mathematical model to a set of experimental data generating the lowest possible value for ε. After the MLS vector, $\beta containing$ parameters can be obtained as:

$$\beta = (x^T x)^{-1}(x^T y) = C x^T y \tag{7}$$

, where $C = (x^T x)^{-1}$

This equation is used to construct the response surfaces that describe the behavior of the response in a given experimental domain. Computational software is normally used in this process. In MLS method it is assumed that errors are independent of each other with zero mean value and a common variance value. Therefore, the variance estimated in equation (7) is obtained by repetitions of the central point where C is a square matrix value. By calculating the square root value of C , the standard error for coefficient β is obtained. The final process in this step is to determine whether the chosen mathematical model is fitting to the data in the studied experimental domain. It is evaluated using application of analysis of variance (ANOVA), where it compares the variation due to the changes in parameters with the variation due to random

errors occurred during response measurments.[4] General steps carried out in ANOVA are described as follows. Variation of data is obtained by calculating sum of the square value of the deviation of each observation (y_i) or its replicates (y_{ij}) with relation to media ($\bar{y}$) by,

$$\sum d_i^2 = \left(y_{ij} - \bar{y}\right)^2 \tag{8}$$

using the above equation sum of square of deviation due to the regression (SS_{reg}) and sum of square of deviation due to residual generated by the model (SS_{res}). Summation of these values is equal to the total sum of squares of deviation (SS_{tot}),

$$SS_{tot} = SS_{reg} + SS_{res} \tag{9}$$

Due to the repetition of central point observation error can be associated with the repetition values. Therefore the sum of squares of deviation is further divided into two components as

$$SS_{res} = SS_{pe} + SS_{lof} \tag{10}$$

, where SS_{pe} is the sum of squares due to pure error and SS_{lof} is sum of square due to the lack of fit of the model.

The next step is to determine the media of square (MS) depending on the respective degree of freedom gained for each variation (total, regression, residual or lack of fit).

Variance of sources	Sum of the square	Degree of freedom	Media of the square
Regression	$SS_{reg} = \sum_i^m \sum_j^{n_1} (\hat{y}_i - \bar{y})^2$	$p-1$	$MS_{reg} = \frac{SS_{reg}}{p-1}$
Residuals	$SS_{res} = \sum_i^m \sum_j^{n_1} (y_{ij} - \hat{y}_i)^2$	$n-p$	$MS_{reg} = \frac{SS_{res}}{n-p}$
Lack of fit	$SS_{lof} = \sum_i^m \sum_j^{n_1} (\hat{y}_i - \bar{y}_i)^2$	$m-p$	$MS_{lof} = \frac{SQ_{lof}}{m-p}$
Pure error	$SS_{pe} = \sum_i^m \sum_j^{n_1} (y_{ij} - \bar{y}_i)^2$	$n-m$	$MS_{pe} = \frac{SS_{pe}}{n-m}$
Total	$SS_{tot} = \sum_i^m \sum_j^{n_1} (y_{ij} - \bar{y})^2$	$n-1$	

Table 2-1 Analysis of variance for fitted mathematical model to an experimental data set using multiple regression[1]

Where n_i: number of observation

m : total number of levels in the design

p : number of parameter of model

$\hat{y}_i$: estimated value by the model for the level i

$\bar{y}$: overall media

y_{ij}: replicates performed in each individual levels

$\overline{y_i}$: media of replicates performed in the same set of experimental conditions

Once the regression calculations are performed, there are two ways to determine the fitness of the chosen mathematical model with respect to the experimental data. The first method is to perform a significance of regression analysis, given by the ratio between media of square values of regression (MS_{reg}) and residual (MS_{res}) values. The value is compared with the Fisher distributions (*f* test) for corresponding degrees of freedom values.

$$\frac{MS_{reg}}{MS_{res}} \approx F_{v_{reg},v_{res}} \tag{11}$$

If the statistical significance for the above ratio is higher than the tabulated *f* value, the mathematical model is well fitted to the experimental model. The other method is to evaluate the lack of fit test where it compares the ratio between media of square values of lack of fit (MS_{lof}) and pure error (MS_{pe}) with *f* test values.

$$\frac{MS_{lof}}{MS_{pe}} \approx F_{v_{lof},v_{pe}} \tag{12}$$

If the ratio is higher, than the tabulated data model is not fitted well to the experimental data and it needs to be improved by carrying out repetitive experiments.

2.1.3 Evaluation of Response Plots and Determination of Optimal Conditions

The final step of the optimization process is the visualization of the predicted model equation by constructing the response surface plots and contour plots. The response surfaces are the theoretical three-dimensional representation of the response versus independent variables while the contour plots are two-dimensional displays of the responses over the plane of independent variables. For quadratic models the critical point on the response surfaces can be a maximum, a minimum, or a saddle. Coordinates of the critical points are calculated by means of the first derivative of mathematical function, which is equal to zero,

$$y = f(x_1, x_2) = b_0 + b_1 x_1 + b_2 x_2 + b_{11} x_1^2 + b_{22} x_2^2 + b_{12} x_1 x_2 \quad (13)$$

the stationary point is calculated by solving the following equations,

$$\frac{\partial y}{\partial x_1} = b_1 + 2b_{11} x_1 + b_{12} x_2 = 0 \quad (14)$$

$$\frac{\partial y}{\partial x_2} = b_2 + 2b_{22} x_2 + b_{12} x_1 = 0 \quad (15)$$

When there are three or more variables are present in the system, one or more variables are set to constant values in order to construct the contour plots or response surfaces. Some of the common response surfaces and contour plots are shown in the next diagram.

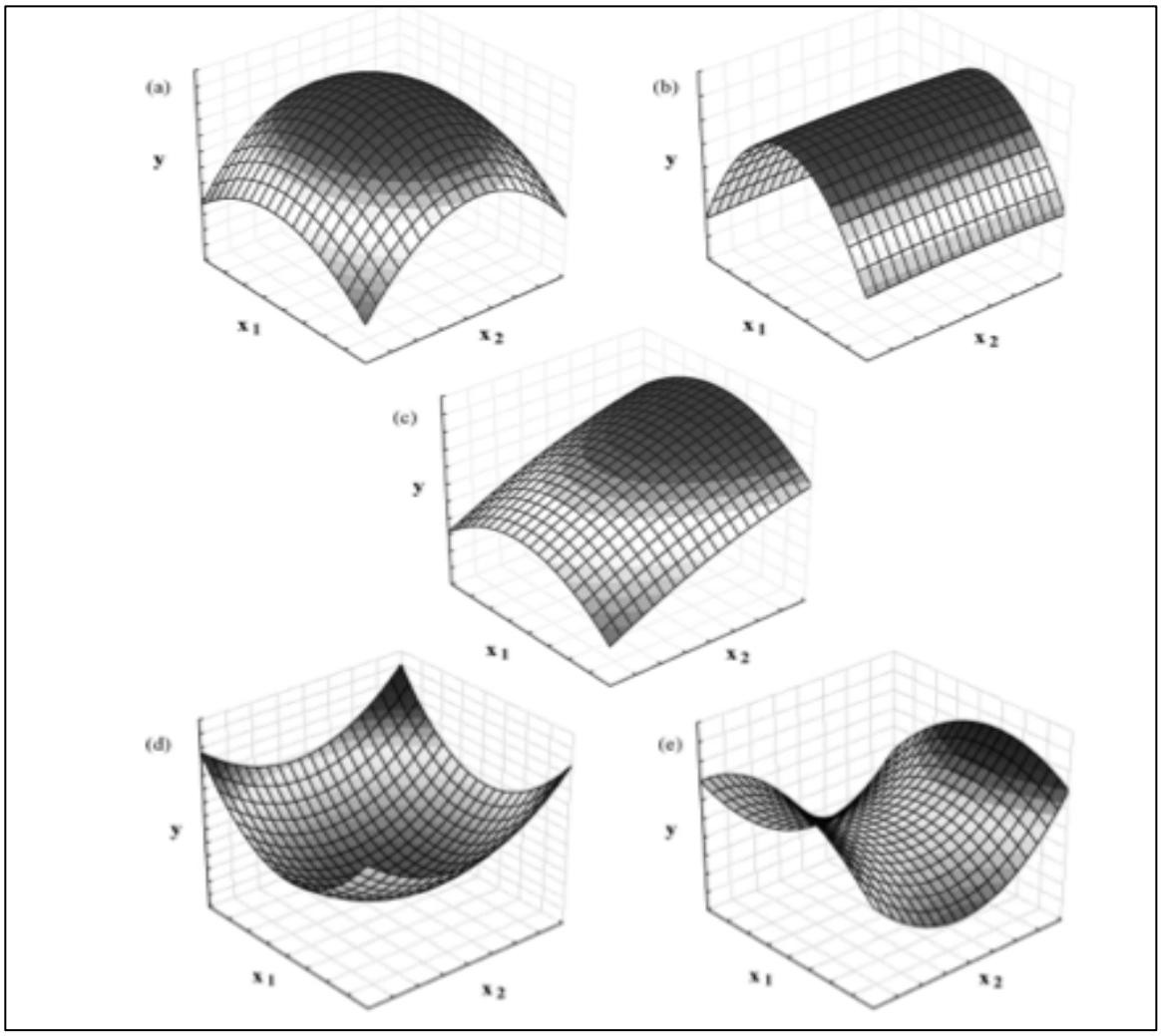

Figure 2.1 Some profiles of surface response generated from a quadratic model in the optimization of two variables. (a) maximum, (b) plateau, (c) maximum outside the experimental region, (d) minimum, and (e) saddle surfaces[1]

The response surface represented in figure 5(b) is a plateau relative to variable x_2, which indicates that the response is independent on any level of variable x_2. Another interesting response is shown in figure (e), which is a saddle. Here, neither a minimum nor a maximum response is obtained. This means that the chosen variables did not represent optimal conditions. Therefore, careful displacement of the experimental region is carried out to obtain optimal conditions for the system.

RSM has several advantages over classical one-variable-a-time optimization such as it provides more information from a small number of experiments, and it is capable of evaluating interactions between variables and their effects on the responses[2].

The success of the optimization process is greatly relying on the selection of the proper experimental design. As mentioned earlier, some of the common symmetrical second order experimental designs are full factorial designs, Box-Behnken designs, central composite designs, and Doehlert design. Among these methods, Doehlert experimental design is the experimental design model that has been used during the research.

2.2 Doehlert Design

David Doehlert developed this method in 1970 as a practical and economical method that can be used as an alternative for second order experimental designs, such as central composite design or Box-Behnken designs.[6] Both central composite design and Box-Behnken methods are symmetrical and possess characteristic orthogonal and rotatable behaviors, while the unsymmetrical Doehlert design is neither orthogonal nor rotatable.[7] A given experimental design is categorized as symmetrical if it has same number of levels for each independent variable that is studied in the system.[2] According to the original article published by David Doehlert, his design describes a circular domain for two variables, spherical domain for three variables and hyperspherical domain for variables above three with uniform space filling ability throughout the experimental domain.[6] The characteristic features of Doehlert matrix are listed below[1]:

1. Requires *N* number of experiments according to $N = k^2 + k + c_p$ where k is the number of independent variables that are studying and c_p is the replicate number of central point.

2. Each variable can be studied at different levels depending on their importance towards the response as well as their restrictions such as cost or instrument constraints etc.
3. The intervals between its levels represent a uniform distribution thus it is originally named as uniform shell designs.
4. Experimental matrix can be displaced through the experimental domain via adjacent points present in original matrix to obtain new experimental region.

For two variables the Doehlert design is represented by a regular hexagon with six points at the hexagon and one central point. The hexagon is generated using regular simplex, which is an equilateral triangle, and the coordinates of the triangle represent the central point and two other points at the hexagon. The other points of the hexagon are obtained from subtracting every run in the triangle from each other. Coordinates of the regular hexagon for two variables are given in coded units as shown below.

Run	X_1	X_2	Subtraction
1	**0.0**	**0.0**	
2	**1.0**	**0.0**	
3	**0.5**	**0.866**	
4	-1.0	0.0	1-2
5	-0.5	-0.866	1-3
6	-0.5	0.866	3-2
7	0.5	-0.866	2-3

Table 2-2 Coded factor levels for two variable Doehlert design

The real experimental values corresponding to the coded values can be obtained from the equation (2) mentioned in the part 2.1.1. It can be clearly seen the unsymmetrical nature of the

design matrix that variable X_1 is studied at five levels while X_2 is only studied at three levels. Depending on the importance of the variable studied levels can be interchanged. The graphical representation and possible displacement of the hexagon over the experimental region is given below.

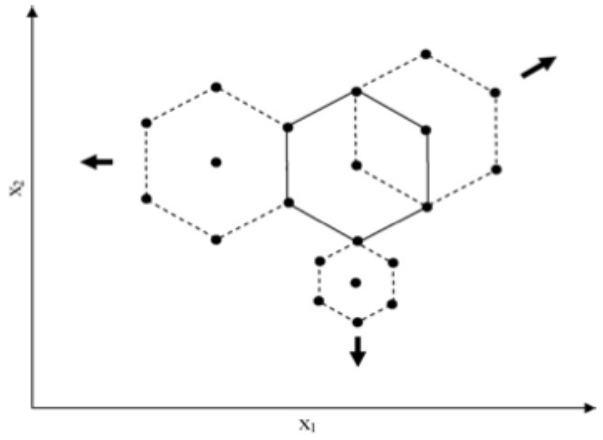

Figure 2.2 Graphical representation of hexagonal Doehlert design in experimental domain[1]

One of the major advantages of the Doehlert matrix is its space filling ability with a uniform grid of points, regardless of the irregularity of the experimental domain. The experimental matrix can also be displaced to regions with high response values while keeping some of the previous experimental coordinates, which ultimately reduces the number of experiments required in the new experimental matrix. Furthermore, the coded limit between the coordinates can be lowered in order to obtain the optimal response in the area of interest. The experimental matrices for three and four variables are listed below.

Applications of Doehlert matrix in optimization have increased in recent years due to the efficiency and several advantages over other second order models[1, 4, 6].

A study comparing the efficiencies of Composite design, Box-Behnken Design and Doehlert Design in comparison has found that for any independent variable value, Doehlert design is the most efficient among the three systems.[3] It is more practical and economical, as the

number of experiments need to be carried out is low and some experiments data can be re-used with the ability of displacement of the matrix over the experimental region.[7] Since the synthesis of nanoplatforms for cancer treatment is time-consuming and costly, Doehlert Design offers the opportunity to decrease the number of required nanoplatforms during the optimization of the nanoplatform for maximal efficacy.

Run	Three-factor			Four factor			
	x_1	x_2	x_3	x_1	x_2	x_3	x_4
1	0	0	0	0	0	0	0
2	1	0	0	1	0	0	0
3	0.5	0.866	0	0.5	0.866	0	0
4	0.5	0.289	0.817	0	0.289	0.817	0
5	0.5	0	0	0	0.289	0.204	0.791
6	-1	-0.866	0	-1	0	0	0
7	-0.5	-0.289	-0.817	-0.5	-0.866	0	0
8	-0.5	-0.866	0	-0.5	-0.289	-0.817	0
9	0.5	-0.289	-0.817	-0.5	-0.289	-0.204	-0.791
10	-0.5	0.866	0	0.5	-0.866	0	0
11	0	0.577	-0.817	0.5	-0.289	-0.817	0
12	-0.5	0.289	0.817	0.5	-0.289	-0.204	-0.791
13	0	-0.577	0.817	-0.5	0.866	0	0
14				0	0.577	-0.817	0
15				0	0.577	-0.204	-0.791
16				-0.5	0.289	0.817	0
17				0	-0.577	0.817	0
18				0	0	0.613	-0.791
19				-0.5	0.289	0.204	0.791
20				0	-0.577	0.204	0.791
21				0	0	-0.613	0.791

Table 2-3 Doehlert matrix for three and four independent variables[1]

References

1. Bezerra, M.A.; Santelli, R.E.; Oliveira, E.P.; Villar, L.S.; Escaleira, L.A., Response SurfaceMethodology (RSM) as a Tool for Optimization in Analytical Chemistry. *Talanta* **2008**, 76, 965–977
2. Bas, D.; Boyaci, I. H., Modeling and Optimization I: Usability of Response Surface Methodology *Journal of Food Engineering* **2007**, 78(3), 836–845
3. Ferreira, S.L.C.; Dos Santos, W.N.L.; Quintella, C.M.; Neto, B.B.; Bosque-Sendra, J.M., Doehlert Matrix: A Chemometric Tool for Analytical Chemistry. *Talanta* **2004**, 63, 1061-1067.
4. Kuehl, R.O., Design of Experiments: Statistical Principles of Research Design and Analysis. Duxbury Press. **2000**, 124-197
5. Myers, R. H.; Montgomery, D. C., Response Surface Methodology: Process and Product Optimization using Designed Experiments. New York: John Wiley & Sons, Inc. **1995**
6. Doehlert, D.H., Uniform Shell Designs. *Appl. Statist.***1970**, 19, 231-239
7. Ferreira, S.L.C.; Bruns, R.E.; Da Silva, E.G.P.; Dos Santos, W.N.L.; Quintella, C.M.; David, J.M.; De Andrade, J.B.; Breitkreitz, M.C.; Jardim, I.C.S.F.; Neto, B.B., Statistical Designs and Response Surfac Techniques for the Optimization of Chromatographic Techniques. *J. Chromatogr. A* **2007**, 1158, 2-14

Chapter 3 - Synthesis and Characterization of a Fe/Fe_3O_4 Based Drug Delivery System

3.1 Iron Nanoparticles in Drug Delivery

Particles with a diameter within 1 to 100 nm are considered nanoparticles. With the emergence of nanotechnology, tailored nanomaterials have shown a wide variety of applications in engineering and biomedical techniques. In modern medicine, applications include both diagnosis and treatment of various disease conditions by using them as contrasting agents for magnetic imaging, and as drug delivery agents, or as a drug itself.[1] Nanoparticles have characteristic properties, such as chemical reactivity, energy absorption, and mobility that greatly depend on their size.[2] Among various types of nanoparticles, metallic nanoparticles, such as gold nanoparticles, silver nanoparticles, and iron oxide nanoparticles, are currently showing promising results in biomedical applications as diagnostic or therapeutic tools.[3,4]

Iron is an abundant metal and has been used since ancient times in many industrial applications and as therapeutic agent.[5] Therefore, iron has become a potential candidate in nanotechnology-based applications of metallic nanoparticles. Iron has three main oxides FeO, Fe_2O_3, and Fe_3O_4. Bulk Fe_2O_3 and Fe_3O_4 are paramagnetic, whereas they are superparamagnetic when nanoscopic.[6] Due to the characteristic properties of Fe_2O_3 and Fe_3O_4, such as magnetism, and biocompatibility, they have potential applications as contrast agents in magnetic resonance imaging, targeted drug delivery, hyperthermia, gene delivery and early detection of inflammatory diseases and cancers.[6,7,8] In the area of targeted drug delivery, nanoparticles, and here especially the iron oxide nanoparticles, are advantageous due to their high surface areas that can be easily modified with chemical ligands. For targeted drug activity *in vivo,* Fe_2O_3 is considered one of the

best candidates due to the presence of iron (III) in the nanoparticle core, which is less toxic to human body. On the other hand Fe_3O_4 is considered an excellent contrasting candidate for magnetic resonance imaging and hyperthermia.[9]

Iron is an essential mineral for biological systems (including humans) due to its activity as electron donor and acceptor. For instance, it is the vital component in hemoglobin and required for proper activity of numerous enzymes within the body.[10] Therefore, leaching of iron form the delivery systems will not cause drastic toxic effects, as ferric/ferrous ions will be either stored or excreted from the body by general elimination mechanisms.[9] Size plays a major role in prolonged blood circulation of nanoparticles due to the uptake of nanoparticles by the reticuloendothelial system (RES) in the body. Larger nanoparticles with diameter above 200 nm are accumulated within the spleen by mechanical filtration while nanoparticles less than 10 nm will be removed from the blood circulation system by renal excretion and extravasation. Therefore, nanoparticles with diameters ranging from 10 nm-100 nm feature optimal sizes in order to maintain prolonged blood circulation and selective accumulation within the tumor compartment for efficient drug delivery mechanisms.[11]

3.2 Uptake Mechanisms of Nanoparticles by Cancer Tissues

Once the nanoparticles are intravenously administered to the blood stream, they are selectively delivered to the tumor compartments via passive targeting and active targeting mechanisms. In passive targeting mechanisms, nanoparticles with correct dimensions are selectively accumulated in the cancer compartments due to enhanced permeability and retention effects of the cancerous tissues.[12] During tumor propagation, tumor-surrounding areas are highly vascularized in order to provide sufficient nutrients and oxygen supply for rapid growth of tumor

cells. Therefore, the rapid formation of tumor blood vessels through angiogenesis causes deficient blood vessels with leaky irregular endothelial cells compared to normal healthy tissues. As a result, the tumor vasculature becomes more permeable for macromolecular transportation through the gaps formed between the endothelial cells.[13] Properly synthesized nanoparticles with correct dimensions have ability to permeate through the endothelial cells and selectively accumulate within the tumor environments.

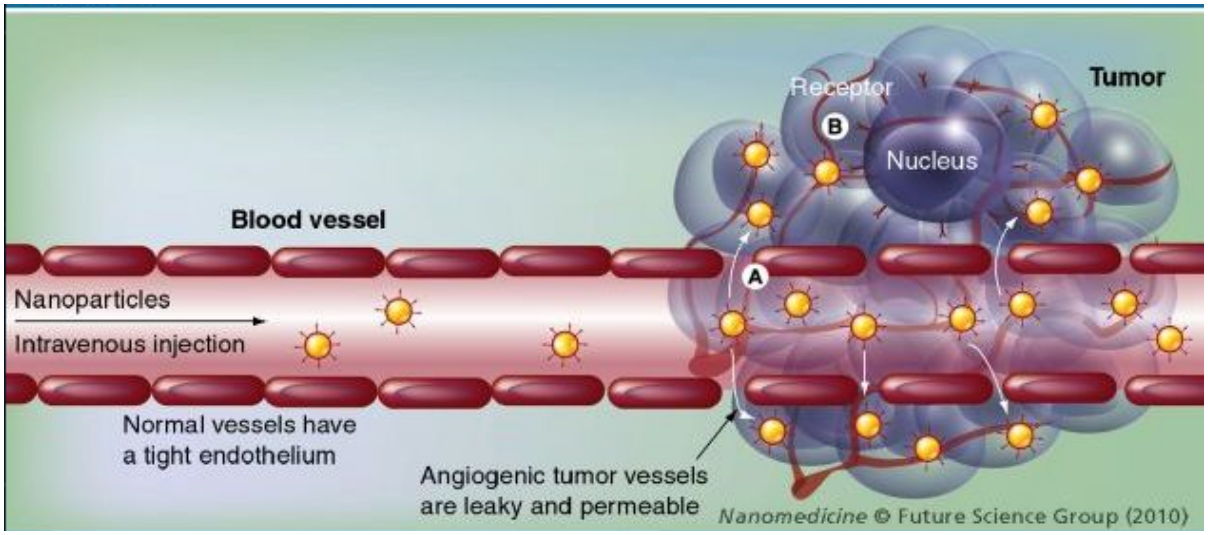

Figure 3.1 Passive targeting of the nanoparticles in cancer cells via enhanced permeable retention effects[14]

In addition to passive targeting, nanoparticles are also capable of selectively delivering their cargo to the tumor periphery via active targeting, as already discussed in chapter 01. Active targeting of nanoparticles is achieved by introducing antibodies or targeting ligands onto the surface of nanoparticles, which selectively bind to overexpressed receptors present on tumor blood cells or tumor vasculature.

3.2.1 Tumor Homing Peptides in Tumor Specific Active Targeting

A short peptide sequence (CGKRK) is used in my nanoparticle based drug delivery system as the tumor homing sequence, which is bound to the dopamine ligands present on the Fe/Fe_3O_4 nanoparticles. CGKRK facilitates the active targeting of tumors. The RGD peptide is the first tumor targeting peptide that has been discovered.[15] To date, RGD is still one of the widely used homing sequences. It selectively targets integrin receptors present on the tumor cells. Other than the RGD sequence, several other peptides sequences are currently under investigations for their homing activity in cancer research, such as CGKRK, NGR, TCP-1, iRGD etc.[16]

As already discussed, CGKRK has been used in this research as the targeting moiety, due to its dual targeting nature, as its targeting receptor heparan sulfate is present on both, neovascular endothelial cells and tumor cells. Hoffmann and coworkers reported evidence to support this fact when luminol labeled CGKRK was used for studying the uptake mechanism. Luminol associated CGKRK is found on the surface of the endothelium cells, as well as in the tumor periphery. They further reported that this phenomenon is observed only with CGKRK and not with other peptides labeled with the fluorescein dye. Therefore, accumulation of CGKRK on tumor vasculature is not due to the EPR effect, but a rather specific targeting mechanisms that is followed by this short peptide sequence.[17] Other than enhancing cellular uptake of the drugs by most tumors, CGKRK also targets the mitochondria and nuclei once it has entered the tumor cells. CGKRK is a cationic molecule. Therefore it selectively binds to the anionic phospholipid receptors on the cells. CGKRK in bulk quantities is inexpensive and commonly carried out by means of solid phase peptide synthesis.

3.2.1.1 Solid Phase Peptide Synthesis

In chemical synthesis, reactions can be carried out in gas, liquid or solid phases. Solid phase synthesis has become more prominent in peptide synthesis and DNA synthesis. Generally, in solid phase synthesis molecules are bound to a solid support and stepwise reactions are carried out in a reactant medium where byproducts or unreacted materials are easily removed by washing with suitable solvents. In peptide synthesis, the peptide chain is synthesized from the C terminus to the N terminus by introducing one amino acid at a time via amide bond formation. The first amino acid is coupled to a polystyrene resin, which act as the solid support. Functional groups of the side chains of the amino acids are protected by protecting groups to avoid coupling reactions with upcoming amino acids. Finally, the peptide is cut from the resin to obtain the desired sequence. A schematic representation of solid phase synthesis is summarized in Figure 3.2, as shown below.

The terminal amine groups of their corresponding amino acids are generally protected with Fmoc (9-fluorenylmethyloxycarbonyl) and Boc (t-butyloxycarbonyl) groups that can be selectively cleaved by acids or bases.[18] The side chain protecting groups are stable under reaction conditions, but eventually removed at the final stage to obtain the desired peptide sequence.

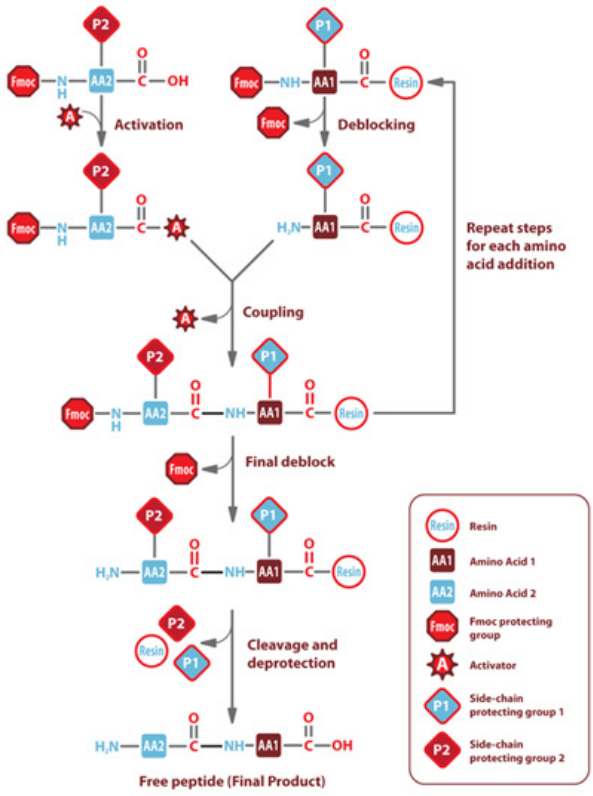

Figure 3.2 Schematic representation of solid phase peptide synthesis[19]

3.3 Synthesis and Surface Functionalization of Fe/Fe_3O_4 nanoparticles

Iron nanoparticles can be synthesized by several methods such as thermal decomposition of iron pentacarbonyl, sonochemical decomposition of iron carbonyl, reduction of iron salts/oxides, and synthesis by vapor phase are well established.[20] Successful synthesis of monodispersed Fe(0) nanoparticles via thermal decomposition of iron pentacarbonyl ($Fe(CO)_5$) is carried out in the Bossmann laboratories. Formation of a thin layer of Fe_3O_4 around the core Fe(0) particles is achieved in-situ by selective oxidation by air with the aid of hexadecylammonium chloride.

3.3.1 Surface Functionalization of Fe/Fe_3O_4 Nanoparticles

Iron nanoparticles are highly sensitive to atmospheric oxygen thereby undergoing further oxidation and reduction of the volume of the Fe(0) core. Therefore, a strongly adhesive Fe_3O_4 layer is synthesized around the Fe(0) core by air oxidation (see above) to protect the zero-valent iron core. The surface of the outer iron oxide layer can be functionalized with various types of materials to minimize the biocorrosion when they are used in biological applications.

Rajh *et al* have reported that bidentate ligands, such as dopamine have the ability of converting the under-coordinated surface sites of magnetite nanoparticles to a bulk like lattice structure with octahedral geometry for oxygen coordinated irons. This lattice formation enhances a tight binding of the dopamine to the surface of nanoparticles. Furthermore, a Langmuir isotherm of dopamine chemisorption indicates that desorption of dopamine from Fe_3O_4 surfaces is less favorable than adsorption.[21,22] Thus, stable interaction between iron and dopamine is established, which minimizes the bio corrosion of iron nanoparticles by their surrounding aqueous media. In addition to the stabilization of the Fe_3O_4 surface of the nanoparticles, dopamine also provide versatile linkage to couple other ligands or therapeutic components to the nanoparticle via amide bond formation reactions with the terminal primary amine of dopamine. Finally, the hydrophilic nature of the primary amine group enhances the satisfactory solubility of the drug delivery system in physiological media.

Iron oxide nanoparticles are further functionalized with dopamine-maleimide ligands to couple the homing peptide sequence and desired drug onto the nanoparticles. Maleimide is an unsaturated imide and important molecule in chemical synthesis due to its reactivity toward Diels-Alder reactions and Michael addition reactions. The main purpose of introducing the maleimide moiety onto the nanoparticles through dopamine is to couple the homing peptide

sequence and doxorubicin via Michael addition reactions. Dopamine and dopamine maleimides, as well as adsorption to nanoparticles are shown in Figure 3.3 below.

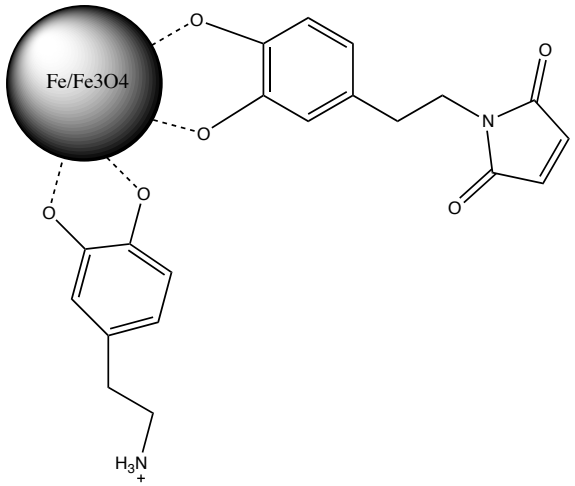

Figure 3.3 Iron oxide nanoparticles functionalized with dopamine and dopamine maleimide ligands

3.4 Experiments and Results

3.4.1 Synthesis of Core/shell Fe/Fe_3O_4 Nanoparticles

Fe/Fe_3O_4 nanoparticles were synthesized by thermal decomposition of $Fe(CO)_5$ in the presence of oleylamine and hexadecylammonium chloride (HADxHCl) using 1-octadecene (ODE) as solvent originally published in Sun et al.[23] This reaction produces Fe(0) atoms, which aggregate to form the initial sub-nanometer clusters. The reaction temperature is then lowered to 180^{o}C. The Fe(0) clusters are capable of catalyzing the thermal decomposition of $Fe(CO)_5$. In the presence of the binary ligand system oleylamine/ hexadecylamine x HCl this process leads to the controlled growth of iron(0) nanoparticles. Depending on the iron pentacarbonyl concentration, initial reaction time and temperature, as well as the duration and temperature of the subsequent ripening procedure, near monodisperse (polydispersity < 1.03) nanoparticles possessing

diameters between 5 nm and 100 nm can be prepared.[24] The second step in nanoparticle synthesis consists in the defined oxidation of the surface Fe(0) to Fe_3O_4. Dr. Hongwang Wang has optimized this procedure in the Bossmann group by bubbling O_2/N_2 mixtures through a dispersion of the initially prepared nanoparticles at room temperature. By selecting the duration of air oxidation, various chain thicknesses can be achieved. The transmission electron microscopy (TEM) images and high-resolution transmission electron microscopy (HRTEM) image of the obtained nanoparticles are shown in Figure 3.4. The nanoparticles have a well-defined core/shell structure, with the average Fe(0) core diameter of 20 ± 0.5 nm and the Fe_3O_4 shell thickness of 2.0 ± 0.5 nm, respectively. The TEM characterization revealed that the bulk Fe(0) phase is crystalline, but not monocrystalline. Several crystallites are combined in the Fe(0) core of each nanoparticle. The outer Fe_3O_4 layer, is able to protect the Fe(0) core against aqueous buffers and under air. However, slow oxidation of the Fe(0) cores is observed in cell experiments (see Figure 3.4).

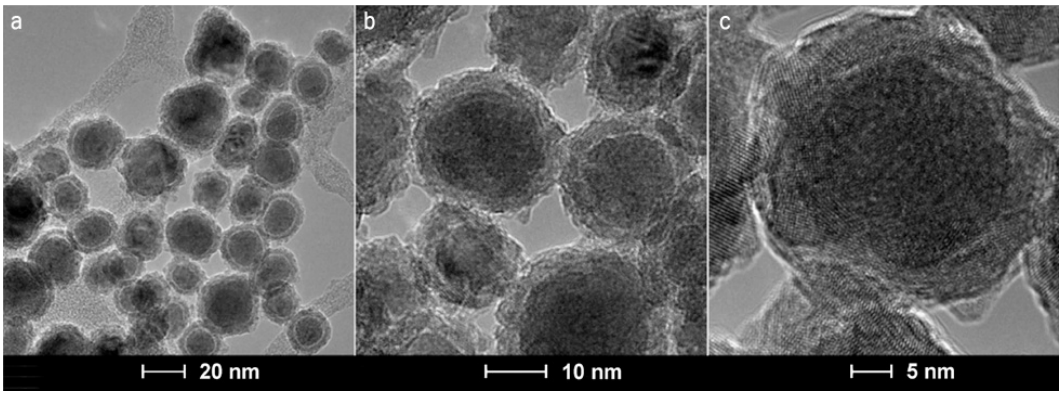

Figure 3.4 (a, b) TEM and (c) HRTEM images of Fe/Fe_3O_4-core/shell nanoparticles

This synthetic procedure was scaled up to 100g batches in 2013 in the Bossmann group. Kansas State University Research Foundation (KSURF) in collaboration with Kansas State University's Institute for Commercialization (KSU-IC) is currently pursuing a combined patent

with Battelle Memorial Institute, Columbus, OH. The resulting nanoparticles were further characterized by means of XRD and XPS.

Powder X-ray diffraction (XRD) patterns were obtained on a Bruker D8 X-ray diffractometer with Cu Kα radiation.[25] The XRD pattern (as shown in Figure 3.5) is indicative of the presence of bcc Fe(0) as bulk phase.

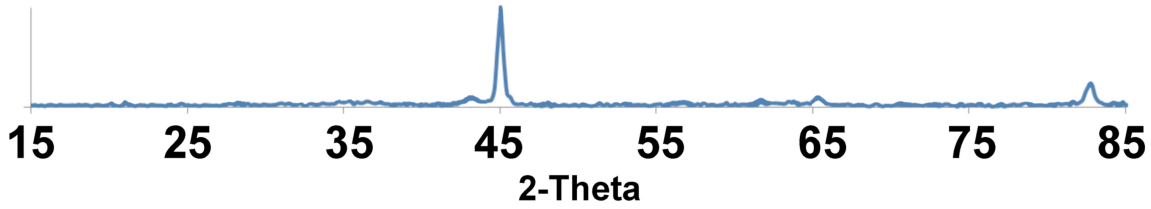

Figure 3.5 XRD pattern of the synthesized Fe/Fe_3O_4 nanoparticles after ligand exchange oleylamine/ hexadecylamine x HCl vs. dopamine

X-ray photoelectron spectroscopy (XPS) data[26] was recorded with a Perkin–Elmer PHI 5400 electron spectrometer using acrochromatic Al Kα radiation (1486.6 eV). Analysis was carried out under vacuum less than 5×10^{-9} Torr and heated to 120 ^{o}C to remove any adsorbed molecules on the surface. The XPS binding energies were measured with a precision of 0.025 eV. The analyzer pass energy was set to 17.9 eV, the contact time was 50 ms, and the area scanned was 4 mm^2.

XPS is able to reveal the chemical surface composition of the nanoparticles. Typically, it can analyze nanoparticles to a depth of 1-2 nm. Therefore, it is unable to discern the bulk composition. The XPS measurements shown in Figure 3.6 were performed by Dr. Myles Ikenberry in the group of Prof. Dr. Keith Hohn, Department of Chemical Engineering, Kansas State University. Shown is the surface composition after nanoparticle synthesis and after exchange of oleylamine/ hexadecylamine x HCl against dopamine. XPS clearly indicates the

presence of Fe_3O_4 at the nanoparticles' surface, as a comparison with literature findings indicates.[27]

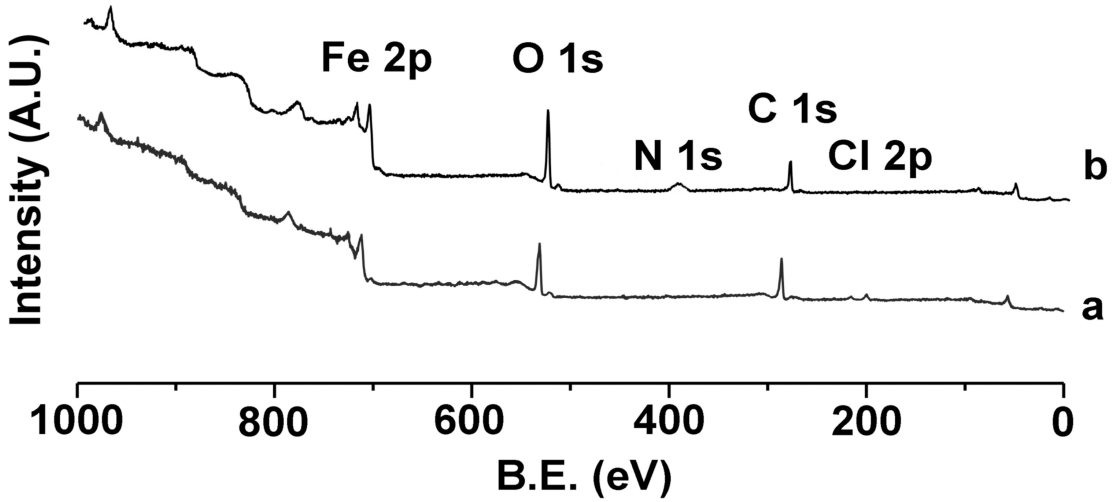

Figure 3.6 Iron, oxygen, nitrogen, carbon and chloride content at the catalyst surface, as determined by XPS. a) Freshly synthesized Fe/Fe_3O_4 nanoparticles (after air oxidation). b) Fe/Fe_3O_4 nanoparticles after ligand exchange with dopamine.

Sample	Fe	O	N	C	Cl
a) Fe/Fe_3O_4 featuring oleylamine/ hexadecylamine x HCl at the surface	3.5	29.7	2.7	60.6	3.5
b) Dopamine exchanged Fe/Fe_3O_4 nanoparticles	4.7	33.4	11.1	50.6	0.2

Table 3-1 Iron, oxygen, nitrogen, carbon and chloride content at the catalyst surface, as determined by XPS. a) Freshly synthesized Fe/Fe_3O_4 nanoparticles (after air oxidation). b) Fe/Fe_3O_4 nanoparticles after ligand exchange with dopamine.

In both nanoparticles, the inorganic surface consisted of Fe_3O_4. The observed increase in nitrogen and oxygen content, together with a decrease in carbon and chlorine content at the

surface indicates exchange of oleylamine/ hexadecylamine x HCl against dopamine. Unfortunately, XPS is only a semiquantitative analysis method.

3.4.1.1 Determination of Iron Content in the Nanoparticles

Inductively coupled plasma optical emission spectroscopy (ICP-OES) is used for the quantitative measurement of the iron content of the nanoparticles. This is an emission spectroscopic technique very specific for a given element, and the intensity of the energy emitted at the chosen wavelength is proportional to the amount (concentration) of that element in the analyzed sample.[28]

A standard series of Fe(II) ranging from 10-50 ppm was prepared from the 1000 ppm ICP standard stock solution using 20% HNO_3. Dopamine ligand modified Fe/Fe_3O_4 core/shell nanoparticle samples were subjected to ICP studies. The samples were prepared by dissolving the nanoparticle samples in conc. HNO_3 for 1 hour with constant stirring. Then the samples were filtered and diluted with distilled water. The measurements were conducted using the inductively coupled plasma optical emission spectrophotometer (Varian 720-ES) at the Department of Agronomy. The excitation wavelength was 259.94 nm. The test concentrations were determined using the standard curve.

3.4.2 Functionalization of Core/shell Fe/Fe_3O_4 Nanoparticles with Dopamine Ligands

3.4.2.1 Synthesis of Dopamine Maleimide Ligands

Dopamine maleimide ligand synthesis was carried out with modified procedures, previously published in Geiseler *et al*.[29] Initially, maleimide was activated by reacting with ethyl

chloroformate in the presence of N-methylmorpholine to obtain N-ethoxycarbonylmaleimide. This intermediate product was then reacted with dopamine hydrochloride in saturated $NaHCO_3$ solution in absence of light followed by acid treatment to obtain the final product. The final product is further purified by column chromatography and characterized by ^1H NMR.

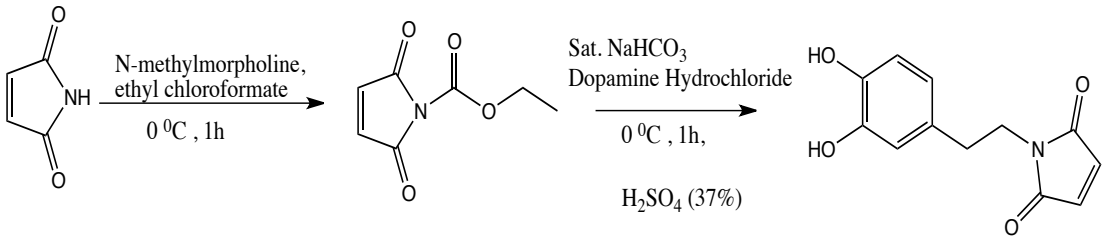

Figure 3.7 Synthesis of the dopamine maleimide ligand

3.4.2.2 Surface Modification of Nanoparticles with Dopamine Ligands

The surface of the iron/iron oxide nanoparticles was modified with both dopamine hydrochloride and dopamine maleimide ligands. The number of ligands required to form a complete monolayer on the nanoparticle surface is calculated assuming a Poisson distribution. There were mainly two assumptions taken into consideration during this calculation. We assumed that the nanoparticles are perfect spheres and the space demand of one dopamine linker is 1.094×10^{-18} m^2, as calculated from its Connolly solvent excluded volume of 1.075×10^{-28} m^3.[30] This data is available from the program package Chemdraw 3D (Cambridge Soft Corporation, 1999). The space demand was calculated by assuming a sphere for dopamine. This permitted the calculation the area of the circle with the same diameter than the sphere.

We further assumed that each ligand has the same affinity towards surface binding so that the binding of multiple ligands that form a monolayer at the surface of the nanoparticle can be described by a Poisson distribution.

Poisson distribution is used to predict the number of events occurring in a specified interval such as area and volume, with a known average rate and independently of the time since the last event.

$$f(k,\lambda) = \frac{\lambda^k e^{-\lambda}}{k!}$$

Where λ: expected number of occurrences

k: integer number of occurrences

f: probability for exactly k occurrences

As it is shown in the Figure 3.6 the number of dopamine or dopamine-based ligands is 1150 if the nanoparticle has a diameter of 20 nm. Furthermore, in order to maintain the sufficient water solubility of the Fe/Fe_3O_4 nanoparticles up to 230 maleimide-functionalized dopamines are tethered onto the surface of the nanoparticles.

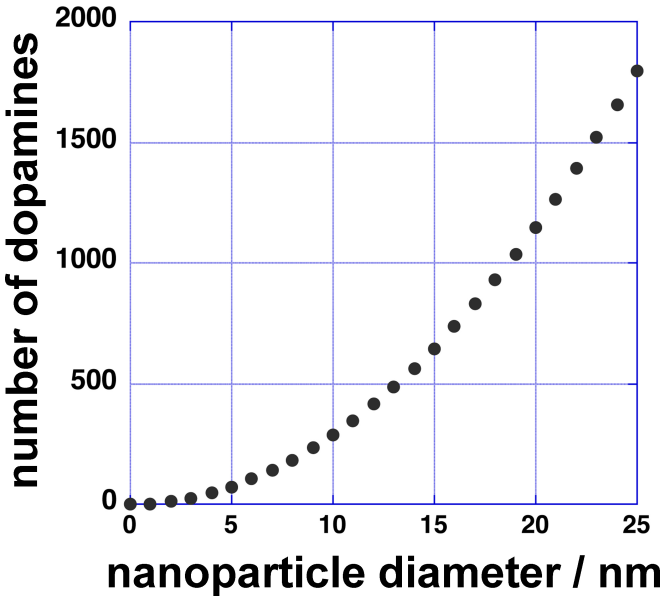

Figure 3.8 Number of dopamines per nanoparticle surface, assuming a dense packing of dopamine molecules at a spherical surface.

The coating of nanoparticles with dopamine ligands is achieved by reaction of nanoparticles and dopamine in chloroform solution. In brief, dopamine and dopamine maleimide ligands (4:1 ratio) in chloroform solution was added to Fe/Fe_3O_4 nanoparticles dispersed in chloroform. This dispersion was sonicated for 30 min and shaken on mechanical shaker for 1 hour. This step was repeated for 6-7 hours. The nanoparticles are collected by centrifugation and washed with chloroform for 3 times. Finally, the nanoparticles are dispersed in chloroform until further use. The following Figure 3.7 shows the increase of water solubility of the Fe/Fe_3O_4 nanoparticles once functionalized with dopamine/dopamine maleimide ligands compared to "bare" nanoparticles with no/minimum surface functionalized ligands.

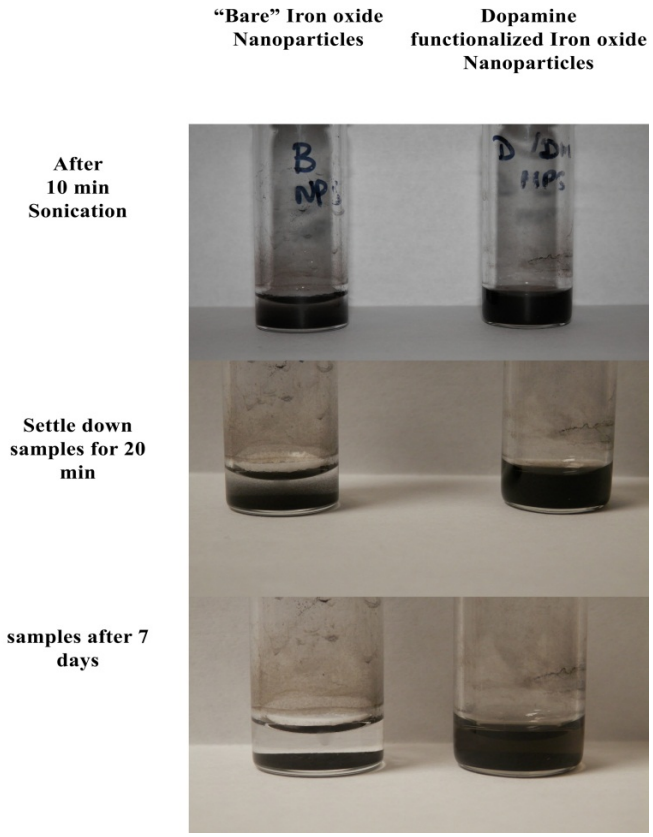

Figure 3.9 Fe/Fe_3O_4 solubility before and after with surface functionalization using dopamine and dopamine maleimide ligands

Characterization of the dopamine bound nanoparticles is carried out by IR spectroscopic methods. As shown in Figure 3.8, the IR spectra clearly indicate the surface modifications of the iron/iron oxide nanoparticles with dopamine due to the presence of characteristic peaks of the dopamine ligands, such as the broad peak at 1644cm^{-1} due to the aromatic C=C stretching, the peak at 1483cm^{-1} due to C=C bending, and the strong peak at 1263cm^{-1} due to the C-O stretching of the dopamine moiety.

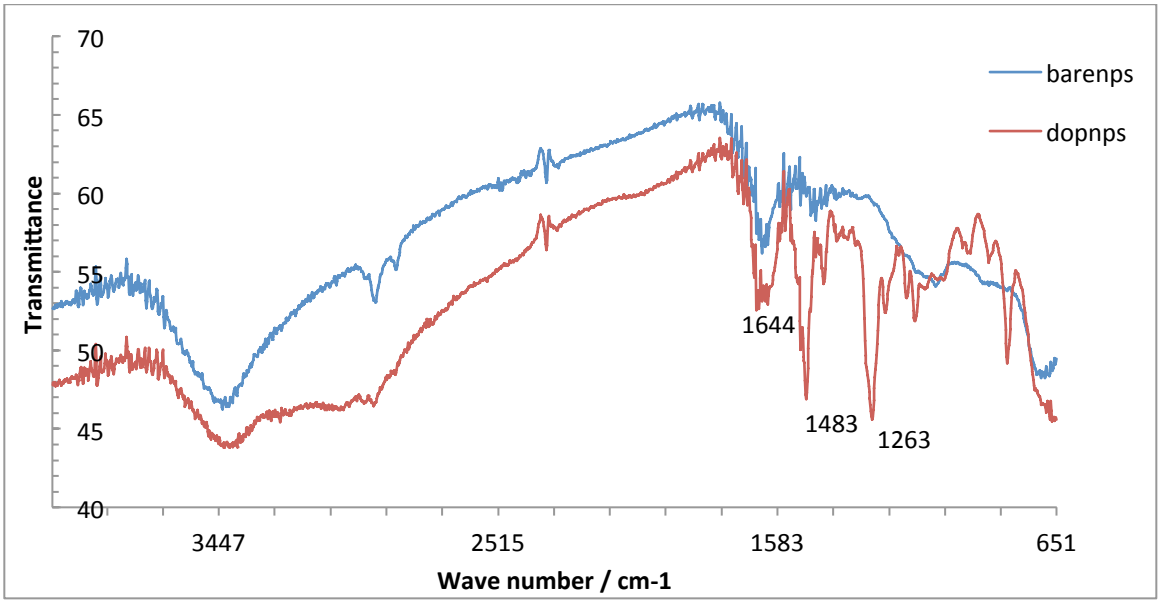

Figure 3.8 IR spectra of "bare" Fe/Fe_3O_4 nanoparticles and dopamine functionalized Fe/Fe_3O_4 nanoparticles

Iron/iron oxide nanoparticle based drug delivery systems were constructed using the dopamine-functionalized nanoparticles and coupling the targeting ligand, the CGKRK peptide and doxorubicin as model drug, onto the nanoparticles via dopamine maleimide ligands. A series of nanoparticle based drug system was constructed by simply changing the ratio between the number of molecules of CGKRK and doxorubicin following the experimental design method as explained in chapter 2. Two Doehlert matrices were constructed where one matrix studies the

homing activity at five levels and the second matrix studies the doxorubicin effect on topoisomerase inhibition at five levels. Following the design of the two matrices, 14 different nanoparticle based systems were synthesized. The corresponding Doehlert matrices are tabulated in Tables 3.1 and 3.2.

Run	Coded value X_1	Real value X_1 (No. of CGKRK molecules)	Coded value X_2	Real value X_2 (No. of Doxorubicin molecules)
1	0	80	0	80
2	1	128	0	80
3	0.5	104	0.866	120
4	-1	32	0	80
5	-0.5	56	-0.866	40
6	0.5	104	-0.866	40
7	-0.5	56	0.866	120

Table 3-2 Doehlert matrix to study the nanoparticle efficacy where it investigates CGKRK homing activity at five levels and topoisomerase II inhibitor activity at three levels

Run	Coded value X_1	Real value X_1 (No. of Doxorubicin molecules)	Coded value X_2	Real value X_2 (No. of CGKRK molecules)
8	0	80	0	80
9	1	128	0	80
10	0.5	104	0.866	120
11	-1	32	0	80
12	-0.5	56	-0.866	40
13	0.5	104	-0.866	40
14	-0.5	56	0.866	120

Table 3-3 Doehlert matrix to study the nanoparticle efficacy where it investigates topoisomerase II inhibitor activity at five levels and CGKRK homing activity at three levels

Coupling of CGKRK molecule to the free dopamine ligand was carried out prior to the binding of doxorubicin to the nanoplatform to optimize the conditions for the Michael Addition at the surface of the nanoparticle.

3.4.3 Coupling of CGKRK and Doxorubicin to Dopamine Maleimide

The thiol (-SH) group present in cysteine amino acid of CGKRK selectively reacts with the double bond of the maleimide moiety via Michael addition reaction under favorable pH conditions (pH 6.5-7.5).[31] Dopamine-maleimide and CGKRK were reacted in 1:1 mole ration in phosphate saline buffer buffer (PBS) with the pH at 7.0. The pH value of the medium controls the reaction. Consequently, alteration of the pH (to values outside the optimal range) led to poor reaction without desired coupling product. The synthetic scheme is given below in Figure 3.9. After 24 h of reaction, the mixture was lyophilized and the coupling product was characterized by mass spectrometry. This optimized condition (pH=7.0) was used to couple GCKRK to dopamine maleimide on the iron/iron oxide nanoparticles.

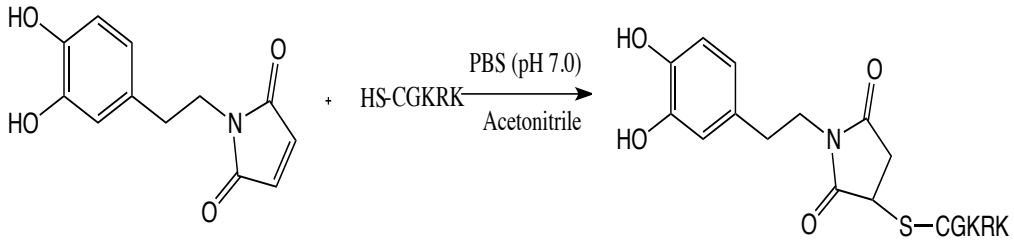

Figure 3.9 Coupling of CGKRK to dopamine maleimide

The quantitative analysis of CGKRK bound to the dopamine-maleimide ligands on the Fe/Fe_3O_4 nanoparticles was carried out by measuring the sulfur (S) content using ICP-OES measurements. The samples prepared for the analysis of iron content were also analyzed for sulfur content using a standard series of S(1000 ug/ml S in water, prepared with high purity

H_2SO_4 in water) ranging from 2-10 ppm prepared from the 1000 ppm ICP standard stock solution using 20% HNO_3. The excitation wavelength was 181.97 nm. The test concentrations were then determined using the standard curve. The amount of S present in each sample is directly relates to the number of CGKRK molecules attached on to the nanoparticles via thiol maleimide double bond formation.

Primary amines also undergo Michael addition reactions with maleimide double bonds. When both thiol and primary amine groups are present, the primary amines add to maleimide in competition to thiol groups. This reaction also favors slightly basic conditions, where the pH is higher than pH > 7.0.[31]Therefore, the coupling of hydrophobic doxorubicin to the maleimide double bond was also carried out in similar manner in PBS buffer with dopamine-maleimide present on the iron/iron oxide nanoparticles. Doxorubicin is commercially available as hydrochloride salt to increase its clinical applications. Therefore, hydrophobic doxorubicin with free primary amine is obtained via reaction with triethyl amine. Briefly, two molar equivalents of triethyl amine were added to doxorubicin hydrochloride, dissolved in DMF, and the mixture was stirred overnight. Hydrophobic doxorubicin was extracted using methylene chloride. Dry solid hydrophobic doxorubicin was obtained by evaporating the methylene chloride. The Michael addition reaction between the dopamine-maleimide and the hydrophobic doxorubicin was also carried out in phosphate saline buffer medium for 24 hours.

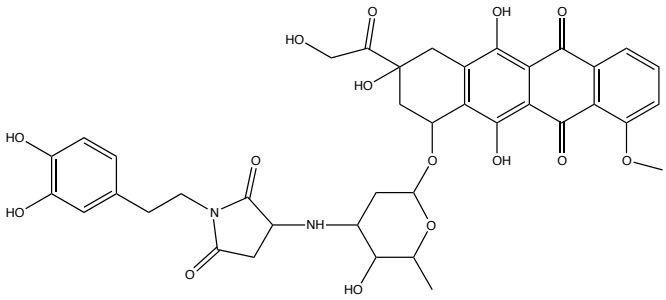

Figure 3.10 Structure of Doxorubicin coupled dopamine maleimide

After the reaction nanoparticles were thoroughly washed with 1x PBS solution for four times, these washings were analyzed using UV-Vis spectrophotometry to check the presence of unbound doxorubicin in the washing solutions. As Figure 3.11 shown below, washing solutions did not show the presence of free doxorubicin, as indicated by its missing absorption peak at 480 nm. Hence, it can be concluded that doxorubicin is coupled to the maleimide moieties on the nanoparticles via Michael addition reactions.

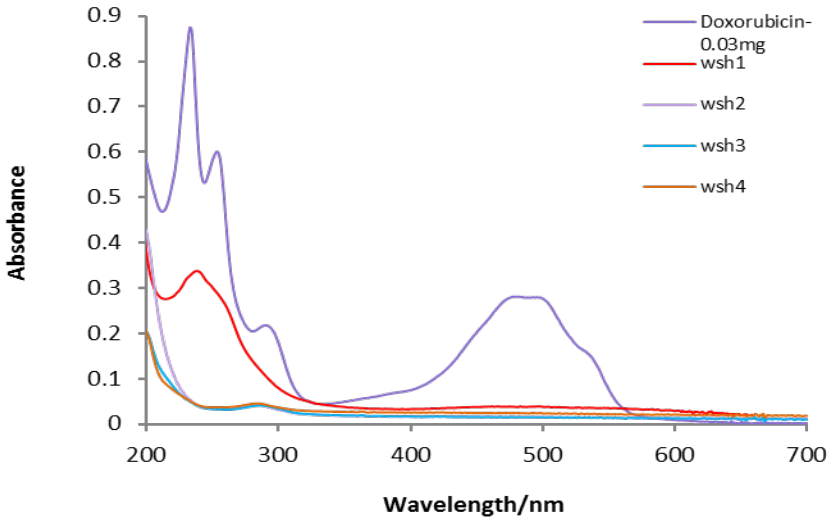

Figure 3.11 UV-Vis absorbance spectra of washing solutions of doxorubicin coupled iron/iron oxide nanoparticles

The doxorubicin-attached iron/iron oxide nanoparticle system was also characterized by fluorescence measurements in order to verify the presence of doxorubicin on the nanoparticle. The data is shown in Figure 3.12. Doxorubicin fluorescence emission occurs at 560-590 nm. Doxorubicin bound nanoparticles showed two emission peaks in the range of 550-600 nm, indicating the presence of doxorubicin on the nanoparticle system.

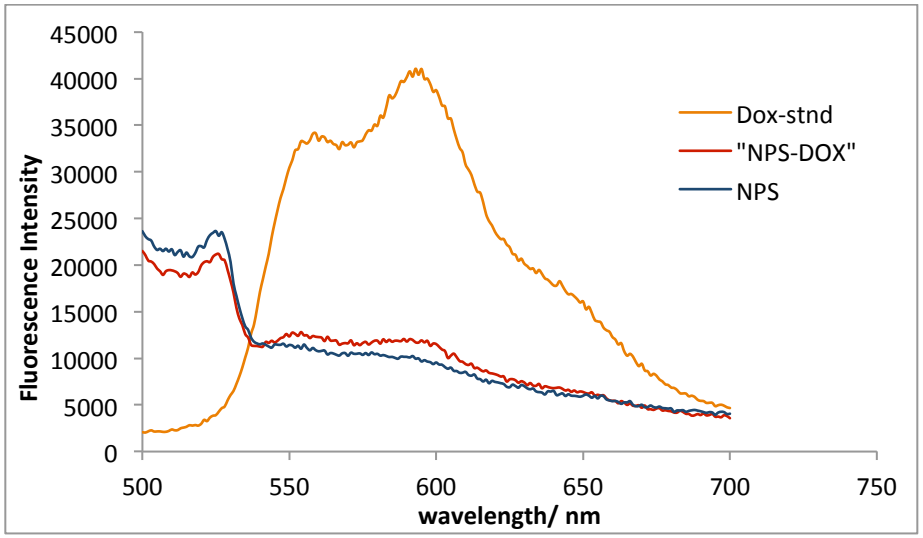

Figure 3.10 Fluorescence emission spectra for free doxorubicin and nanoparticle bound doxorubicin in the drug delivery system

The presence of doxorubicin on the iron/iron oxide nanoparticles was further studied by HPLC analysis. The standard doxorubicin hydrochloride has a retention time of 5.6 min when using a standard reverse phase C18 column and a acetonitrile:water (30:80 v/v) mixture as eluent Doxorubicin coupled iron/iron oxide nanoparticles (sample number 17 – 200 doxorubicin molecules per nanoparticle) were treated with 10% HCl solution and mechanically shaken for 10 min. Once all the iron/ron oxide nanoparticles dissolved in the solution and the solution became clear, free doxorubicin was extracted into methylene chloride solution. This procedure used 1.00 mL of CH_2Cl_2 and 1.00 mL of aqueous HCl-containing solution. It was intensely stirred for 20

min. at ambient temperature, prior to separating the organic phase by using a syringe. Methylene chloride layer was filtered using 0.25 µm poltcarbonate filters. This solution was directly used for the HPLC-analysis. The two chromatograms were shown below (Figure 3.11).

HPLC data provide evidence for the presence of doxorubicin bound to the nanoparticles and the release of the doxorubicin from the nanoparticles at lower pH values (10% HCl in the medium). However, this method is not suitable to distinguish between chemisorbed and physisorbed doxorubicin, because the Michael addition reaction coupling doxorubicin to maleimide is revesible at strongly acidic pH.

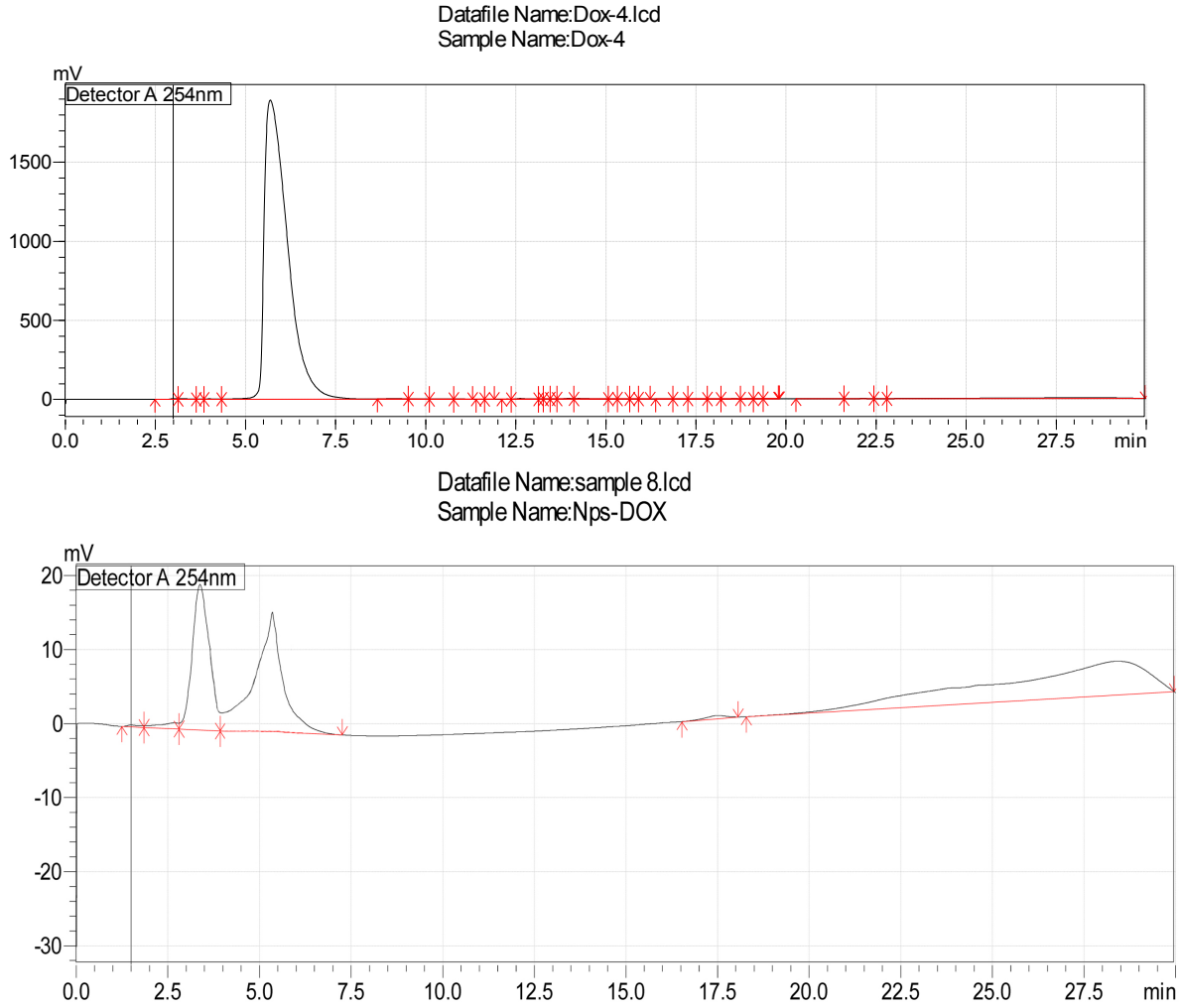

Figure3.11 HPLC chromatogram for standard doxorubicin hydrochloride and doxorubicin released from the iron/iron oxide nanoparticles treated with 10% HCl

3.4.4 Particle Size Evaluation of the Fe/Fe_3O_4 Nanoparticles Based Drug Delivery System

Dynamic Light scattering (DLS) experiments were carried out to evaluate the effective diameters of the iron/iron oxide nanoparticles based drug delivery system, as the size of the nanoparticles play an important role in blood circulation and passive uptake mechanisms by tumor vasculature. As shown in Figure 3.13, dopamine functionalized Fe/Fe_3O_4 nanoparticles featured an average diameter of 440 nm – 485 nm in deionized water (50 μl of nanoparticle solution (1.0 mg ml^{-1}) diluted in 3 ml of deionized water).

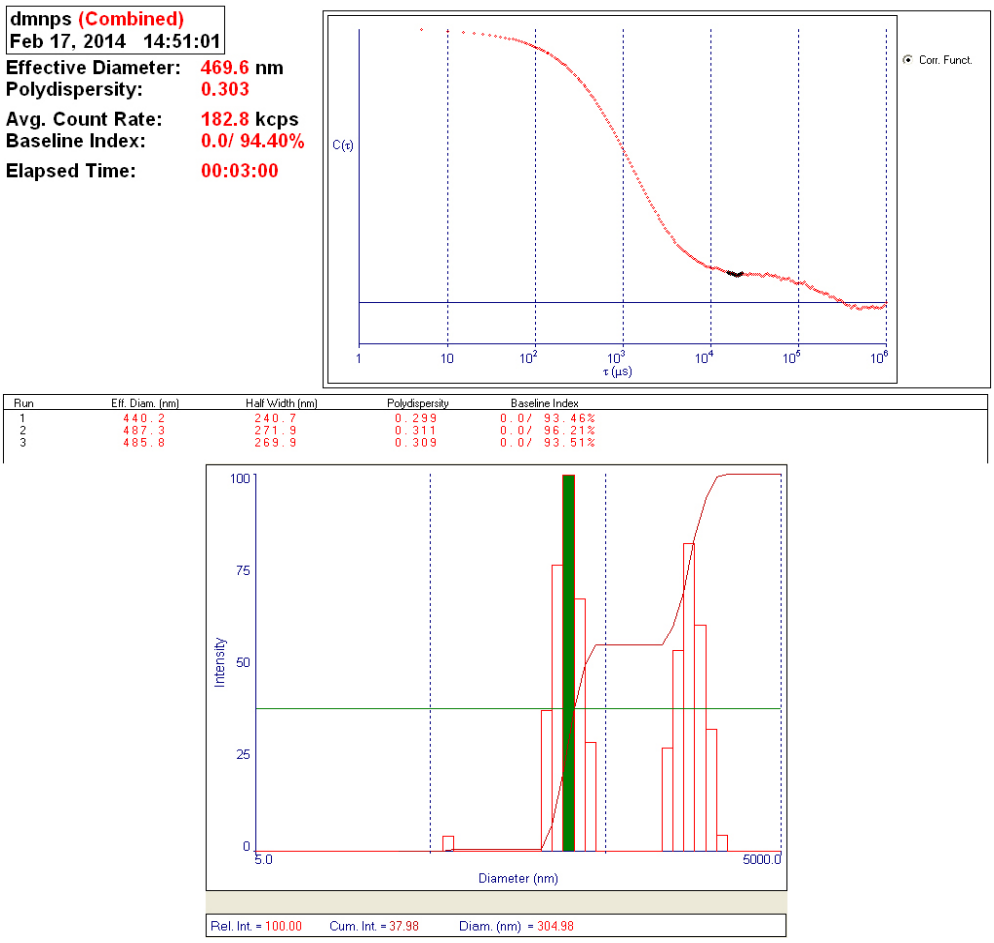

Figure 3.12 DLS data for dopamine functionalized Fe/Fe_3O_4 nanoparticles

The polydispersity value ranged from 0.29% - 0.31%, which indicates a low polydispersity of the iron/ iron oxide nanoparticles in deionized water medium. Similarly, when homing peptide and doxorubicin were coupled to iron / iron oxide nanoparticles, they were also of low polydispersity in deionized water, ranging from 0.28% to 0.35%, even though they tend to aggregate in the aqueous medium. The effective diameters of the drug-loaded nanoparticles were about 450 nm to 500 nm. The DLS results are shown in Figure 3.14.

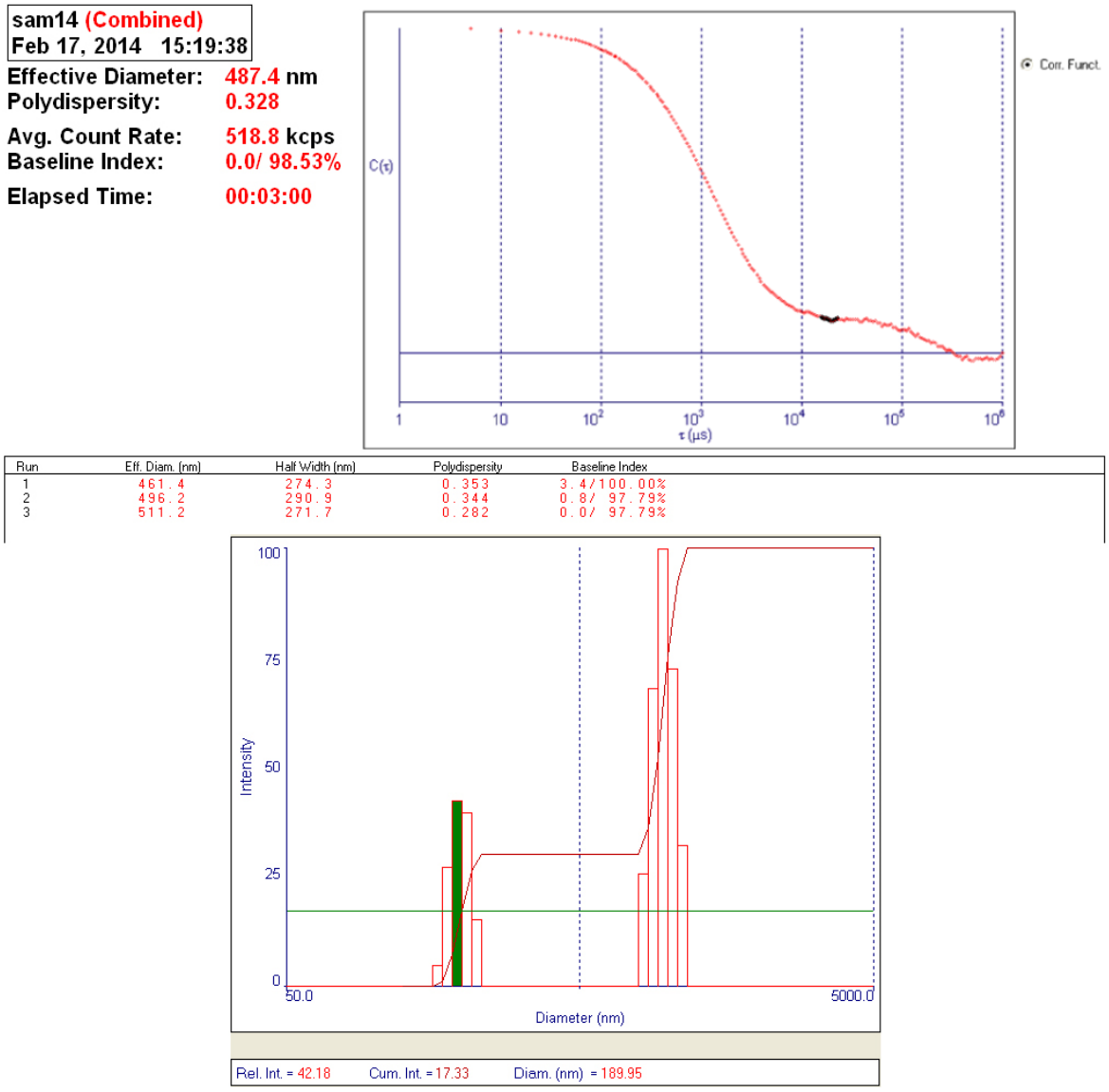

Figure 3.13 DLS data for drug-loaded dopamine functionalized Fe/Fe_3O_4 nanoparticles

3.5 Conclusions

Synthesis of iron / iron oxide nanoparticles, which resemble a core/shell Fe/Fe_3O_4 structure, was successfully carried out using a thermal decomposition method of iron pentacarbonyl. The obtained nanoparticles have a low polydispersity. Their effective diameter is about 20 ± 2 nm. Furthermore, the surfaces of the Fe/Fe_3O_4 nanoparticles were functionalized with dopamine and dopamine-maleimide ligands to enhance their water solubility. Then, the coupling of theranostic components, which are homing sequences and chemotherapeutic drugs (CGKRK and doxorubicin, respectively) was achieved. The double bond of the maleimide moiety was used for the coupling of both, CGKRK and doxorubicin, to the iron / iron oxide nanoparticles to develop the drug delivery system in accordance with the proposed model based on the Ringsdorf model. Thus, a series of iron / iron oxide based nanoparticle systems were constructed with different ratios between the homing peptide and topoisomerase inhibitor doxorubicin. The therapeutic efficacy of the system was evaluated using pancreatic cancer cell lines Pan02 cells.

3.6 Experimental

All the chemicals and solutions used in the synthetic procedures were purchased form Sigma-Aldrich, Fisher Scientific or Agros International, unless otherwise noted. Characterization techniques were carried out using instrumentation available in Kansas State University; Varian 720-ES ICP-OES spectrophotometer in Department of Agronomy; Shimadzu Prominence LC-6AD-20A HPLC machine w/ UV/Vis at Department of Grain Science and Industry; 400MHz Varian NMR spectrophotometer, Cary 630 FTIR (DR/ATR) spectrophotometer in Department of Chemistry; API 2000 LC/MS/MS spectrophotometer (Dr. Duy Hua's lab), Fluoromax2

spectrophotometer (Dr. Daniel Higgins lab) and ZetaPALS zeta potential analyzer are also used for the characterization processes.

3.6.1 Synthesis of the CGKRK Peptide

CGKRK was synthesized using standard solid phase peptide synthesis methods. BrieflyH-Lys(Boc)-Trityl resin was swirled in methylene chloride for 10 min and washed with dimethyl formamide. Then, Fmoc protected arginine(R) was added with O-Benzotriazole-N,N,N',N'-tetramethyl-uronium-hexafluoro-phosphate(HBTU) as coupling agent in a mixture of diisopropylethylamine (DIEA) and dimethyl formamide (DMF). Fmoc protection of the arginine was removed by reaction with 20% piperidine and Fmoc protected lysine(L) was added with a mixture of HBTU, DIEA in DMF. These two steps were repeated until the sequence is completed. Finally, Fmoc protection of the cysteine was also removed and the CGKRK sequence was cleaved from the resin using TFA/TIPS/H_2O (90/5/5) solution. The peptide was precipitated and washed with cold diethyl ether solution and dried under argon and obtained white precipitate as the product. MS-API: *m/z* 591.5. Molecular weight calculated for 591

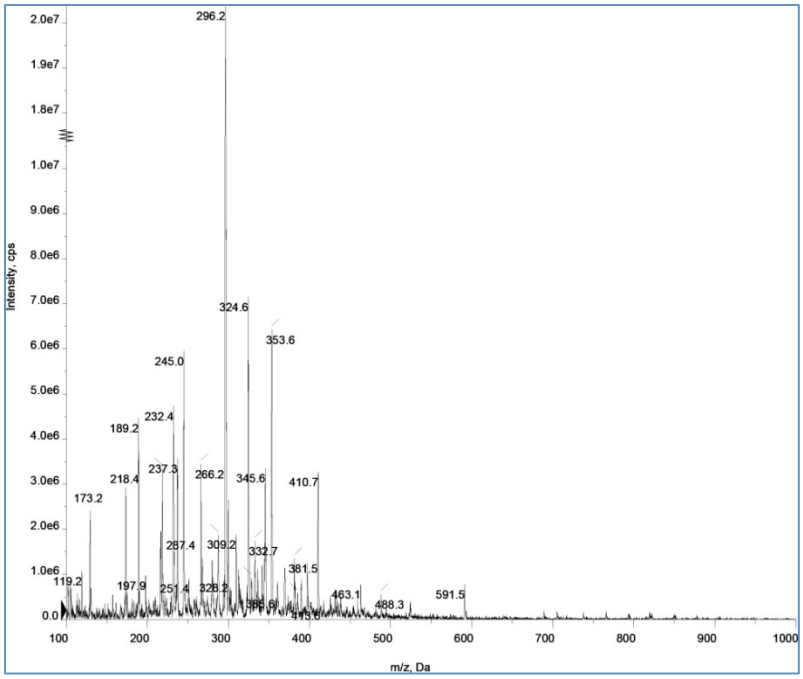

Figure 3.14 MS –API spectrum of CGKRK peptide sequence

3.6.2 Synthesis of Fe/Fe_3O_4 Nanoparticles

Iron nanoparticles were prepared by means of a slight modification of a literature procedure described by Lacroix et al.[23] The apparatus for the synthesis of nanoparticles consisted of a 250 mL, three-necked, round-bottom flask utilizing a cold water jacket condenser on the middle neck, one septum and one temperature probe on each of the outer necks were attached and a spin vane. Then 60 mL 1-octadecene (ODE), 0.9 mL oleylamine and 0.831 g hexadecylammonium chloride (HADxHCl) were added into the flask. The reaction system was connected to a Schlenk line through the top of the jacket condenser. The reaction mixture was degassed at 120^0C for 30 min under vigorous stirring. After being refilled with argon, the reaction mixture was heated to 180^0C. Three portions of 0.7 mL $Fe(CO)_5$ were injected into the reaction mixture via syringe, every 20 min. The reaction mixture was kept at 180^0C for another 20 min after the last injection, and then cooled to room temperature naturally. The supernatant

was decanted, and the iron nanoparticles accumulated on the magnetic stir bar were washed with hexane and ethanol. The product was dried in vacuum and stored in chloroform at 4^0C under argon for further use.

3.6.2.1 Iron/Iron Oxide Nanoparticle Characterization Using Transmission Electron Microscopy (TEM)

Sample preparation and data collection are similarly described in the literature.[32] Briefly, samples were prepared by suspending the catalyst in ethanol and agitating in an ultrasonic bath for 15 minutes. 10 μL of catalyst sample was placed onto copper mesh grid with lacey carbon film. The wet grids were allowed to air-dry for several minutes prior to being examined under TEM. The catalyst particle size and morphology were examined by bright-field and dark-field transmission electron microscopy (TEM) using an FEI Technai G_2 transmission electron microscope at an electron acceleration voltage of 200 kV. High resolution images were captured using a standardized, normative electron dose and a constant defocus value from the carbon-coated surfaces.

3.6.3 Determination of Iron Content in Fe/Fe_3O_4 Nanoparticles

A standard curve for the Fe^{2+} used for the iron quantification using ICP-OES was constructed in the range of 10 – 50 ppm solution. The iron content of Fe/Fe_3O_4 nanoparticles was found to be 700mg/L.

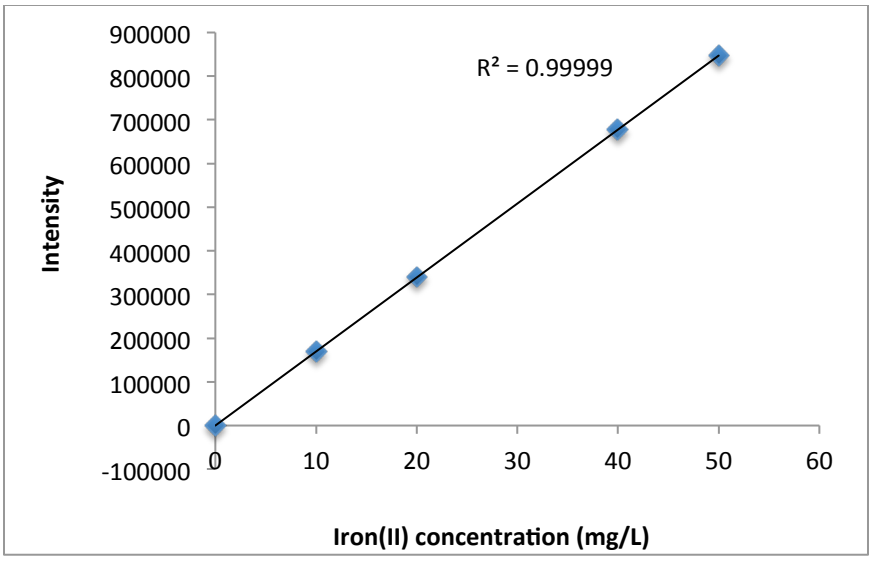

Figure 3.15 Standard calibration for Fe(II) concentration in ICP-OES measurements

3.6.4 Synthesis of Dopamine Maleimide Ligands

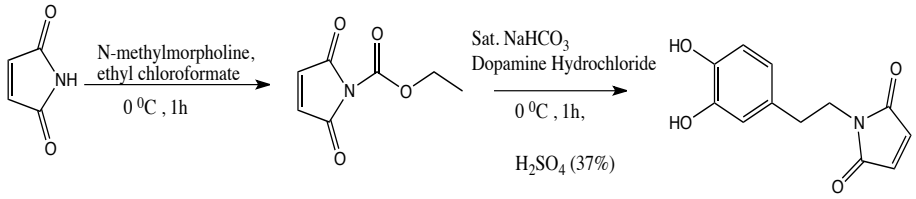

Synthesis of dopamine maleimide was obtained by a modified procedure of an earlier published report by Geiseler *et al*.[29] Initially, maleimide (1.0g, 1.0 eq) was dissolved in ethyl acetate (40 ml) in a round bottom flask and the mixture was cooled to 0 ^{o}C. N-methyl morpholine (1.0 ml, 1.1 eq), dissolved in 5 ml of ethyl acetate, was added drop-wise to the mixture during 10min. Then, a solution of ethyl chloroformate (0.932 ml, 1.0eq), dissolved in 2.5 ml of ethyl acetate, was added drop-wise while keeping the temperature at 0 ^{o}C. The mixture was warmed to room temperature and stirred for 1 hr. A solid was filtered followed by three washings with ethyl acetate. Combined ethyl acetate solutions were washed respectively with sat. sodium bicarbonate solution (25 ml x 3), water (20 ml x 2) and brine solution (20 ml). Ethyl acetate layer was dried upon anhydrous magnesium sulfate and filtered. Finally, the solvent was

evaporated under reduced pressure. The purple product was obtained in 90% yield. ^{1}H NMR ($CDCl_3$) δ: 6.65 (s, 2H); 4.33 (q, 2H); 1.33(t, 3H).

Dopamine maleimide are obtained as followed. In a 125 ml round bottom flask, Dopamine hydrochloride (200 mg, 1.0eq) was dissolved in 8 ml of sat. sodium bicarbonate solution at 0^0C in the absence of light. Then N-ethoxycarbonylmaleimide (219 mg, 1.0 eq) was added to the mixture and stirred for another 10min at 0 ^{0}C, and then brought to room temperature. Water (35 ml) was added and further stirred for 40 min, followed by adjusting of pH to 1.5 with 30% H_2SO_4. This solution was extracted with ethyl acetate (25 ml x 4), dried with anhydrous magnesium sulfate, filtered, and evaporated under vacuum to obtain the crude product. The product was purified by means of silica column chromatography with methylene chloride: methanol 10:1 as mobile phase to obtain a pure yellow solid with 65% yield. ^{1}H NMR (DMSO-*d*6) δ: 8.72(s, 1H); 8.61(s, 1H); 6.92(s, 2H); 6.55(d, 1H); 6.49(s, 1H); 6.49(d, 1H); 3.47(t, 2H); 2.56(t, 2H).

3.6.5 Coupling of CGKRK and Doxorubicin to Dopamine Maleimide

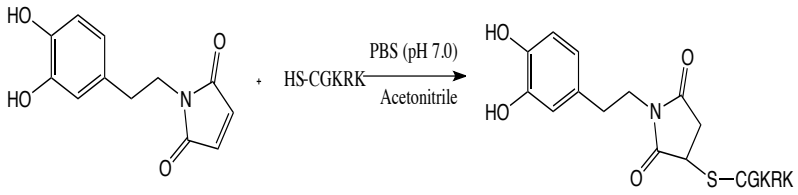

Dopamine maleimide (10 mg, 1.0eq) was dissolved in 2 ml of 1X phosphate saline buffer (PBS) with the aid of 1 ml of acetonitrile under argon environment. Then, CGKRK (25mg, 1.0eq), dissolved in 1 ml of 1X PBS, was added to the mixture and stirred for 24hrs at pH= 7.2

under argon. After 24hr the mixture was lyophilized to obtain a pale yellow solid. MS-API: *m/z* 824.6. Calculated molecular weight is 824.

Doxorubicin hydrochloride (100 mg, 1 eq) and triethyl amine (35 ul, 2.0eq) were mixed in dry dimethyl formamide (5 ml) under constant stirring for 12 hrs. Then 5 ml of distilled water was added to the medium, mixed properly, and hydrophobic doxorubicin was extracted with methylene chloride (3 x 25 ml). The methylene chloride layer was dried with anhydrous $MgSO_4$ and concentrated in vacuum to yield a dark red solid with a yield of 80%. The obtained hydrophobic doxorubicin was also coupled to dopamine maleimide following the same procedure as mentioned above for CGKRK. MS-API: *m/z* fragments observed at 412.9; 251.4; 379.1, molecular weight calculated for is 776.7.

3.6.6 Coupling of CGKRK and Doxorubicin to Dopamine Maleimide on Iron/Iron Oxide Nanoparticles

Sample number 1:

Initially dopamine and dopamine maleimide coated Fe/Fe_3O_4 nanoparticles 25 mg was dispersed in 1 ml solution of 1x PBS buffer was sonicated for 15 min. Then 110 µl of CGKRK solution (1 mg in 1 ml of 1x PBS) was added to the nanoparticle mixture. Further sonicated for 5 min. After that vial containing the mixture was mechanically stirred for 24 h. on a mechanical shaker. Then Fe/Fe_3O_4 nanoparticles were collected by centrifugation at 10000 rpm for 5 min. Nanoparticles were washed with 1x PBS solution for three times. Collected nanoparticles were dispersed again in 1 ml of 1x PBS solution and sonicated for 10 min. Then 109 µl of doxorubicin solution (1 mg in 1 ml of 1x PBS) was added to the nanoparticle solution and stirred for 24 h. on a mechanical shaker. Nanoparticles were washed with 1x PBS solution for three times and dried

under Argon. Finally recovered Fe/Fe_3O_4 sample (20 mg) was stored at 4 ^{0}C until further use. Similar procedure was carried out to synthesize all the other samples as well.

3.6.7 Determination of Loaded CGKRK Content on to The Iron/Iron Oxide Nanoparticles

A standard curve for the Fe^{2+} used for the iron quantification using ICP-OES was constructed in the range of 2-10 ppm solution. The average amount of CGKRK present on each nanoparticle sample is about 400ng/mg.

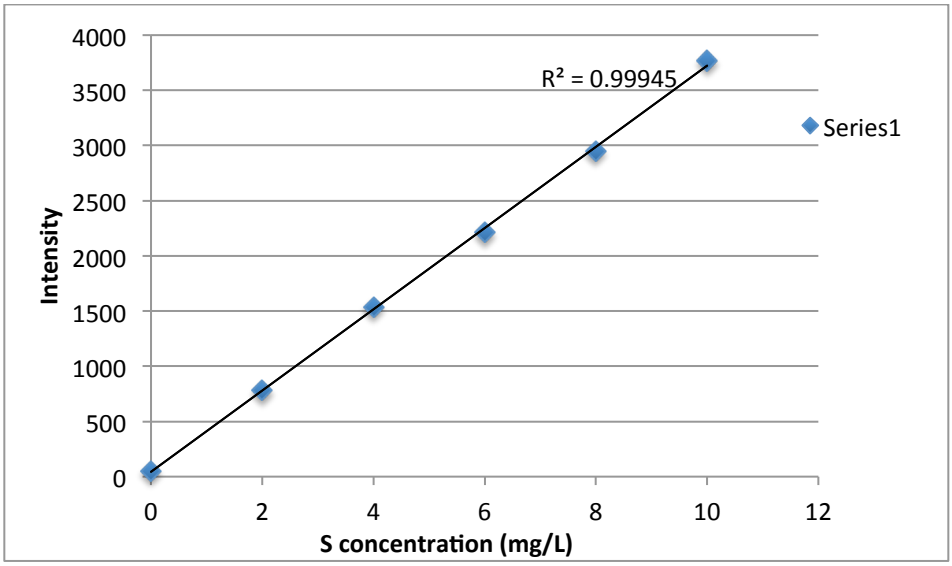

References

1. Auffan, M.; Rose, J.; Bottero, J.Y.; Lowry, G.V.; Jolivet, J.P.; Wiesner, M.R., Towards a Definition of Inorganic Nanoparticles from an Environmental, Health and Safety Perspective. *Nat Nanotechnol* **2009**, 4(10), 634–641
2. http://www.sciencedaily.com/articles/n/nanoparticle.htm
3. Rudge, S.; Peterson, C.; Vessely, C.; Koda, J.; Stevens, S.; Catterall, L., Adsorption and Desorption of Chemotherapeutic Drugs from a Magnetically Targeted Carrier (MTC). *J Control Release.* **2001**,74, 335–40
4. Pankhurst, Q.A.; Connolly, J.; Jones, S.K.; Dobson, J.; Applications of Magnetic Nanoparticles in Biomedicine. *J Phys D Appl Phys.* **2003**, 36, 167-181
5. http://www.cdc.gov/nutrition/everyone/basics/vitamins/iron.html
6. Babes, L.; Denizot, B.; Tanguy, G.; Le Jeune, J.J.; Jallet, P., Synthesis of Iron Oxide Nanoparticles used as MRI Contrast Agents: A Parametric Study. *J Colloid Interface Sci.* **1999**, 212, 474–82
7. Yigit, M.V.; Mazumdar, D.; Lu, Y., MRI Detection of Thrombin with Aptamer Functionalized Superparamagnetic Iron Oxide Nanoparticles. *Bioconjug Chem*. **2008**, 19, 412–417
8. Peng, X.H.; Qian, X.; Mao, H.; Wang, A.Y.; Chen, Z.G.; Nie, S., Targeted Magnetic Iron Oxide Nanoparticles for Tumor Imaging and Therapy. *Int J Nanomed.* **2008**, 3, 311–312
9. Marcu, A.; Pop, S.; Dumitrache, F.; Mocanu, M.; Niculite, C.M.; Gherghiceanu, M.; Lungu, C.P.; Fleaca, C.; Ianchis, R.; Barbut, A.; Grigoriu, C.; Morjan, I., *Appl. Surf. Sci.* **2013**, 281, 60–65
10. http://www.nelsonsnaturalworld.com/en-us/uk/our-brands/spatone/iron-essentials/role-of-iron-in-the-body/
11. Gupta, A.K.; Wells, S., Surface-Modified Superparamagnetic Nanoparticles for Drug Delivery: Preparation, Characterization, and Cytotoxicity Studies. *IEEE Trans Nanobioscience* **2004**, 3(1), 66-73

12. Nie, S. M., Understanding and Overcoming Major Barriers in Cancer Nanomedicine. *Nanomedicine* **2010**, 5, 523–528

13. Grossman J. H.; McNeil S. E., Nanotechnology in Cancer Medicine. *Phys. Today* **2012**, 65, 38–42

14. Dong, X.; Mumper, R.J., Nanomedicinal Strategies to Treat Multidrug-resistant Tumors: Current Progress. *Nanomedicine* **2010**, 5(4), 597-615

15. Allen, T.M., Ligand-Targeted Therapeutics in Anticancer Therapy. *Nature Reviews Cancer* **2002**, 2, 750-763

16. Zhang, X.X.; Eden, H.S; Chen, X., Peptides in Cancer Nanomedicine: Drug Carriers, Targeting Ligands and Protease Substrates. *J. Control Release* **2012**, 159, 2-13

17. Hoffman, J. A.; Giraudo, E.; Singh, M.; Zhang, L.; Inoue, M.; Porkka, K.; Hanahan, D.; Ruoslahti, E., Progressive Vascular Changes in a Transgenic Mouse Model of Squamous Cell Carcinoma. *Cancer Cell* **2003**, 4, 383–391

18. Amblard, M.; Fehrentz, J.A.; Martinez, J.; Subra, G., Methods and Protocols of Modern Solid Phase Peptide Synthesis. *Mol. Biotechnol.* **2006**, 33, 239–254

19. http://www.sigmaaldrich.com/content/dam/sigma-aldrich/life-science/pepscreen-brochure/solid-phase-peptide-synthesis.jpg

20. Huber, D. L.; Synthesis, Properties, and Applications of Iron Nanoparticles. *Small* **2005**, 1, 482-501

21. Rajh, T.; Chen, L. X.; Lukas, K.; Liu, T.; Thurnauer, M. C.; Tiede, D. M., Surface Restructuring of Nanoparticles: An Efficient Route for Ligand-Metal Oxide Crosstalk. *J. Phys. Chem. B* **2002**, *106*, 10543

22. Xu, C.; Xu, K.; Gu, H.; Zheng,R.; Liu,H.; Zhang, X.; Guo, Z.; Xu, B. Dopamine as A Robust Anchor to Immobilize Functional Molecules on the Iron Oxide Shell of Magnetic Nanoparticles. *J. Am. Chem. Soc.*, **2004**, *126* (32), 9938–9939

23. Lacroix, L.M.; Frey, H. N.; Ho, D.; Sun, X.; Cheng, K.; Sun, S., Stable Single-Crystalline Body Centered Cubic Fe Nanoparticles. *Nano Lett.* 2011, 11, 1641–1645

24. Perera, A. S.; Wang. H.-W.; Yapa, A. S.; Bossmann, S. H., Final Report to Battelle

Memorial Institute, Columbus/OH "Upscaling of core/shell magnetic nanoparticles for catalytical applications", **2013**

25. Wang, H.; Shrestha, T. B.; Basel, M. T.; Dani, R. K.; Seo, G.-M.; Balivada, S.; Pyle, M. M.; Prock, H.; Koper, O. B.; Thapa, P. S.; Moore, D.; Li, P.; Chikan, V.; Troyer, D. L.; Bossmann, S. H. Magnetic-Fe/Fe3O4-nanoparticle-bound SN38 as carboxylesterase-cleavable prodrug for the delivery to tumors within monocytes/macrophages *Beilstein J. Nanotechnol.* **2012**, *3*, 444
26. Ikenberry, M.; Pena, L.; Wei, D.; Wang, H.; Bossmann, S. H.; Wilke, T.; Wang, D.; Komreddy, V. R.; Rillema, D. P.; Hohn, K. L. Acid monolayer functionalized iron oxide nanoparticles as catalysts for carbohydrate hydrolysis *Green Chem.* **2014**, *16*, 836
27. Wilson, D.; Langell, M. A. XPS analysis of oleylamine/oleic acid capped Fe_3O_4 nanoparticles as a function of temperature *Appl. Surf. Sci.* **2014**, *303*, 6
28. http://www.ime.fraunhofer.de/content/dam/ime/en/documents/AE/SOP_ICP-OES_en.pdf
29. Geiseler, B.; Fruk, L., Bifunctional Catechol Based Linkers for Modification of TiO_2 Surfaces. *J. Mater. Chem.* **2012**, 22, 735-741
30. Connolly, M. L., The molecular surface package *J Mol Graphicsi,* **1993**, 11, 139–141
31. Mather, B. D.; Viswanathan, K.; Miller, K.M.; Long T.M., Michael Addition Reactions in Macromolecular Design for Emerging Technologies. *Prog. Polym. Sci.* **2006**, 31, 487–531
32. Wang, H.; Udukala, D. N.; Samarakoon, T. N.; Basel, M. T.; Kalita, M.; Abayaweera, G.; Manawadu, H.; Malalasekera, A.; Robinson, C.; Villanueva, D.; Maynez, P.; Bossmann, L.; Riedy, E.; Barriga, J.; Wang, N.; Li, P.; Higgins, D. A.; Zhu, G.; Troyer, D. L.; Bossmann, S. H. Nanoplatforms for highly sensitive fluorescence detection of cancer-related proteases *Photochem. Photobiol. Sci.* **2014**, *13*, 231

Chapter 4 - *In-Vitro* Evaluation of the Nanoparticle-Based Nanoplatforms for Treating Pancreatic Cancer

4.1 Introduction

Iron/iron oxide nanoparticle based drug delivery systems, constructed according to the Ringsdorf model, were tested on murine pancreatic cancer cell lines (Pan02) and on noncancerous mouse fibroblast cells (STO), to determine the therapeutic activity of the system *in-vitro.* Preliminary studies of the cellular uptake and cytotoxic effects of the different nanoparticle based nanoplatforms in dependence on the ratio between CGKRK and doxorubicin were evaluated using cell-based assays. As mentioned previously, CGKRK enhances the cellular uptake of the nanoparticle-based systems by binding to the phospholipid heparin sulfate receptor. Once the cells take up the nanoparticles, they will selectively accumulated in the lysosomal/early endosomal compartments[1], which ultimately causes release of the topoisomerase II inhibitor doxorubicin. Once released, doxorubicin is transported to the nucleus.

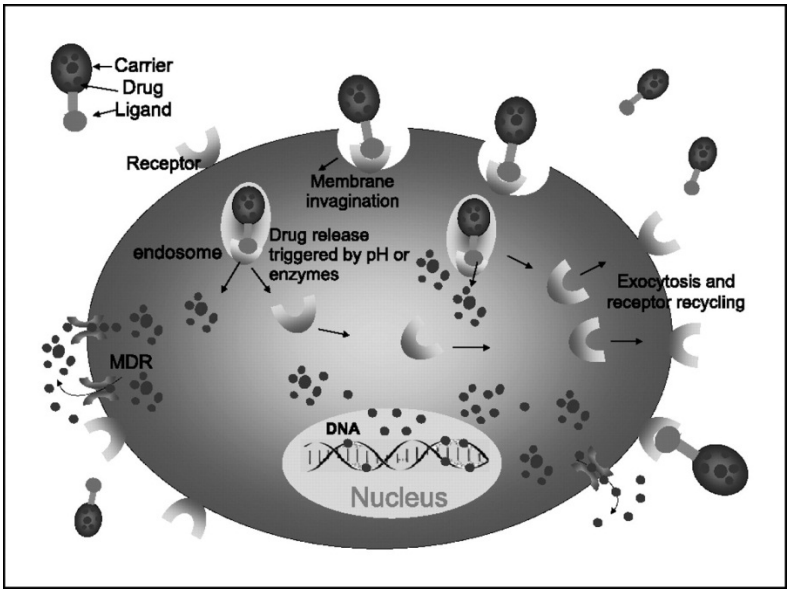

Figure 4.1 Cellular uptake mechanism and fate of the nanoparticle based drug delivery system[1]

As shown in Figure 4.1, the targeting ligand CGKRK selectively binds to the receptors present on the cell membrane and enhances the cellular uptake of the iron oxide based nanoplatform into the pancreatic cancer cells by means of endocytosis. Once the late endosome is formed by fusion of the early endosome and the lysosome, the environment inside the lysosomal/endosome compartments becomes acidic (pH < 5). This acidic environment is responsible for the release of the active drug doxorubicin from the nanoparticles. Doxorubicin escapes from the lysosomal membranes and selectively migrates to the nucleus, where it is accumulated. While doxorubicin is inside the nucleus, it inhibits DNA replication by intercalating into double stranded DNA, which renders topoisomerase II inactive. This induces apoptosis of the cells. Furthermore, a fraction of the iron oxide nanoparticle based drug escapes the endosome and will be transported to the mitochondria due to the CGKRK activity, which is known to facilitate transport to this location.

4.2 Experiments and Results

I have carried out the cell-based assays in Dr. Deryl Troyer's lab in the Department of Anatomy and Physiology, College of Veterinary Medicine, Kansas State University.

4.2.1 Analysis of Cellular Uptake of the Fe/Fe_3O_4 Nanoparticle Based Drug Delivery System

The cellular uptake levels of the nanoscopic drug delivery system were analyzed by employing the Prussian Blue staining method. It is a well-known staining procedure used for the qualitative determination of the presence of ferric ions in the cells.[2] The Prussian blue reaction involves the treatment of cells with ferrocyanide along with hydrochloride acid. Any ferric ion

(III) present in the cells reacts with the ferrocyanide and results in the formation of a bright blue pigment called Prussian blue, or ferric ferrocyanide.[3]

The iron content of the Fe/Fe_3O_4 nanoparticles was determined to be 700 mg/L by means of ICP-AES measurements. Therefore, the concentrations of the drug systems were varied depending on the total iron concentrations on the solutions. For the cellular uptake mechanisms, low iron concentrations of 5 μg/ml and 10 μg/ml were used. Four different drug formulations with different CGKRK to doxorubicin were used for the cellular uptake studies using Pan02 cells. The loading efficiencies of the nanoparticle-based systems were evaluated using Perl's Prussian Blue stain kit (Polysciences, Inc., Warrington, PA). Pan02 cells plated on 24 well cell plates were incubated over night at 37^0C in humidified containing 5% CO_2 with nanoparticles solutions in RPMI 1640 with 10% fetal bovine serum (FBS) 1% Penicillin-Streptomycin (Penstrap) and 10% 70 kDa dextran. Then, cells were fixed with 10% Neutral Buffered Formalin and incubated for 15min. Wells were washed thoroughly with 1 X PBS buffer and stained with an aqueous solution of 4% potassium ferrocyanide and 4% hydrochloric acid for 10min. again excess staining solutions were washed away with distilled water. Counter staining of the cells were carried out using nuclear fast red for 2-5 min. Finally excess counter stain solutions were also washed away with 1xPBS solutions. Cells were examined under light microscope with 40X magnification. Pan02 cells before and after staining are shown in Figure 4.2 and Figure 4.3.

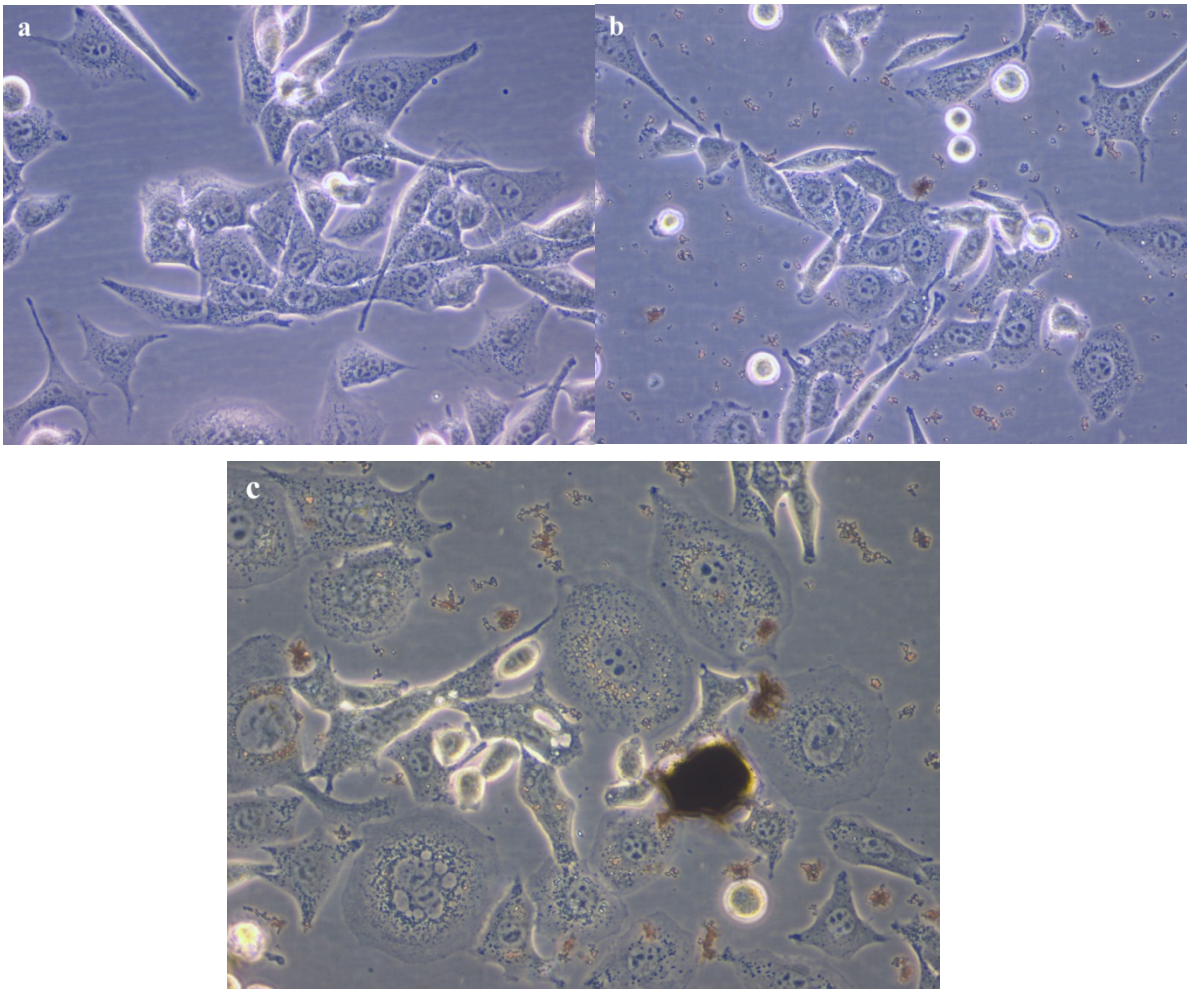

Figure 4.2 a) Pan02 cells incubated in RPMI medium for 24 h; b) Pan02 cells with 10 µg/ml iron oxide nanoparticles at 0 h; c) Pan02 cells incubated with iron oxide nanoparticles at 37^0C in humidified containing 5% CO_2 for 24 h; under light microscope with 40X magnification

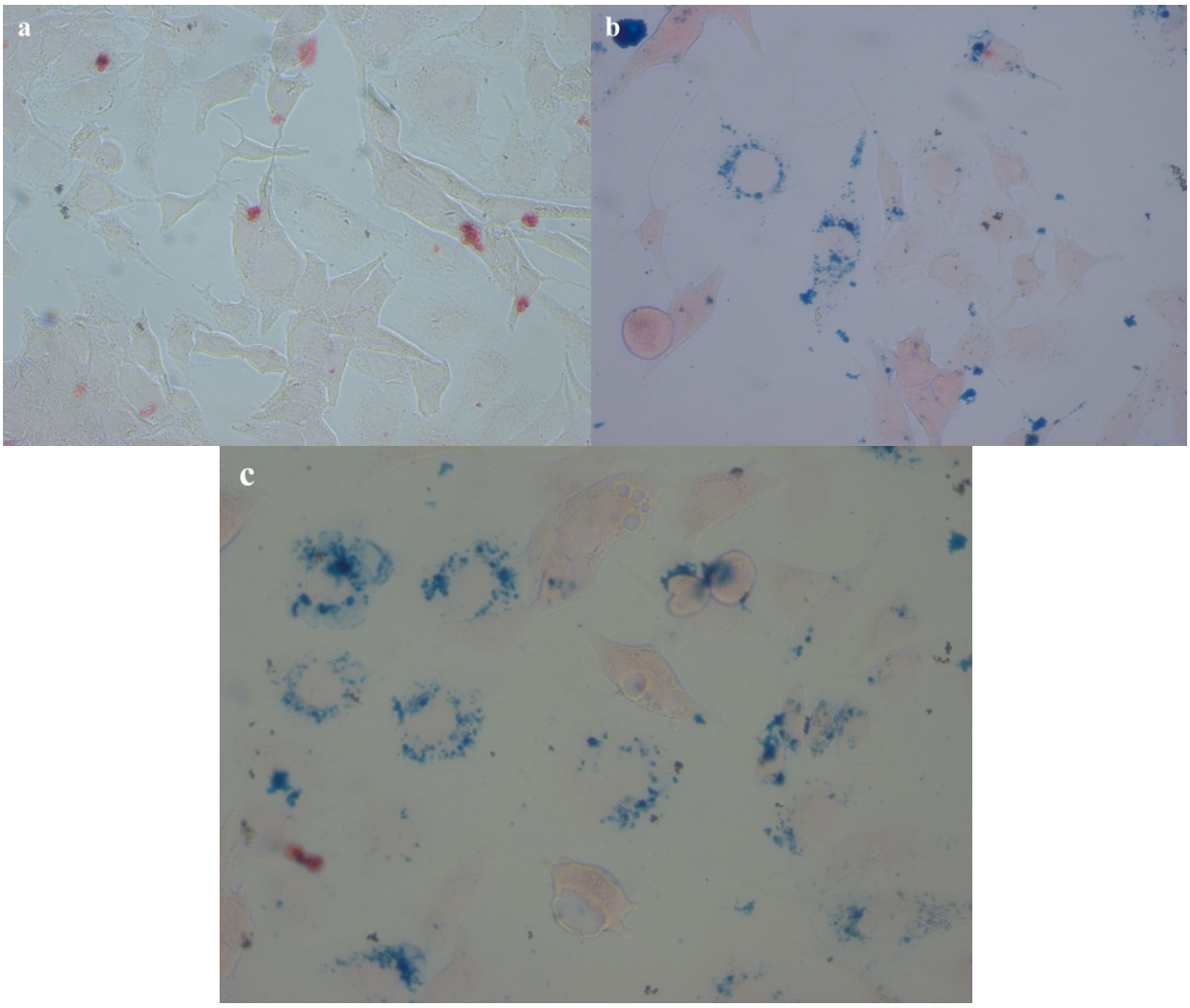

Figure 4.3 Pan02 cells after Prussian Blue staining procedures under light microscope with 40X magnification a) Control Pan02 cells; b) Pan02 cells incubated with 5 µg/ml of iron oxide nanoparticles; c) Pan02 cells incubated with 10 µg/ml of iron oxide nanoparticles

As shown in Figure 4.3, Pan02 cells incubated with iron/iron oxide nanoparticles show presence of blue pigments within the cytoplasm of the cells and selectively accumulated around the nucleus. In both 5 µg/ml and 10 µg/ml concentrations of iron/iron oxide nanoparticles are shown that nanoparticles are selectively taken up by the Pan02 cells, compared to the control sample. This provide evidences to support that the iron oxide nanoparticle based drug delivery system is biocompatible and taken up by the cancer cell lines.

4.2.2 Anti-Proliferating (Cytotoxic) Activity of the Fe/Fe_3O_4 Nanoparticle Based Drug Delivery System

The colorimetric MTT assay is used in the preliminary *in-vitro* cytotoxic assays to evaluate the toxicity effects of the iron/iron oxide nanoparticle based drug system on Pan02 cells. The basic principle of the assay is the reduction of the yellow dye MTT (3-(4,5-Dimethylthiazol-2-yl)-2,5-diphenyltetrazolium bromide, a tetrazole) to its insoluble purple formazan form by the enzymes presence in mitochondria of living cells. Then this insoluble dye is solubilized using a solubilizing buffer and the absorbance of this colored solution is quantified by measuring at a certain wavelength (usually 550 nm) by a UV-VIS spectrophotometer, depending on the solution medium used for cell growth.[4] Formation of the formazan is proportional to the amount of viable cells as mitochondrial enzyme activity is responsible of reduction of MTT.

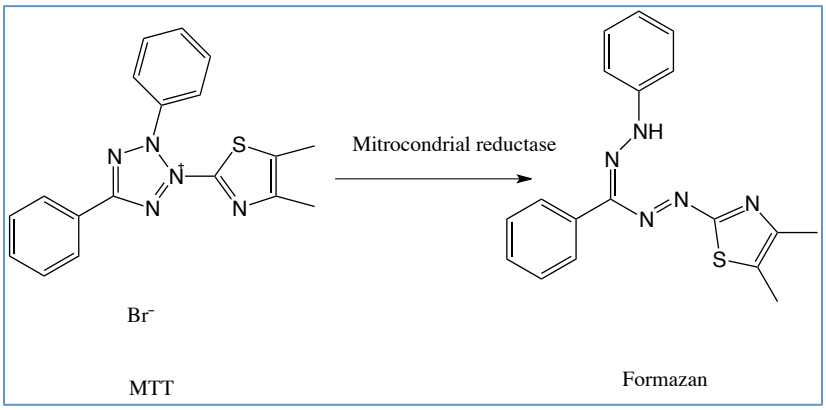

Figure 4.4 Conversion of MTT to formazan dye by mitochondrial reductase enzymes

Three different concentration values (10 μg/ml, 50 μg/ml and 100 μg/ml with respect to iron) were prepared from each iron/iron oxide nanoparticle based drug delivery systems along with the dopamine/dopamine maleimide coated iron/iron oxide nanoparticles. All the samples were tested upon murine pancreatic cancer cells (Pan02) and mouse fibroblast cells (STO) as control cells. Mouse fibroblast cells are non-cancerous and therefore used for comparison

purposes. The main purpose of the cytotoxicity assays are to evaluate the therapeutic efficacy of the drug delivery system and to determine effective ratio between the homing sequence CGKRK and topoisomerase II inhibitory doxorubicin content in each nanoparticle system. The sample numbers and their corresponding compositions are listed below in table 4.1 for easy identification. The samples were constructed using experimental method "Doehlert design" as explained in the chapter 03.

Sample number	No. of CGKRK molecules	No. of Doxorubicin molecules
1	80	80
2	128	80
3	104	120
4	32	80
5	56	40
6	104	40
7	56	120
8	80	80
9	80	128
10	120	104
11	80	32
12	40	56
13	40	104
14	120	56
D	-	-

Table 4-1 Iron oxide nanoparticle based drug system with corresponding sample number for preliminary tests

Dopamine/dopamine maleimide coated iron oxide nanoparticles, doxorubicin drug itself and cells incubated in the growth media were used as controls to evaluate the drug delivery

system efficacy with respect to each other. The MTT assay protocol is briefly described in the next paragraph.

Originally, Pan02 cells were cultured in 96 well plates at a concentration of 12500 cell per square centimeter in RPMI 1640 medium with 10% FBS and 1% penstrap and incubated at 37^0C in humidified air containing 5% CO_2 overnight. Growth medium was removed from the cell suspensions and iron oxide nanoparticle samples prepared from growth medium are introduced to the cells as shown in Figure 4.5.

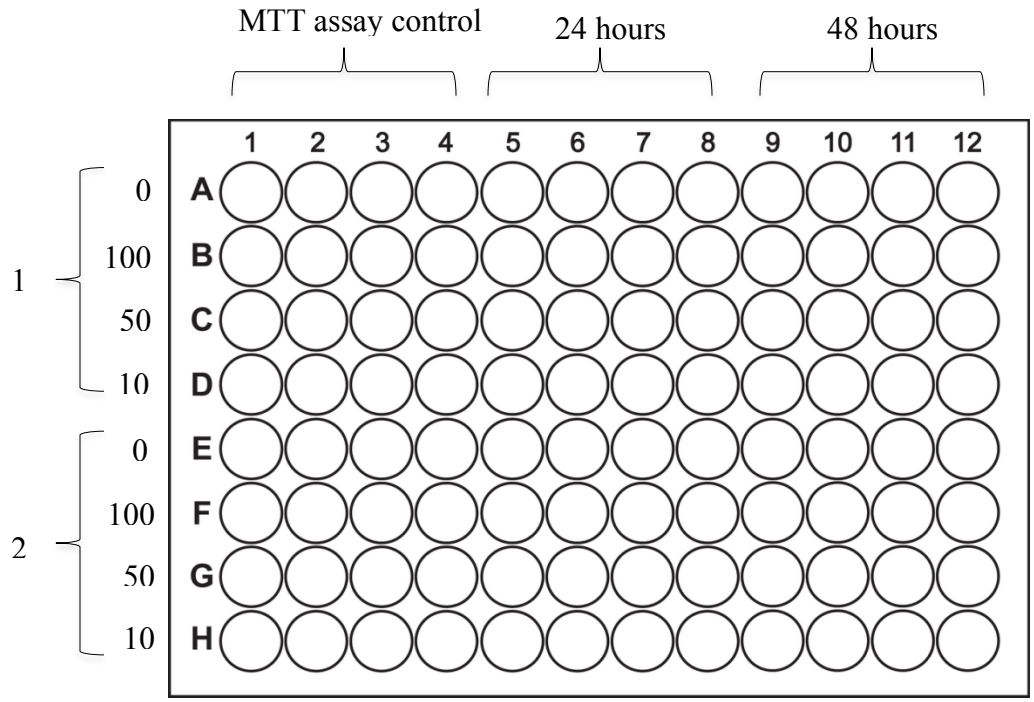

Figure 4.5 Iron oxide nanoparticle addition layout on the 96 well plates

For each sample a negative control was carried out incubating the cells without any iron/ iron oxide nanoparticles and it is denoted as 0 μg/ml. Similarly, 8 plates were used to carry out the toxicity assays for all the samples mentioned in the table 4-1. Once the nanoparticles are introduced to the cells plates were incubated at 37^0C in humidified air containing 5% CO_2 for 24 hours. MTT solution was added to the wells in 5-8 columns and incubated again for 4 hours.

Insoluble purple formazan pigments were solubilized using solubilizing buffer and same procedure was carried out after 48 h for the wells in column 9-12. After 72 hours with initial cell incubation on the plates color development was measured at 560 nm and 690 nm using the UV-Vis spectrophotometry. Absorbance of purple formazan dye is measured at 560 nm and absorbance of MTT solution is measured at 690 nm. The schematic representation of the assay procedure is shown in figure 4.6.

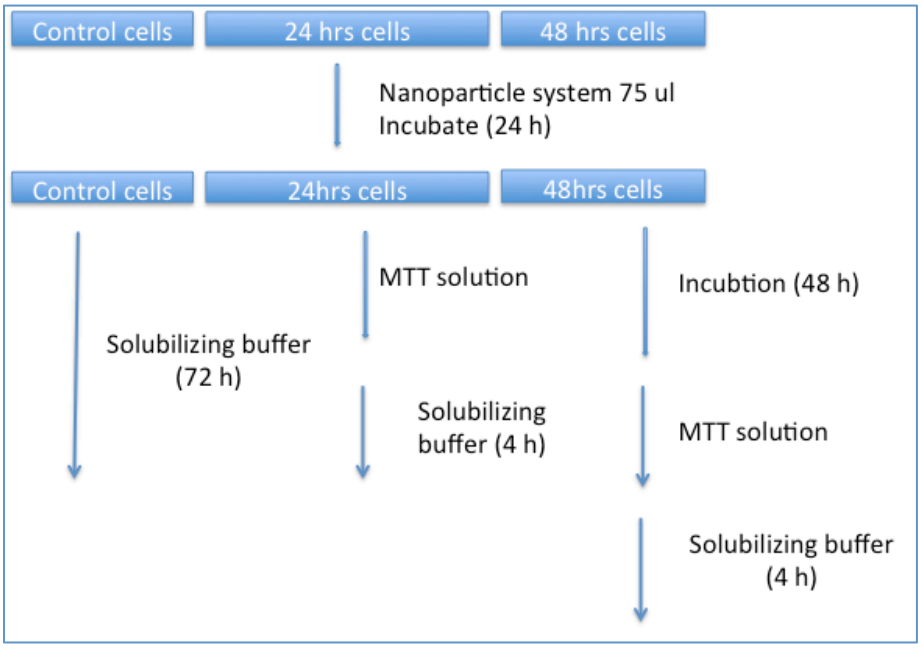

Figure 4.6 Schematic representation of the MTT assay procedure

As shown in Figure 4.5 each concentration of the sample is quadruplicate. Therefore the viability of the cells depending on the iron nanoparticle concentrations was calculated using the equation below.

$$cell\ viability\ (\%) = \frac{(\bar{a} - \bar{b})}{(\bar{c} - \bar{d})}\ X\ 100\%$$

where, $\bar{a}$ is the mean of sample absorbance ($Abs_{560} - Abs_{690}$)

$\bar{b}$ is the mean of MTT assay control absorbance for sample ($Abs_{560} - Abs_{690}$)

$\bar{c}$ is the mean of negative control absorbance ($Abs_{560} - Abs_{690}$)

$\bar{d}$ is the mean of MTT assay control absorbance for negative control ($Abs_{560} - Abs_{690}$)

The cell viability of Pan02 cells as a function of the nanodelivery systems used after 24 h and 48 h incubation are shown in the graphs below (Figure 4.7). It is clearly visible that the cell viability is over 80% for most of the samples in all three concentrations. When the cells were examined under the light microscope it is further evident that the nanoparticles were aggregated together in the media and the cell uptake of the nanoparticles are considerably low where there were only small fractions of cells with nanoparticle accumulated in the cytoplasm.

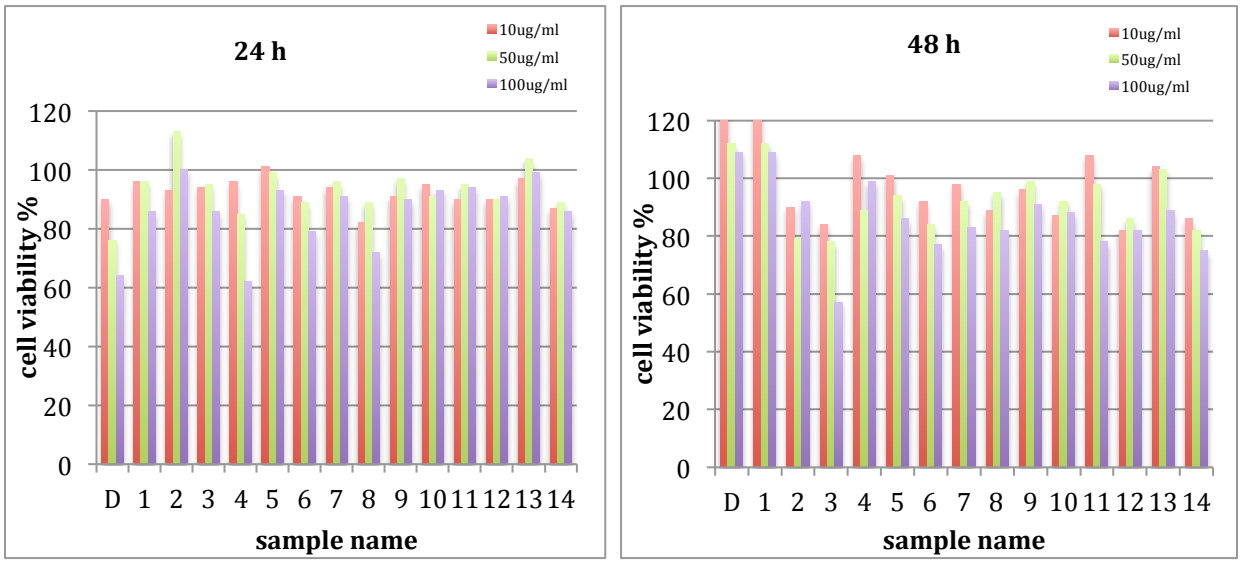

Figure 4.7 Percentage cell viability of Pan02 cells with various iron oxide nanoparticle systems after 24 and 48 hours

In order to minimize the nanoparticle aggregation, dextran has been used successfully in the Bossmann laboratories in the project carried out for the early detection of cancers using iron / iron oxide based nanoparticle systems. Therefore, the same strategy was used in the *in-vitro* cytotoxic assay measurements, where 10 mg of Dextran (70 kDa) is used for each 1 ml of growth medium when preparing the concentration series for the iron/ iron oxide nanoparticles. The MTT assay was repeated again, and the percentages for the cell viabilities are shown in Figure 4.8.

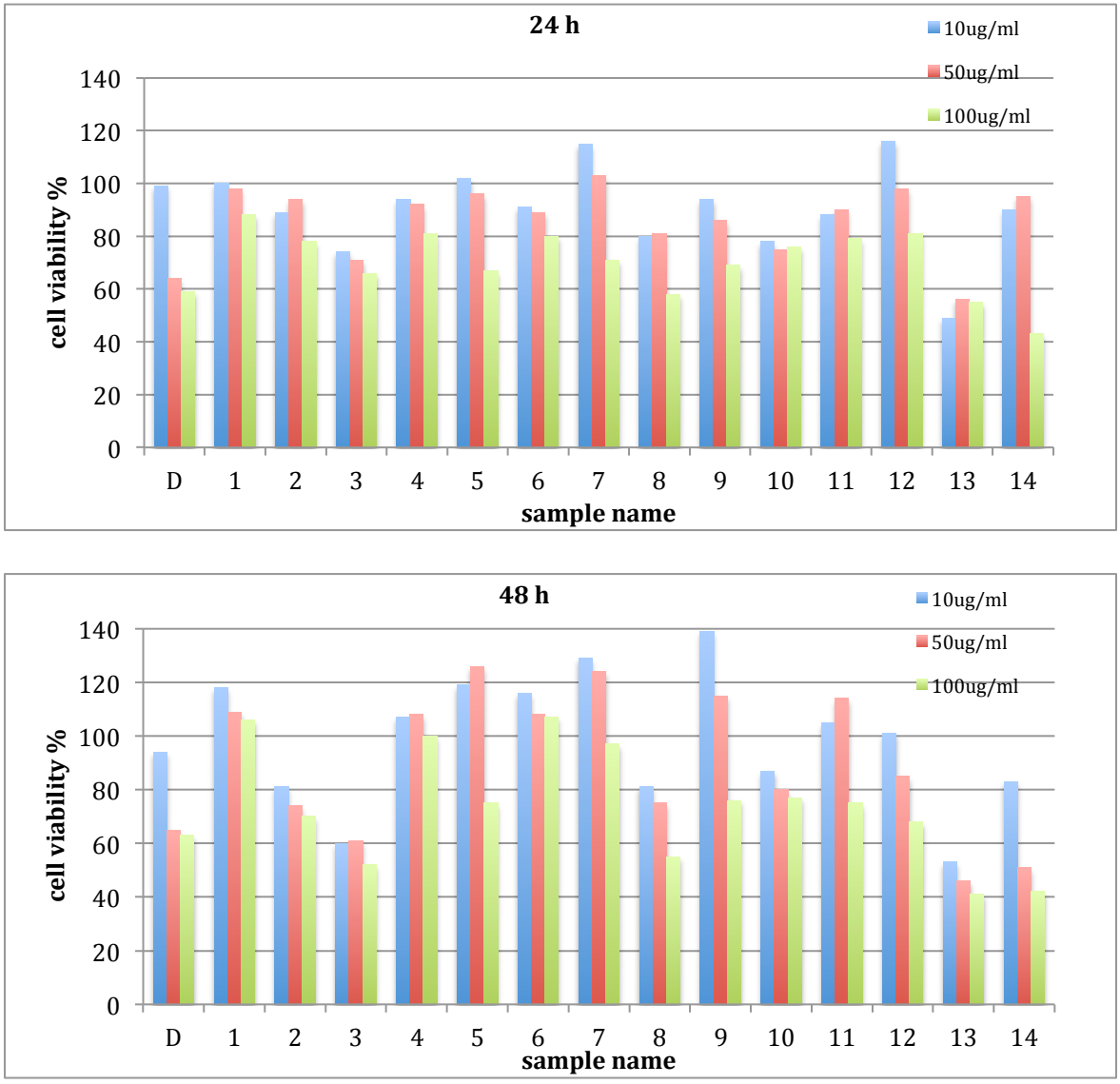

Figure 4.8 Percentage cell viabilities of the Pan02 cells after 24 and 48 hours with iron oxide nanoparticle systems

As shown in Figure 4.8, the percentages of the cell viabilities of the Pan02 cells were considerably low compared to the cell viabilities shown in Figure 4.7. This clearly indicated that the dextran reduces the aggregation of iron / iron oxide nanoparticles in the growth medium. As a result, nanoparticles uptake and cytotoxic activity of the drug system were elevated, which ultimately reduced the cell viability of the cancerous Pan02 cells due to the presence of a dispersed drug delivery system. Moreover, it clearly indicates that with increasing concentration of the iron / iron oxide nanoparticles the cell viability decreases in all the samples. Most notably, it shows very high toxicity in samples number 3, 8, 13 and 14 in both 24 hours and 48 hours. Since the iron / iron oxide nanoparticle based drug systems comprise of different ratios of CGKRK to doxorubicin, a simple correlation of the cell viability with respect to the homing ability of CGKRK or doxorubicin does not yield a straightforward result. Therefore, we have to assume that a synergistic effect causes the observed cytotoxic activity inside the pancreatic tumor cells. In order to evaluate this synergistic effect of the cytotoxicity data and to arrive at the best ratio of the two components, a response surface has been drawn with the use of statistical analysis method mentioned in the chapter 02. The consequences of its shape will be discussed further in chapter 05.

The MTT assays for all the iron oxide based systems were also carried out on noncancerous mouse fibroblast cells (STO) in a similar manner for the comparison of the toxicity with respect to the nanoparticle based drug systems on healthy cells. Mouse fibroblast cells were cultured in Dulbecco's Eagle Medium (DMEM) with 10% FBS, 1% penstrap. Iron / iron oxide nanoparticle samples were prepared using the same growth medium and dextran (10%) was also introduced to the medium. The results for the cell viabilities (again in percentages) are summarized in Figure 4.9.

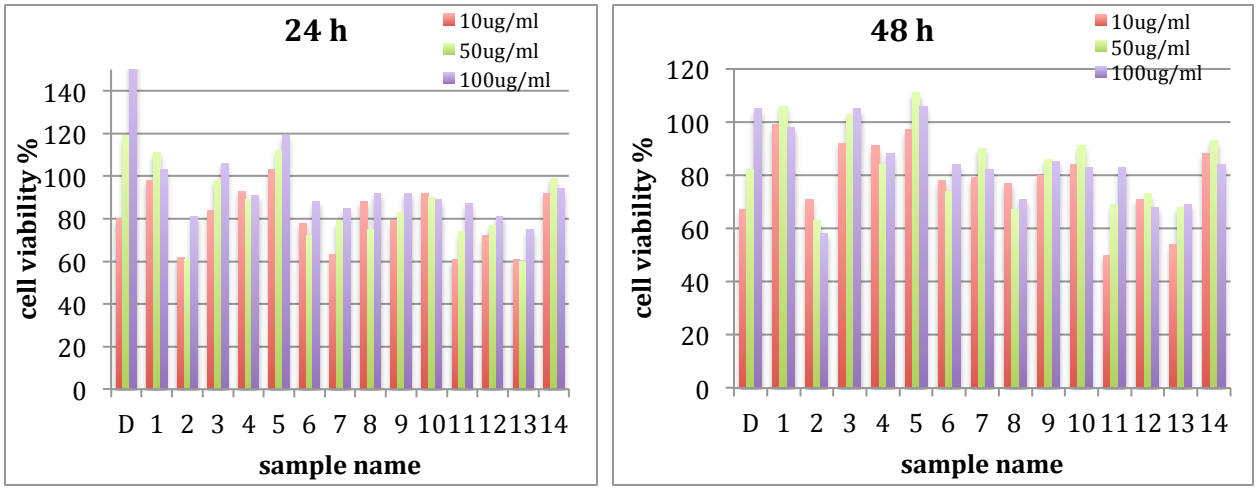

Figure 4.9 Percentage cell viabilities of the STO cells after 24 and 48 hours with iron oxide nanoparticle systems

The percentage cell viabilities of the STO cells are ranging between 60% to 100% in all of the samples. Among them most compositions of Fe/Fe_3O_4 nanoparticles, CGKRK and doxorubicin show more than 80% viability, except samples 2, 7, 11 and 13. In most of the samples, the highest toxicity values were observed for the lowest nanodelivery platform concentrations (10ug/ml), which is not a common feature observed in MTT cell viability assays. Interestingly, the iron / iron oxide drug delivery systems 3, 8 and 14 ((104,120), (80, 80) and (120, 56) respectively) that showed the highest toxicity on Pan02 cells, did not show significant cytotoxicity effects on STO cells at all tested concentrations. However, drug delivery system number 13 (40,104) shows about 60% cytotoxicity effects whereas the cytotoxicity values for Pan02 cells was about 40%. Based on these results, our studies showed that the iron / iron oxide nanoparticle based drug delivery system has potential as anticancer agent in the treatment of pancreatic cancers, because compositions can be chosen that are more toxic to cancer cells than to healthy cells.

The MTT assay has also been carried out using free doxorubicin with Pan02 cells to evaluate the cytotoxicity capacity with the same concentrations that were incorporated into the iron / iron oxide nanoparticles during the design of the drug delivery system. Depending on the number of doxorubicin molecules introduced into the nanoparticle systems, the average number of doxorubicin molecules was calculated. The corresponding concentrations for doxorubicin were 1 µg/ml, 0.5 and 0.1 µg/ml, for iron oxide nanoparticle concentrations of 100 µg/ml, 50 µg/ml and 10 µg/ml respectively. The percentage cell viabilities are shown in Figure 4.10 below.

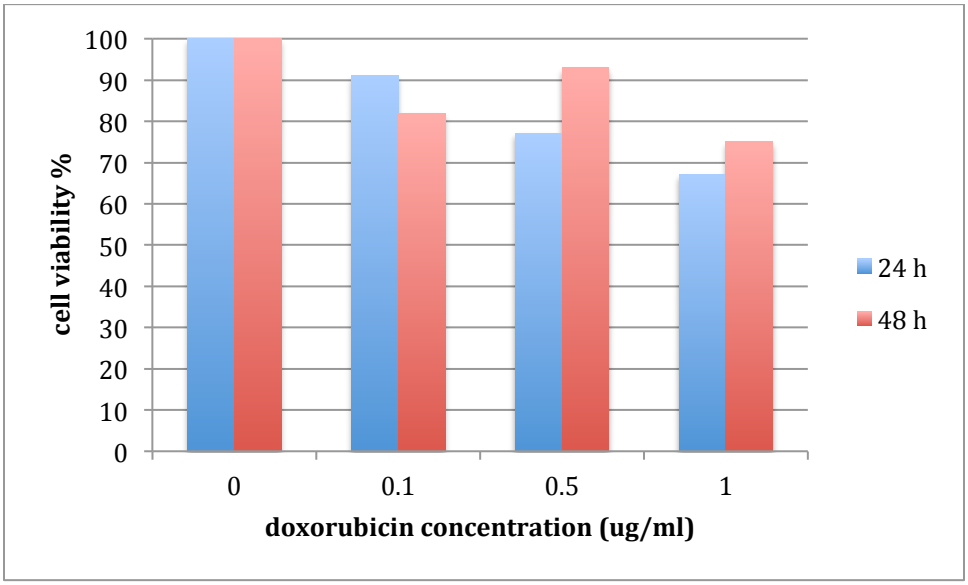

Figure 4.10 Percentage cell viabilities of the Pan02 cells incubated with free doxorubicin after 24 and 48 hours

According to the percentage viability data for free doxorubicin, the hydrophobic drug is not very cytotoxic at the given concentration range, except at 1 µg/ml where it has the highest cytotoxicity values for 24 hours. Therefore, it can be concluded that when the drug is incorporated into the nanoparticles, its uptake efficacies are higher and the therapeutic activity becomes more significant, compared to free doxorubicin. The higher therapeutic capacity of the iron / iron oxide nanoparticle based drug systems may be due to the synergistic effect of both

CGKRK and doxorubicin. There could be also an added cytotoxic effect due to the presence of iron.

4.1.1 Anti-Proliferating (Cytotoxic) Activity of the Fe/Fe_3O_4 Nanoparticle Based Drug Delivery System for Extended Doehlert Matrices

From the preliminary data obtained by means of Prussian blue staining and MTT assays, it can be concluded that the constructed systems show potential as anticancer drug delivery agents in treating pancreatic cancers. The Prussian blue staining method shows satisfactory nanoparticle uptake by the Pan02 cells, while the MTT assay data show low cell viabilities of Pan02 cells, compared to higher cell viabilities of the non-cancerous STO cells. This is especially valid in samples number 3, 8 and 14. When looking into the nanoparticle compositions that showed higher cytotoxicity activity, we have observed that samples with higher amount of doxorubicin showed higher cytotoxicity activity towards Pan02 cells. Therefore, in order to further evaluate a potential synergistic effect of CGKRK and doxorubicin on nanoparticles towards cell cytotoxicity of Pan02 cells, two additional Doehlert matrices were constructed. As described in the chapter 02, the space filling ability of the Doehlert designs was taken into consideration when constructing the new matrices. This is clearly an added advantage that reduces the experimental time and cost when expanding the cytotoxicity studies in order to find the optimal conditions of the nanoparticle system as anticancer therapeutic agent. Iron/iron oxide nanoparticles with higher cytotoxicity effects that were obtained from original matrices were incorporated in the new matrices with additional iron/iron oxide nanoparticle samples with high numbers of CGKRK and doxorubicin molecules.

In order to synthesize the new nanoparticle systems (15-22), the total number of dopamine maleimides on the nanoparticles was increased. Consequently, the new dopamine to

dopamine maleimide ratio is set to 1:3, as opposed to the previous 1:4 ratio. Coupling of CGKRK and doxorubicin onto the nanoparticles was carried out in a similar manner as mentioned in the section 3.4.3 in 1X PBS buffer medium. CGKRK and doxorubicin loaded iron/iron oxide nanoparticles were dried and stored at 4^0 C until further use.

Corresponding new matrices are tabulated in Tables 4.2 and 4.3. Samples from the initial matrices are denoted in purple columns.

Run	Coded value X_1	Real value X_1 (No. of CGKRK molecules)	Coded value X_2	Real value X_2 (No. of Doxorubicin molecules)
3	0	104	0	120
22	1	152	0	120
21	0.5	128	0.866	160
7	-1	56	0	120
1	-0.5	80	-0.866	80
2	0.5	128	-0.866	80
20	-0.5	80	0.866	160

Table 4-2 New Doehlert matrix to evaluate the nanoparticle efficacy studying topoisomerase II inhibitor activity at five levels and CGKRK homing activity at three levels

Run	Coded value X_1	Real value X_1 (No. of Doxorubicin molecules)	Coded value X_2	Real value X_2 (No. of CGKRK molecules)
15	0	152	0	120
17	1	200	0	120
18	0.5	176	0.866	160
10	-1	104	0	120
9	-0.5	128	-0.866	80
16	0.5	176	-0.866	80
19	-0.5	128	0.866	160

Table 4-3 New Doehlert matrix to evaluate the nanoparticle efficacy studying topoisomerase II inhibitor activity at five levels and CGKRK homing activity at three levels

Spatial arrangements of the new nanoparticle samples with respect to the original samples are shown in Figure 4.10 and Figure 4.11.

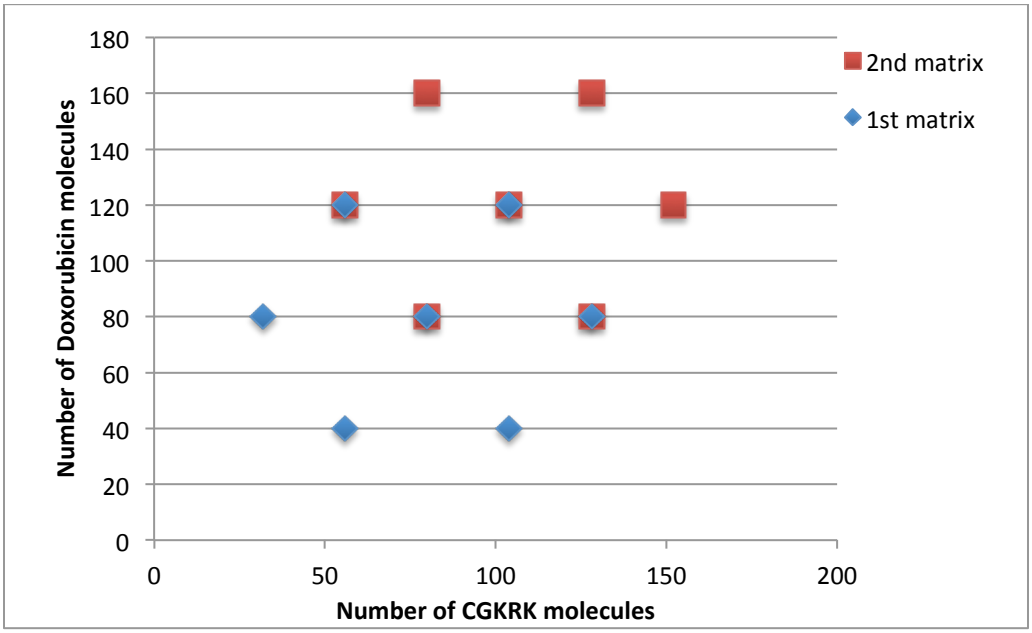

Figure 4.11 Spatial arrangement of the 2nd Doehlert matrix with respects to initial matrix, which studied CGKRK in five levels

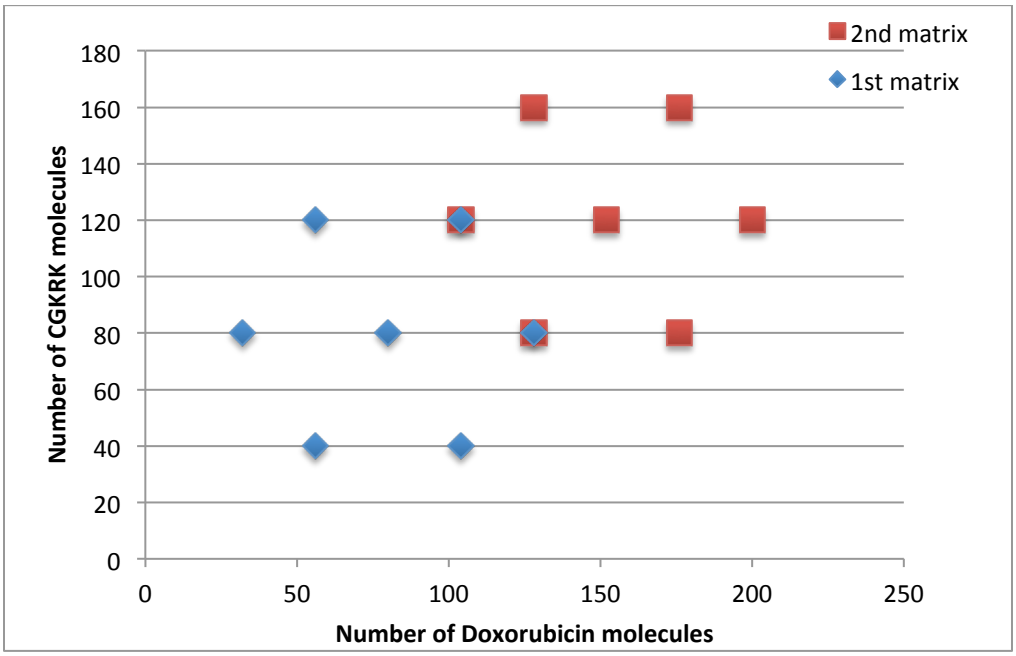

Figure 4.12 Spatial arrangement of the 2nd Doehlert matrix with respect to the initial matrix, which studied Doxorubicin in five levels

Antiproliferation assays using newly synthesized nanoparticle systems (15-22) against both Pan02 cells and STO cells (control assays) were carried out following the same procedures as described in section 4.2.2. It was found in our initial study that the 48 hours cell cytotoxicity assays are not statistically significant for any concentrations. Therefore, only the 24 hours cell cytotoxicity assays were conducted for the new samples. Cell cytotoxicity data for Pan02 cells with respect to all concentrations of each sample are shown in the graphs below. (Figure 4.13).

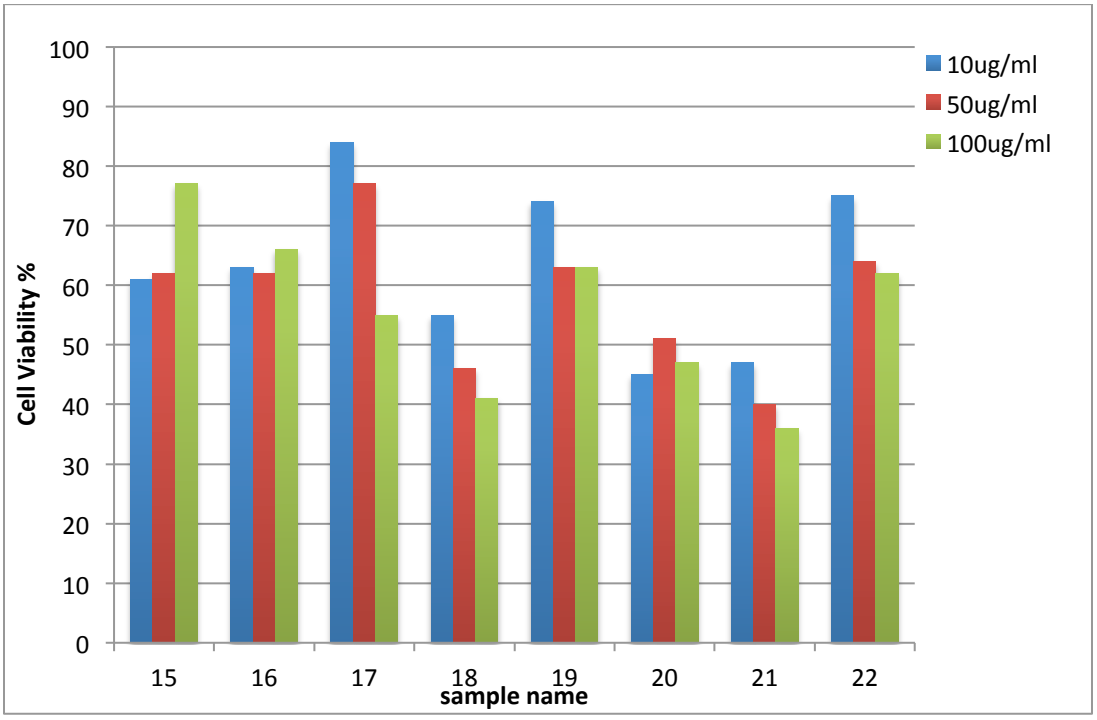

Figure 4.13 Percentage cell viabilities of the Pan02 cells after 24 hours incubation with iron / iron oxide nanoparticle systems

According to Figure 4.13 it is clearly evident that the cell cytotoxicity is further reduced when a high doxorubicin content is present on the nanoparticle samples (15-22), compared to the previous samples (1-14). Most of the samples show linear correlation with the nanoparticle concentration where the percentage cell viability decreases with the increase of concentration.

According to the preliminary statistical analysis, the percentage cell viability was not affected by the number of CGKRK molecules present on each nanoparticle system (the CGKRK parameters were statistically not significant in the chosen model). Assuming that this is still valid for the new iron/iron oxide nanoparticle systems, an interesting correlation between the percentage cell viability and number of doxorubicin can be derived from the data. It shows the reduction of percentage cell viability of the Pan02 cells with increasing number doxorubicin molecules until a certain number of doxorubicin molecules is reached. If the concentration of doxorubicin on the nanoparticle is further increased, the observed cell viability starts to increase back (showing a negative effect on cell cytotoxicity). For example, samples 16, 18 (176 doxorubicin molecules per nanoparticle) and sample 17 (200 doxorubicin molecules per nanoparticle) show lower cytotoxicity effects than sample 20 and 21 (160 doxorubicin molecules per nanoparticle), which show the highest cytotoxicity values. It is interesting that the samples 16 and 18, which have the same number of doxorubicin molecules at the nanoparticles' surface (176), show different cytotoxicity effects towards Pan02 cells. This behavior may be due to the difference in the number of CGKRK molecules present on each nanoparticle (80 molecules in sample 16 and 160 in sample 18). Based on the data, prediction of simple correlation between the cell cytotoxicity and nanoparticle composition is quite ineffective; therefore a refined statistical analysis of the data using response surface methodology was carried out to evaluate potential synergistic effect of both CGKRK and doxorubicin against Pan02 cells. To minimize the error term associated with the mathematical model, cell cytotoxicity assays for the central point of each Doehlert matrices were carried out in triplicates, as described on page 22 chapter 02.

Comparison of the cell cytotoxicity data of iron/iron oxide nanoparticles for each concentration in both Pan02 cells and STO cells are summarized in the Figure 4.14.

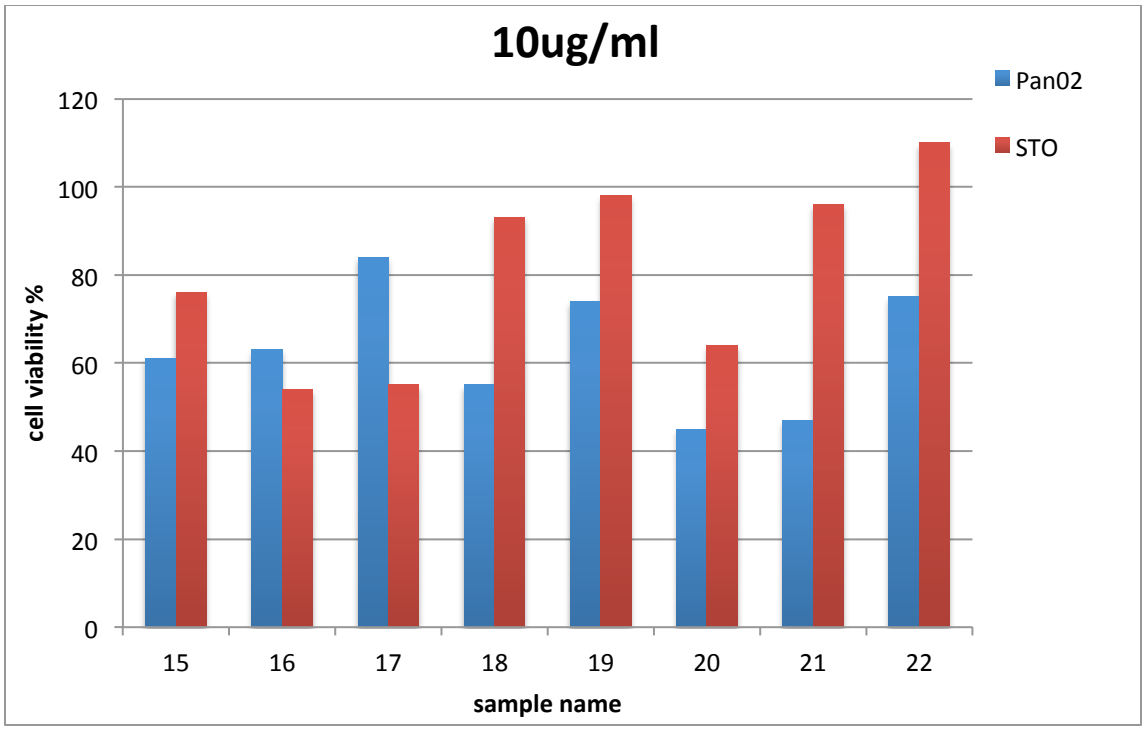
10ug/ml
Pan02
STO
120
100
80
60
40
20
0
cell viability %
15
16
17
18
19
20
21
22
sample name

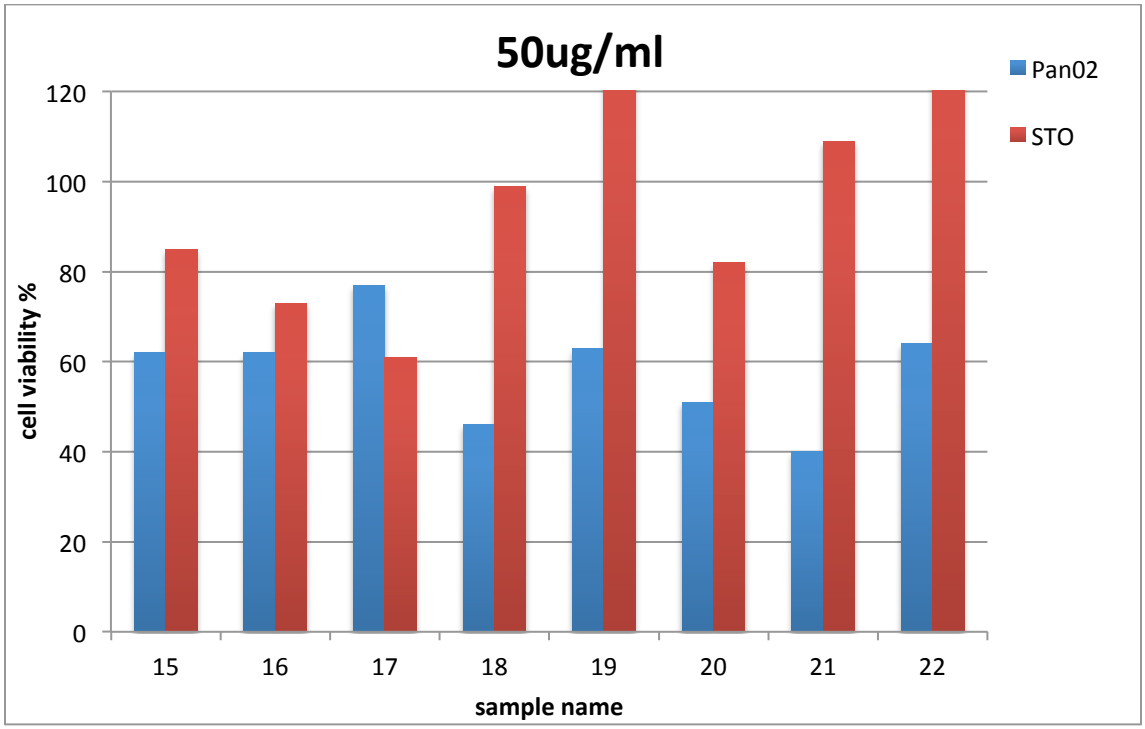
50ug/ml
Pan02
STO
120
100
80
60
40
20
0
cell viability %
15
16
17
18
19
20
21
22
sample name

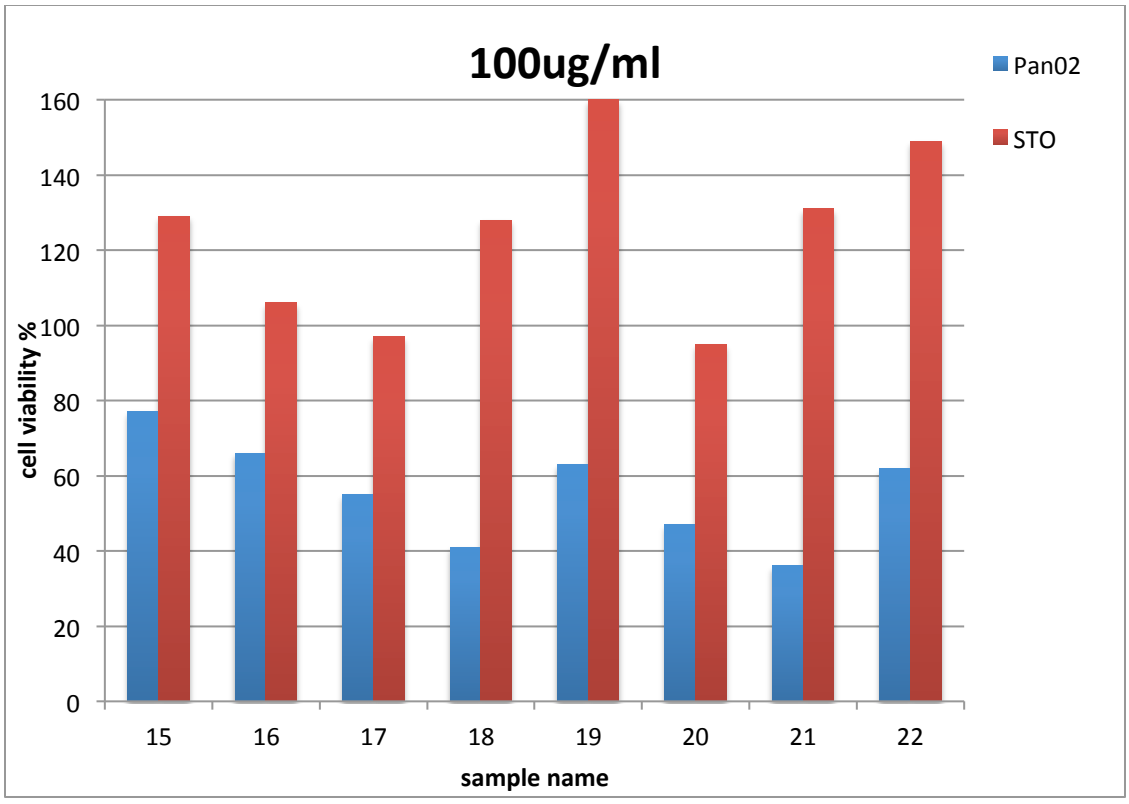

Figure 4.14 Percentage cell viability comparison of Pan02 cells and STO cells treated with iron/iron oxide nanoparticle systems for 10 µg/ml, 50 µg/ml and 100 µg/ml respectively

Among the group of 10 µg/ml concentrations, samples 16 and 17 showed higher toxicity towards noncancerous STO cells compared to cancerous Pan02 cells. Cell toxicity of sample 17 is the highest. This behavior is attributed to the high doxorubicin content on the samples, which is highly toxic to the normal STO cells. All the other samples show lower toxicity towards STO cells than Pan02 cells, especially samples 20 and 21, which showed higher toxicity effects on Pan02 cells. Similar trends are observed at the concentrations of 50 µg/ml and 100 µg/ml for all the samples, except sample 17 that showed higher toxicity towards STO cells Pan02 cells at 50 µg/ml concentration. Based on these data it is clear that the secondary data obtained from the cytotoxicity assays are compatible with the preliminary data. This iron/iron oxide nanoparticle based system showed promising results in establishing a novel nanoformulation with potential in

the treatment of pancreatic cancer. However, in order to determine whether the activity is based on doxorubicin itself or due to the synergistic effect of both CGKRK and doxorubicin, a detailed statistical analysis using RSM method was carried out. The RSM methodology and the results of the statistical analysis and will be discussed in the next chapter.

4.2 Conclusion

In conclusion, the iron / iron oxide nanoparticle based drug delivery system that was designed in accordance with the Ringsdorf model, has been successfully used in *in-vitro* cell-based assays to determine the cytotoxicity on the murine pancreatic cancer cell line Pan02 and on noncancerous mouse fibroblast cells (STO). The cytotoxicity data reported here was further studied using by using response surface methodology for determining the best ratio between the homing activity and the topoisomerase inhibitory activity. A detailed discussion of the statistical analysis will be provided in the next chapter. Even from only preliminary MTT data, it can be concluded that the nanoparticle based system shows potential toxicity effects on Pan02 cells, while showing minimum cytotoxicity to healthy STO cells. This data gives a clear indication that constructing a nanoplatform for drug delivery based on Doehlert methodology has potential. Response surface methodology allowed the development of targeted drug delivery in the treatment of pancreatic cancers using a nanoparticle as drug carrier. Iron/ iron oxide nanoparticles have great potential as universal delivery system capable of treating many cancers by changing the targeting moiety or/and drug.

Therefore, this system will be further developed in the Bossmann group. Potential improvements comprise the use of better targeting peptides and the simultaneous use of more than one drug to minimize side effects towards non-cancerous cells. Forty years after it has been proposed, the Ringsdorf paradigm is still very alive, as this data indicates.

4.3 Experimental

All the experiments were carried out in Dr. Deryl L. Troyer's lab at Department of Veterinary Medicine. Murine pancreatic cancer cell lines (Pan02) and mouse fibroblast cells (STO) were cultured in the Troyer laboratories for assay purposes. All the chemicals and solutions used in the assay procedures were obtained from the Dr. Troyer's lab.

4.3.1 Iron / Iron Oxide Nanoparticle Solution Preparation

Initially, 1.0 mg of iron/ iron oxide nanoparticles from each sample (14 drug delivery systems and dopamine coated nanoparticles) were measured and dissolved in 700 ul of appropriate medium (RPMI 1640 for Pan02 cells and DIEM for STO cells) containing 10% FBS, 1% Penstrap and 10% dextran. The solutions were sonicated for 10 min until the nanoparticles dissolved in the solution. The original concentration of each sample is 1.0 mg/ml with respect to iron in the nanoparticle system. Then, a dilution series was carried out to prepare 100 μg/ml, 50 μg/ml and 10 μg/ml as assay sample solutions by diluting the stock solution with the same media. For each concentration 1.0 ml was prepared.

4.3.2 Prussian Blue Staining Procedure

Pan02 cells plated on 24 well cell plates were incubated overnight at 37^0C in humidified air containing 5% CO_2 with 500 ul of nanoparticles solutions with concentration of 10 μg/ml and 5 μg/ml. Then, cells were fixed with 500 ul of 10% Neutral Buffered Formalin and incubated for 15min. Wells were washed thoroughly with 1 X PBS buffer and stained with 300ul of an aqueous solution of 4% potassium ferrocyanide and 4% hydrochloric acid for 10min. Again, excess staining solutions were washed away with distilled water. Counter staining of the cells was carried out using 250 ul of nuclear fast red for 2-5 min. Finally, excess counter stain

solutions were also washed away with 1xPBS solutions. Cells were examined under a light microscope with 40X magnification.

4.3.3 MTT Assay Procedure

Pan02 cells were cultured in 96 well plates at a concentration of 12500 cells per square centimeter in RPMI 1640 medium with 10% FBS and 1% penstrap and incubated at 37^0C in humidified air containing 5% CO_2 overnight. The growth medium was removed from the cell suspensions and 75 ul of iron / iron oxide nanoparticle samples prepared were introduced to the cells and incubated for 24 h under same incubation conditions. After the 24 h 7.5 ul of MTT solution were added to the cells in rows number 5-8 and 75 ul of solubilizing buffer were added to the same cells after 4 h of incubation. Likewise, the same procedure was carried out for rows number 9-12 after 48 h. Both, cell groups were treated with 75 ul of solubilizing agents after 4 h of incubation. Then, the plates were incubated for another 24 h and absorbance measurements were carried out using UV-VIS spectrophotometric plate reader in College of Anatomy and Physiology.

References

1. Cho, K.; Wang, X.; Nie, S.; Chen, S.; Shin, D.M., Therapeutic Nanoparticles for Drug Delivery in Cancer. *Clin Cancer Res* **2008**, 14(5), 1310-1316
2. Frank, J.A.; Miller, B.R.; Arbab, A.S.; Zywicke, H.A.; Jordan, E.K.; Lewis, B.K.;, L. Bryant, H.; Bulte, J.W.M., Clinically Applicable Labeling of Mammalian and Stem Cells by Combining Superparamagnetic Iron Oxides and Transfection Agents. *Radiology* **2003**, 228(2), 480–487
3. http://www.polysciences.com/SiteData/poly/Assets/DataSheets/601.pdf
4. Liu, Y.; Peterson, D.A.; Kimura, H.;Schubert, D., Mechanism of cellular 3-(4,5-dimethylthiazol-2-yl)-2,5-diphenyltetrazolium bromide (MTT) reduction. *J. Neurochem.* **1997**, 69, 581–593

Chapter 5 - Statistical Analysis of Cytotoxicity Measurements of the Nanoparticle Based Drug Delivery System

As mentioned in chapter 02, a statistical analysis was carried out for the evaluation of optimized parameters of the nanoparticle based drug delivery system. The main objective is to find out the optimal values for the ratio between the two therapeutic components CGKRK and doxorubicin, which are both co-attached on the surface of the Fe/Fe_3O_4 nanoparticles. In order to determine whether the chosen concentrations of iron/ iron oxide nanoparticles and drug ratios represent the optimization conditions, the cytotoxicity data was analyzed using statistical analysis (Response surface methodology). The statistical evaluation was carried out in three main steps, following the methodology description given in section 2.1.

The two main independent variables (factors) in the system are the number of CGKRK molecules and the number of doxorubicin molecules per nanoparticle. Their levels are chosen depending on the required solubility parameters of the nanoparticle systems. The lower and upper levels of the independent variables (factors) are mentioned in table 3.1 and 3.2 in chapter 03. These values are mainly depending on the chosen experimental design, which is Doehlert design in our case. Doehlert design has been selected due to its advantages over the other experimental design methods, as described in section 2.2. Since two independent variables are used, the response of the system (percentage cell viability) represents a curvature. Therefore, a quadratic response model is constructed to evaluate the data. Finally, verification of the model equation was carried out to determine the statistical significance of the model, hence to determine the fitness of the chosen mathematical model with respect to the experimental data.

5.1 Statistical Analysis Results

The experimental data was processed using the software STATISTICAL ANAYSIS SOFTWARE (SAS®). Statistical analysis was carried out using SAS proc reg and proc rsreg methods. Response surfaces were constructed using RSREG methods.

5.1.1 Analysis of Preliminary Cytotoxicity Data

	Percentage cell viability (%)						
Sample number	24 hrs			Sample number	48hrs hrs		
	Concentration in µg/ml				Concentration in µg/ml		
	10	50	100		10	50	100
1	100	98	88	1	118	109	106
2	89	94	78	2	81	74	70
3	74	71	66	3	60	61	52
4	94	92	81	4	107	108	100
5	102	96	67	5	119	126	75
6	91	89	80	6	116	108	107
7	115	103	71	7	129	124	97
8	80	81	58	8	81	75	55
9	94	86	69	9	139	115	76
10	78	75	76	10	87	80	77
11	88	90	79	11	105	114	75
12	116	98	81	12	101	85	68
13	49	56	55	13	53	46	41
14	90	95	43	14	83	51	42

Table 5-1 Cell cytotoxicity data for two Doehlert matrices depending on the concentration and incubation time

Six different analyses were carried out, depending on the concentration and incubation time for the experimental data, as summarized in Table 5.1. In all the calculations both, first and second Doehlert matrices were combined to obtain the required replications. Initially, a full quadratic response surface model with both CGKRK and doxorubicin was constructed and analyzed, with the intent to determine the presence of any outliers.

$$cell\ viability = \beta_o + \beta_1 Dox + \beta_2 Dox^2 + \beta_3 CGKRK + \beta_4 CGKRK^2 + \beta_5 Dox * CGKRK + \varepsilon \quad (1)$$

After removing the outlier data points, the quadratic model was analyzed again and to determine the coefficients of the parameters present in the full quadratic model equation. Finally, ANOVA calculations were conducted comparing the variation due to the changes in the parameters with the variation due to the random errors, which occurred during the measurements. This step is performed to determine the suitability of the model equation to fit the experimental data, as discussed in section 2.1.2 in chapter 02.

According to the results obtained for the coefficient parameters and ANOVA analysis for the quadratic model, further modifications of the model equation have been carried out. These modified models were further analyzed using the same protocol until a statistically significant model equation was obtained where the mathematical model fits the experimental data. Non-significant terms of the quadratic model equation were excluded using the backward elimination process. Analysis data of each concentration as a function of time is discussed separately.

5.1.1.1 Cell Viability of 10 µg/ml Nanoparticle Concentration after 24 h Incubation

Cell viability data for samples number 9 and 13 were found to be outliers at 10 µg/ml concentration. The constructed quadratic surface model for the other observations is shown in Figure 5.1 below. The coefficient parameters of the quadratic mathematical model (β_0 to β_5) were calculated and found to be not statistically significant. The requirement for "significant" is P value (P) < 0.05. Furthermore, the ratio between the media of square values of regression (MS_{reg}) and residual (MS_{res}) obtained from ANOVA is lower than the tabulated Fisher distributions (*f* test) Tabulated in Table B.1 (appendix B). Therefore, the mathematical model did not fit the experimental data.

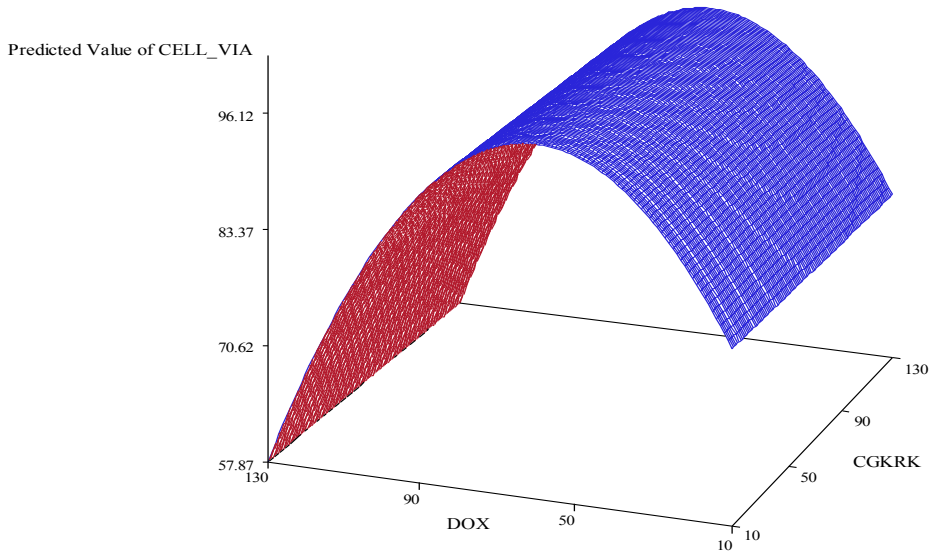

Figure 5.1 Quadratic response surface for the cell viability with respect to CGKRK and doxorubicin at nanoparticle concentration of 10 µg/ml

The reduced mathematical model was constructed as,

$$cell\ viability = \beta_o + \beta_1 Dox + \beta_2 Dox^2 + \beta_3 CGKRK + \varepsilon \quad (2)$$

This model became statistically significant (P < 0.05) as shown in the Table 5.2 below.

Analysis of Variance					
Source	**DF**	**Sum of Squares**	**Mean Square**	**F Value**	**Pr > F**
Model	3	738.60459	246.20153	6.41	0.0160
Error	8	307.06207	38.38276		
Corrected Total	11	1045.66667			

Table 5-2 Regression analysis data for the reduced model (2) for nanoparticle concentration of 10 µg/ml

According to the parameter estimation data as shown below (Table 5.3) CGKRK was not a significant factor (where β_3 is not significant).

Variable	Parameter Estimate	Standard Error	Type II SS	F Value	Pr > F
Intercept	76.18240	15.18406	966.20612	25.17	0.0010
CGKRK	-0.06953	0.06905	38.92233	1.01	0.3434
DOX	0.82632	0.38984	172.45089	4.49	0.0669
DOX2	-0.00688	0.00267	254.75312	6.64	0.0328

Table 5-3 Estimated coefficient parameter values for the reduced quadratic model for 10 µg/ml nanoparticle concentration

Therefore, the number of CGKRK molecules was removed from the equation, and the final mathematical model was obtained as,

$$cell\ viability = \beta_o + \beta_1 Dox + \beta_2 Dox^2 + \varepsilon \quad (3)$$

This model is highly significant with respect to both, DOX and DOX^2 values. The ratio of media of square values of regression (MS_{reg}) and residual (MS_{res}) is higher than the tabulated value (*f*-test). The regression analysis data and parameter estimation are shown in the Table 5.4 and the corresponding response surface for the mathematical model represents a saddle, as shown in the Figure 5.2 below.

a

Analysis of Variance					
Source	**DF**	**Sum of Squares**	**Mean Square**	**F Value**	**Pr > F**
Model	2	699.68226	349.84113	9.10	0.0069
Error	9	345.98440	38.44271		
Corrected Total	11	1045.66667			

b

Variable	**Parameter Estimate**	**Standard Error**	**Type II SS**	**F Value**	**Pr > F**
Intercept	68.23693	12.98319	1061.91627	27.62	0.0005
DOX	0.93136	0.37591	235.97638	6.14	0.0351
DOX2	-0.00778	0.00252	365.41286	9.51	0.0131

Table 5-4 a). Regression analysis data for the final mathematical model (3) and b). parameter estimation for nanoparticle concentration of 10 µg/ml

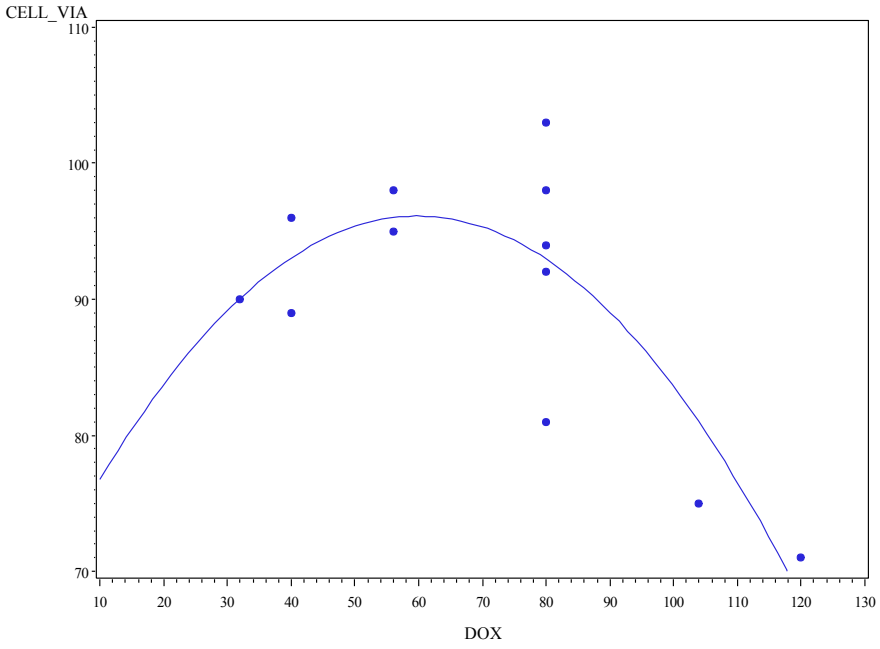

Figure 5.2 Quadratic response surface for cell viability with respect to doxorubicin at 10 µg/ml of nanoparticle concentration

By definition, this response surfaces represents a saddle, due to the quadratic response to DOX concentrations. Therefore, it does not provide either minimum or a maximum critical point within the chosen experimental domain. Therefore, careful displacements of the experimental

domain should be carried out to obtain a minimum in this particular study. Recommended experimental conditions provided by the calculation lie in the range of 110 to 120 molecules of doxorubicin and any number of CGKRK molecules, as it is not significant in this model.

5.1.1.2 Cell Viability of 50 µg/ml Nanoparticle Concentration after 24 h Incubation

Statistical analysis of cell viability responses for 50 µg/ml concentrations of iron oxide nanoparticles provided similar results than 10 µg/ml, as discussed in section 5.1.1. Samples 9 and 13 were outliers, and the analysis of the mathematical quadratic model (equation 1) was performed without accounting for observations 9 and 13. The overall model was not statistically significant, according to the ANOVA results (Table B.2 in Appendix). The quadratic response surface for the full model is given below in Figure 5.3.

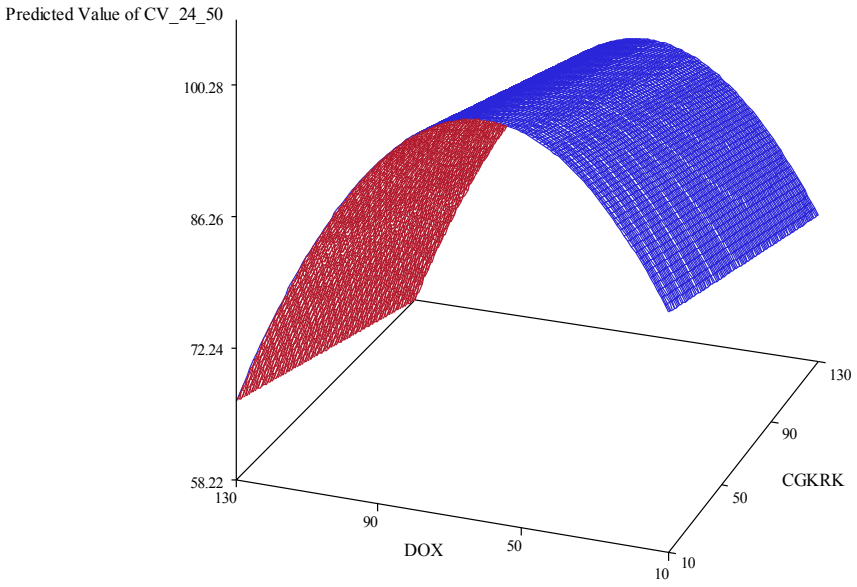

Figure 5.3 Quadratic response surface for the cell viability with respect to CGKRK and doxorubicin at nanoparticle concentration of 50 µg/ml

In analogy to 10 µg/ml, the reduced mathematical model (equation 2) was also analyzed. According to the regression analysis data and parameter estimation data given in the Table 5.5 it is statistically significant without taking CGKRK into account.

a

Analysis of Variance					
Source	**DF**	**Sum of Squares**	**Mean Square**	**F Value**	**Pr > F**
Model	3	738.60459	246.20153	6.41	0.0160
Error	8	307.06207	38.38276		
Corrected Total	11	1045.66667			

b

	Variable	Parameter	Standard	Type II SS	F Value	Pr > F
	Intercept	76.18240	15.18406	966.20612	25.17	0.0010
*	**CGKRK**	-0.06953	0.06905	38.92233	1.01	0.3434
*	**DOX**	0.82632	0.38984	172.45089	4.49	0.0669
	DOX2	-0.00688	0.00267	254.75312	6.64	0.0328
*** Forced into the model by the INCLUDE= option**						

Table 5-5 a). Regression analysis data for the reduced mathematical model (2) and b). parameter estimation for nanoparticle concentration of 50 µg/ml

Therefore, a third model (equation 3) was analyzed again without CGKRK in the model equation. This model became highly significant for both DOX and DOX^2 values hence this mathematical model fits the experimental domain, as proven by ANOVA analysis and represent in Table 5.6.

a

Analysis of Variance					
Source	**DF**	**Sum of Squares**	**Mean Square**	**F Value**	**Pr > F**
Model	2	699.68226	349.84113	9.10	0.0069
Error	9	345.98440	38.44271		
Corrected Total	11	1045.66667			

b

Parameter Estimates					
Variable	**DF**	**Parameter Estimate**	**Standard Error**	**t Value**	**Pr > |t|**
Intercept	1	68.23693	12.98319	5.26	0.0005
DOX	1	0.93136	0.37591	2.48	0.0351
DOX2	1	-0.00778	0.00252	-3.08	0.0131

Table 5-6 a). Regression analysis data for the final mathematical model (3) and b). parameter estimation for nanoparticle concentration of 50 µg/ml

The response surface for the model represents again a saddle, similar to the previous results. Therefore, careful displacements of the experimental domain should be carried out to obtain a critical minimal point for the optimization process of the iron oxide based nanoparticle systems. It should be noted that the solubility of the Fe/Fe_3O_4-nanoparticles will decrease if the doxorubicin loading will increase, due to the hydrophobicity of this drug (log P = 1.42, compared to log P = 0.58 for dopamine and log P = -5.1 for CGKRK, according to Chemdraw).

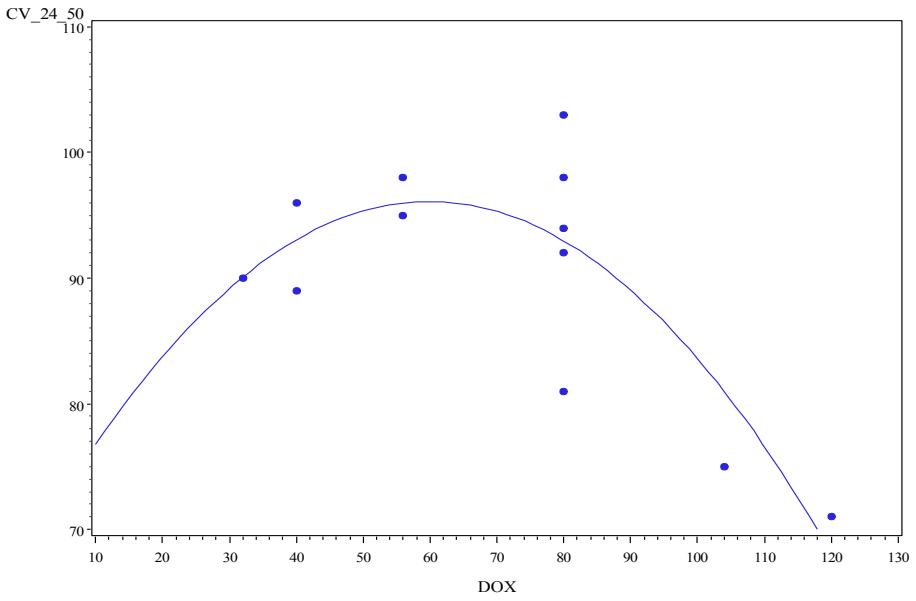

Figure 5.4 Quadratic response surface for cell viability with respect to doxorubicin at 50 µg/ml of nanoparticle concentration

5.1.1.3 Cell Viability of 100 µg/ml Nanoparticle Concentration with 24 h Incubation

Contrary to the two previous matrices for 10 and 50 µg/ml, no outliers were observed when a fully quadratic model (equation 1) was applied to fitting the experimental data obtained with 100 µg/ml. However, the overall model was statistically not significant with $P > 0.05$ for ANOVA. Then, the experimental data were analyzed using a reduced model. Both, CGKRK and DOX were found to be insignificant factors in the model. Similarly, a third model with equation 3 was also found to be not significant for iron/iron oxide nanoparticle concentrations of 100 µg/ml. Even though the fully quadratic response surface model was not significant, it has been used to construct the response surface, which is shown in Figure 5.5.

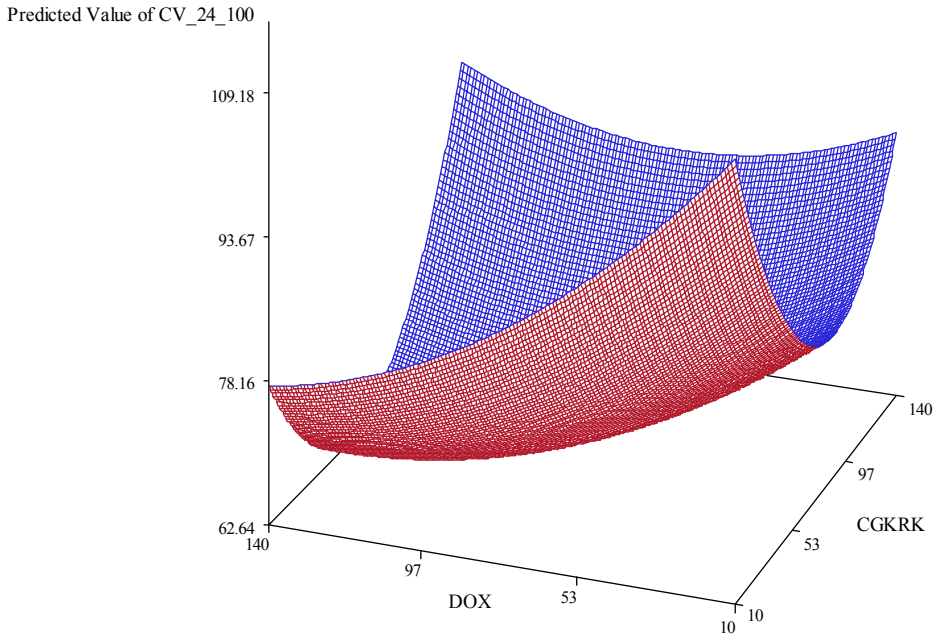

Figure 5.5 Quadratic response surface for the cell viability with respect to CGKRK and doxorubicin at nanoparticle concentration of 100 µg/ml

The quadratic response surface comprises a minimum. The predicated stationary point is 66 CGKRK oligopeptides and 121 doxorubicin molecules per Fe/Fe_3O_4 nanoparticle. The tabulated data is shown in table 5.2. It is noteworthy that the value predicted for the optimal number of doxorubicin molecules per nanoparticle at 100 μg/ml corresponds with the highest observed cytotoxicities at 10 μg/ml and 50 μg/ml. At these concentration levels, statistical significance for linear and quadratic dependencies in the number of doxorubicins per nanoparticle has been achieved.

Factor	Critical Value	
	Coded	Uncoded
CGKRK	-0.282846	66.423407
DOX	0.860735	121.315295
Predicted value at stationary point: 62.641964		

Table 5-7 Coded and experimental values for the critical minimum point in quadratic response surface for cell viability with respect to CGKRK and doxorubicin

Analysis of cell viability with each nanoparticle concentrations for 48 hours incubation time was also carried out in a similar manner using the full quadratic model, the reduced model and the third model, as denoted in equations 1, 2 and 3. For the nanoparticle concentration 10 μg/ml and 48 h of incubation time no output data were obtained as no acceptable error term could be calculated during the statistical analysis. Therefore, testing of the mathematical models with experimental data was not possible for that concentration. For concentrations of 50 μg/ml and 100 μg/ml all three models were analyzed and none of the models were statistically significant for the given experimental domain. In both cases, the full quadratic response surface provided a saddle as the corresponding response surface.

5.1.1.4 Discussion

Based on the analysis of the data, it is clearly evident that response surface methodology can be successfully used for the optimization of the composition of iron / iron oxide nanoparticle based drug delivery systems, as well as to evaluate their therapeutic efficacy in the cancer cell tests. The outcome of the statistical analysis of the data obtained from cytotoxicity tests with PAN02 cells (murine pancreatic cancer) is that a quadratic mathematical model was significant for concentrations of 10 μg/ml and 50 μg/ml and 24h of incubation time. Most interestingly, the model was significant with respect to the linear and quadratic numbers of doxorubicin molecules per Fe/Fe_3O_4-nanoparticle, while it was insignificant with respect to the peptide homing sequence CGKRK. Therefore, it is likely that the short peptide sequence CGKRK is not contributing to the selective uptake of the iron / iron oxide nanoparticles by the cancer cells via receptor mediated targeting. Rather, they are taken up by the cancer cells via a phagocytosis mechanism. It is noteworthy that the iron /iron oxide nanoparticle concentration did not have much of an effect on the therapeutic activity. Similar trends were observed with all three concentrations, even though 24 h of incubation time provided statistically significant responses, compared to the 48 h of incubation. Moreover, the doxorubicin amount on each nanoparticles should be in the upper range of the experimental domain, as it is suggested by the mathematical calculations. However, it may be also worthwhile to explore the cytotoxicity of nanoparticles bearing only 10 to 20 molecules of doxorubicin per nanoparticle, as suggested by the quadratic response. The strength of using a response surface methodology approach is that a mechanistic paradigm is not required for successful data analysis. It is likely that the cytotoxicity towards PAN02 cells at low and high loadings of Fe/Fe_3O_4-nanoparticles with doxorubicin (figures 5.2 and 5.4) is caused by different biochemical mechanism. We speculate that doxorubicin, which is

less hydrophilic than dopamine and especially CGKRK, may cause longer retention of the nanoplatforms in the endosomes, whereas escape from early endosomes may be possible at lower doxorubicin loadings. Further experiments should be carried out in accordance with the predictions provided by the quadratic model. They should be conducted in a narrow experimental region to determine optimized parameters. The results obtained to date clearly show that the use of Doehlert design in experimental design processes contributes to lowering experimental costs by eliminating unnecessary experiments, resulting in more efficient optimization with lower number of experiments and lower time and materials consumption.

5.1.2 Analysis of Secondary Cell Cytotoxicity Data

Statistical analysis of preliminary cytotoxicity data suggest that the further cell experiments need to be carried out in order to find the optimized iron/iron oxide nanoparticle composition with CGKRK and doxorubicin. The suggestion of a new target domain by the statistical analysis of our first set of experimental cell cytoxicity data clearly demonstrates the advantage of the methodology explored here. In using a statistical analysis method to develop nanoparticle-based anticancer agents to successfully treat pancreatic cancer, we were able to save numerous experiments, which otherwise would have to be conducted. This approach also provided the correct directions for the extension of the experimental domain in further studies. Considering all the predictions and suggestions obtained from the preliminary analysis, two extended Doehlert matrices were constructed and cell cytotoxicity measurements were conducted following the same protocols. Percentage cell viability data were obtained, which were then directly used for the statistical analysis in order to determine whether the new matrices represent the optimal conditions for the nanoparticle system for anticancer treatment. Obtained cell viability data are listed on the next page. (Table 5.8).

	Percentage cell viability			
Sample number	24 hrs			composition
	concentration in μg/ml			
	10	50	100	(cgkrk,dox)
3	46	61	51	104,120
3	56	58	51	104,120
3	74	71	66	104,120
1	100	98	88	80,80
2	89	94	78	128,80
7	115	103	71	56,120
20	45	51	47	80,160
21	47	40	36	128,160
22	75	64	62	152,120
				(dox,cgkrk)
9	94	86	69	128,80
10	78	75	76	104,120
16	63	62	66	176,80
17	84	77	55	200,120
18	55	46	41	176,160
19	74	63	63	128,160
15	90	80	76	152,120
15	52	54	75	152,120
15	58	52	81	152,120

Table 5-8 Cell cytotoxicity data for extended Doehlert matrices depending on the concentration for 24 h incubation

Three analyses were carried out for three concentrations combining all the data obtained for each concentration. The statistical analysis results will be discussed below.

5.1.2.1 Percentage Cell Viability of 10 μg/ml Nanoparticle Concentration

Similar to the preliminary data analysis, a full quadratic response surface model (equation 1) was constructed initially and then analyzed, with the intent to determine the presence of any

outliers using Cook's distance criteria (Cook's D < 1.0). No outliers were observed for the input data. Then analysis of variance (ANOVA) was carried out to determine the fitness of the model to the experimental data by regression analysis (the ratio between the media of square values of regression (MS_{reg}) and residual (MS_{res})) and lack of fit test (the ratio between the media of square values of lack of fit (MS_{lof}) and pure error (MS_{pe})) compared to the tabulated Fisher distributions (*f* test). Based on the regression analysis data (Table 5.9), the overall model was not significant at 5% level (α = 0.05) with a P value for the model is 0.12.

a

Analysis of Variance					
Source	**DF**	**Sum of Squares**	**Mean Square**	**F Value**	**Pr > F**
Model	5	3447.31031	689.46206	2.22	0.1200
Error	12	3731.63414	310.96951		
Corrected Total	17	7178.94444			

b

Residual	**DF**	**Sum of Squares**	**Mean Square**	**F Value**	**Pr > F**
Lack of Fit	8	2494.300802	311.787600	1.01	0.5356
Pure Error	4	1237.333333	309.333333		
Total Error	12	3731.634135	310.969511		

Table 5-9 a) Regression analysis; b) Lack of fit test statistical output data for full quadratic model for 10 µg/ml nanoparticle concentration

Nevertheless, as shown in the Table 5.4.b, the lack of fit test carried out at α = 0.05 gave a P value = 0.5356. Therefore, the quadratic model is considered to be adequate. Consequently, coefficient parameters (β) of the quadratic model were calculated to determine the fitness of each term in the model. The results are recorded in the Table 5.10.

Parameter Estimates					
Variable	**DF**	**Parameter Estimate**	**Standard Error**	**t Value**	**Pr > |t|**
Intercept	1	336.98304	102.91704	3.27	0.0066
CGKRK	1	-2.10167	1.10610	-1.90	0.0817
DOX	1	-1.94593	1.03740	-1.88	0.0852
CGKRK2	1	0.00761	0.00467	1.63	0.1290
DOX2	1	0.00559	0.00359	1.56	0.1457
CGKRK_DOX	1	0.00160	0.00550	0.29	0.7765

Table 5-10 Estimated coefficient parameter values for the full quadratic model for 10 µg/ml nanoparticle concentration

The doxorubicin and CGKRK interaction term (DOX*CGKRK) term was not significant with a P value = 0.7765 and excluded from the model. DOX^2 and $CGKRK^2$ terms were marginal at 10% significance level. A reduced model was constructed to evaluate its fitness by omitting the DOX*CGKRK term. The resulting equation is given below.

The Reduced mathematical model:

$$cell\ viability = \beta_o + \beta_1 Dox + \beta_2 Dox^2 + \beta_3 CGKRK + \beta_4 CGKRK^2 + \varepsilon \qquad (4)$$

ANOVA calculations (Table 5.11) were conducted and the model become significant at 10% level with P value = 0.0610.

Analysis of Variance					
Source	**DF**	**Sum of Squares**	**Mean Square**	**F Value**	**Pr > F**
Model	4	3421.10009	855.27502	2.96	0.0610
Error	13	3757.84436	289.06495		
Corrected Total	17	7178.94444			

Table 5-11 Regression analysis data for reduced quadratic model for 10 µg/ml nanoparticle concentration

Coefficient parameters (β) of all the terms in the model are statistically significant at α = 0.10 with coefficient of variation (R^2) value of 47.65% for the model. (Term DOX has a marginal P value = .1066). Parameter values are shown in the Table 5.12.

Variable	Parameter Estimate	Standard Error	Type II SS	F Value	Pr > F
Intercept	321.71591	85.29476	4112.40420	14.23	0.0023
CGKRK	-1.97120	0.97444	1182.88662	4.09	0.0642
DOX	-1.83371	0.92817	1128.23814	3.90	0.0698
CGKRK2	0.00800	0.00432	991.21829	3.43	0.0869
DOX2	0.00583	0.00336	868.73590	3.01	0.1066

Table 5-12 Estimated coefficient parameter values for the reduced quadratic model for 10 µg/ml nanoparticle concentration

Therefore, the estimated quadratic model that represents the experimental percentage cell viability ($\hat{Y}$) can be written as

$$\hat{Y} = 0.0023 + 0.0698Dox + 0.1066Dox^2 + 0.0642CGKRK + 0.0869CGKRK^2$$

Finally the response surface plot and contour plot for the reduced model were constructed and shown in Figure 5. 6 and Figure 5.7, respectively.

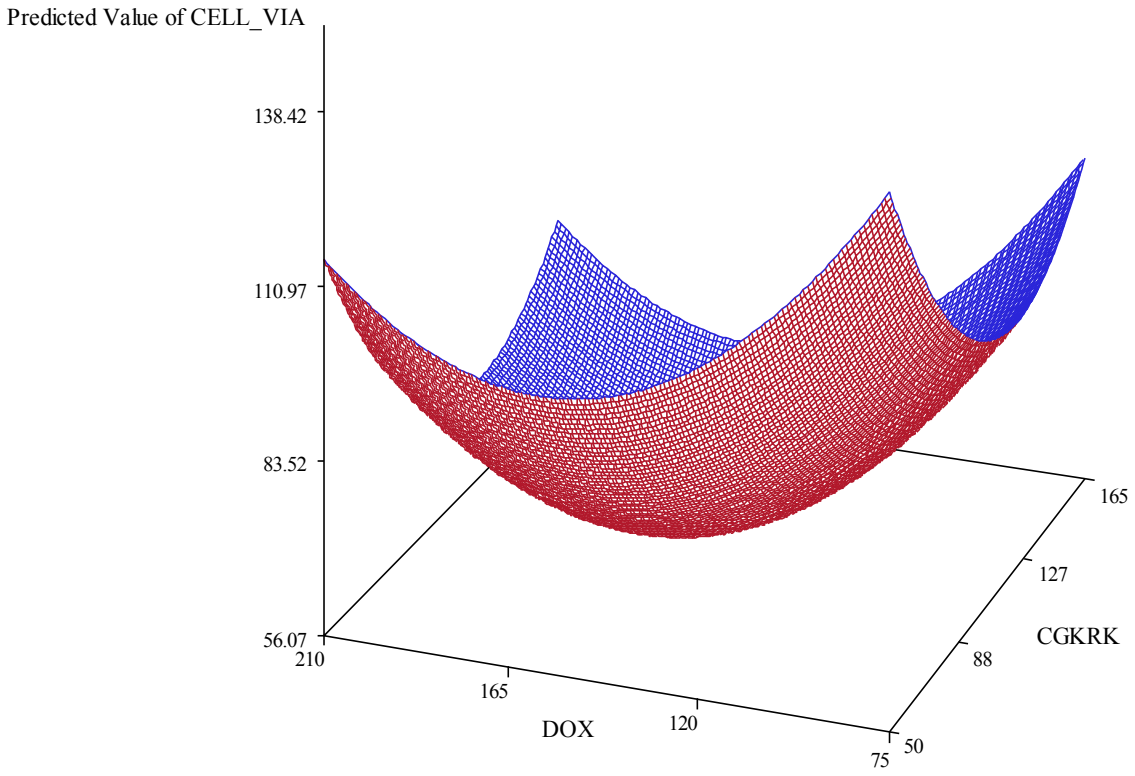

Figure 5.6 Quadratic response surface for the cell viability with respect to CGKRK and doxorubicin at nanoparticle concentration of 10 µg/ml for extended matrices

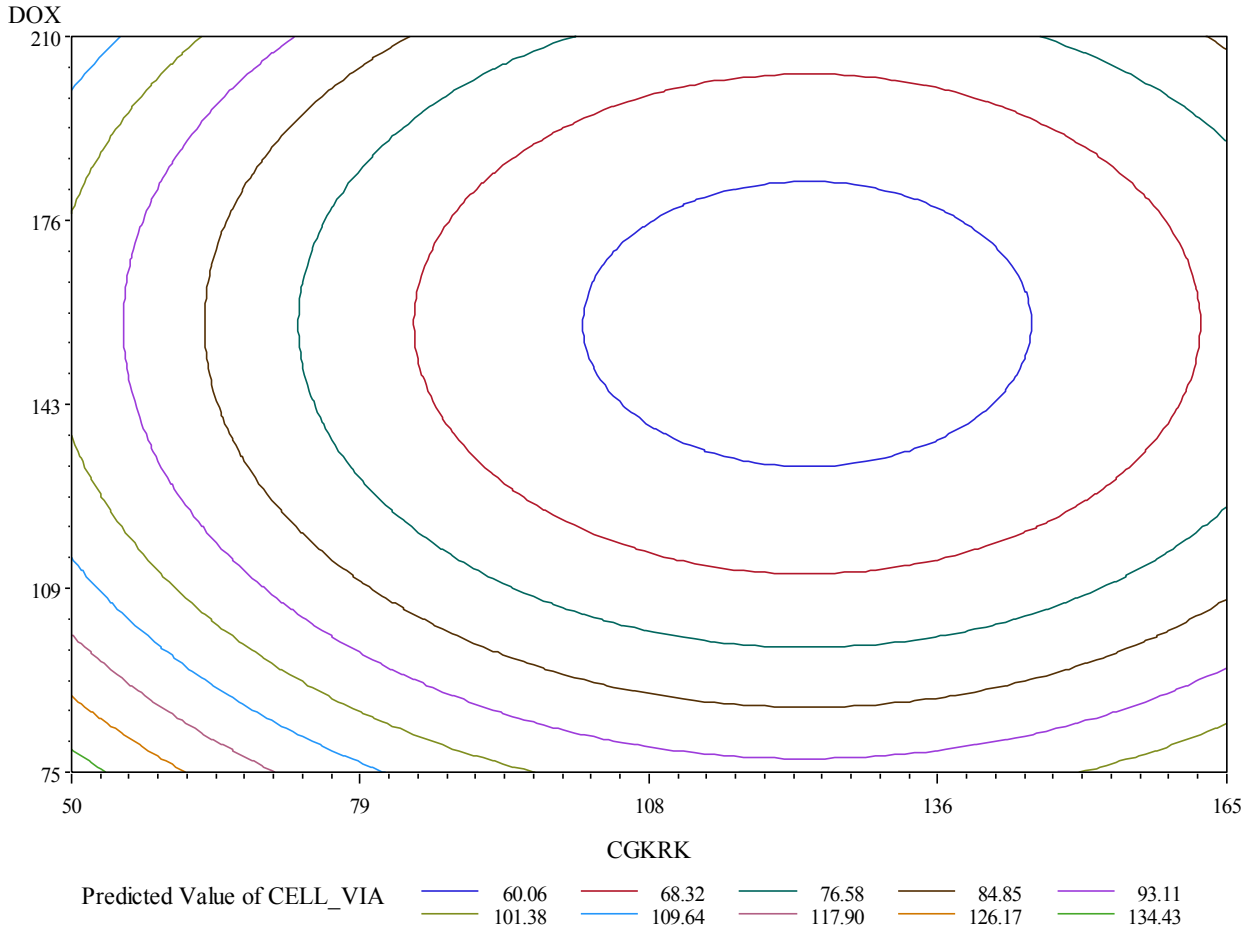

Figure 5.7 Contour plot of the cell viability with respect to CGKRK and doxorubicin at nanoparticle concentration of 10 µg/ml for extended matrices

The response surface for the percentage cell viability with respect to doxorubicin and CGKRK at 10 µg/ml concentration is a minimum, as expected and predicted in the preliminary calculations. The minimum cell viability that can be obtained using the nanoparticle at this concentration is 56.1%, and the composition of the nanoparticle system should be maintained at **156 <DOX<159** and **122 < CGKRK < 125**.

5.1.2.2 Percentage Cell Viability of 50 µg/ml Nanoparticle Concentration

The same statistical analysis procedure was conducted for the nanoparticle concentration 50 µg/ml, as descried in section 5.1.2.1. Initially, the full quadratic response surface model (equation 1) with DOX and CGKRK terms was analyzed using Cook's distance criteria to eliminate any outliers. No outliers were observed for the data obtained using 50µg/ml concentration. Then ANOVA calculations were carried out to determine the fitness of the model to the experimental data by regression analysis and lack of fit test. The overall model was statistically significant at the 5% level with a P value =0.014 from regression analysis (shown in Table 5.13.a).

a.

Analysis of Variance					
Source	**DF**	**Sum of Squares**	**Mean Square**	**F Value**	**Pr > F**
Model	5	3708.65874	741.73175	4.62	0.0140
Error	12	1927.61904	160.63492		
Corrected Total	17	5636.27778			

b.

Residual	**DF**	**Sum of Squares**	**Mean Square**	**F Value**	**Pr > F**
Lack of Fit	8	1346.952370	168.369046	1.16	0.4743
Pure Error	4	580.666667	145.166667		
Total Error	12	1927.619036	160.634920		

Table 5-13 a) Regression analysis and b) Lack of fit test statistical output data for full quadratic model for 50 µg/ml nanoparticle concentration

Moreover, the lack of fit test was conducted at the same significance level ($\alpha = 0.05$) and the model is adequate with a P value = 0.4743 (data shown in Table 5.13.b). Next, coefficient

parameters (β) were calculated (shown in Table 5.14.). Similar to 10µg/ml doxorubicin and CGKRK, the interaction term was not statistically significant and hence excluded from the model.

Parameter Estimates					
Variable	**DF**	**Parameter Estimate**	**Standard Error**	**t Value**	**Pr > |t|**
Intercept	1	105.24831	82.63833	1.27	0.2269
CGKRK	1	0.32977	0.88815	0.37	0.7169
DOX	1	-0.59502	0.83299	-0.71	0.4887
CGKRK2	1	-0.00123	0.00375	-0.33	0.7477
DOX2	1	0.00181	0.00288	0.63	0.5420
CGKRK_DOX	1	-0.00104	0.00442	-0.24	0.8169

Table 5-14 Estimated coefficient parameter values for the full quadratic model for 50 µg/ml nanoparticle concentration

Experimental data were fitted again to the reduced model shown in equation 4. The model is highly significant at the 5% significance level with a P value = 0.0049 with a coefficient of variation value 65.8% for the model. The data is shown below in Table 5.15.

Analysis of Variance					
Source	**DF**	**Sum of Squares**	**Mean Square**	**F Value**	**Pr > F**
Model	4	3708.64940	927.16235	6.25	0.0049
Error	13	1927.62838	148.27911		
Corrected Total	17	5636.27778			

Table 5-15 Regression analysis data for reduced quadratic model for 50 µg/ml nanoparticle concentration

The total variation in the residual can be explained by the fitted reduced model. When coefficient parameters were calculated (Table 5.16) for the model CGKRK and $CGKRK^2$ terms were significant at $\alpha = 0.05$, but become marginal at $\alpha = 0.1$.

Variable	Parameter Estimate	Standard Error	Type II SS	F Value	Pr > F
Intercept	289.95829	61.08923	3340.57924	22.53	0.0004
CGKRK	-1.17785	0.69791	422.33803	2.85	0.1153
DOX	-1.93561	0.66477	1257.11611	8.48	0.0121
CGKRK2	0.00419	0.00309	272.37109	1.84	0.1984
DOX2	0.00605	0.00241	934.32361	6.30	0.0261

Table 5-16 Estimated coefficient parameter values for the reduced quadratic model for 50 µg/ml nanoparticle concentration

Therefore estimated quadratic model that represents the experimental percentage cell viability ($\hat{Y}$) can be written as

$$\hat{Y} = 0.0004 + 0.0121Dox + 0.0261Dox^2 + 0.1153CGKRK + 0.1984CGKRK^2$$

Finally the response surface plot and contour plot for the reduced model were constructed and shown in Figure 5. 8 and Figure 5.9, respectively.

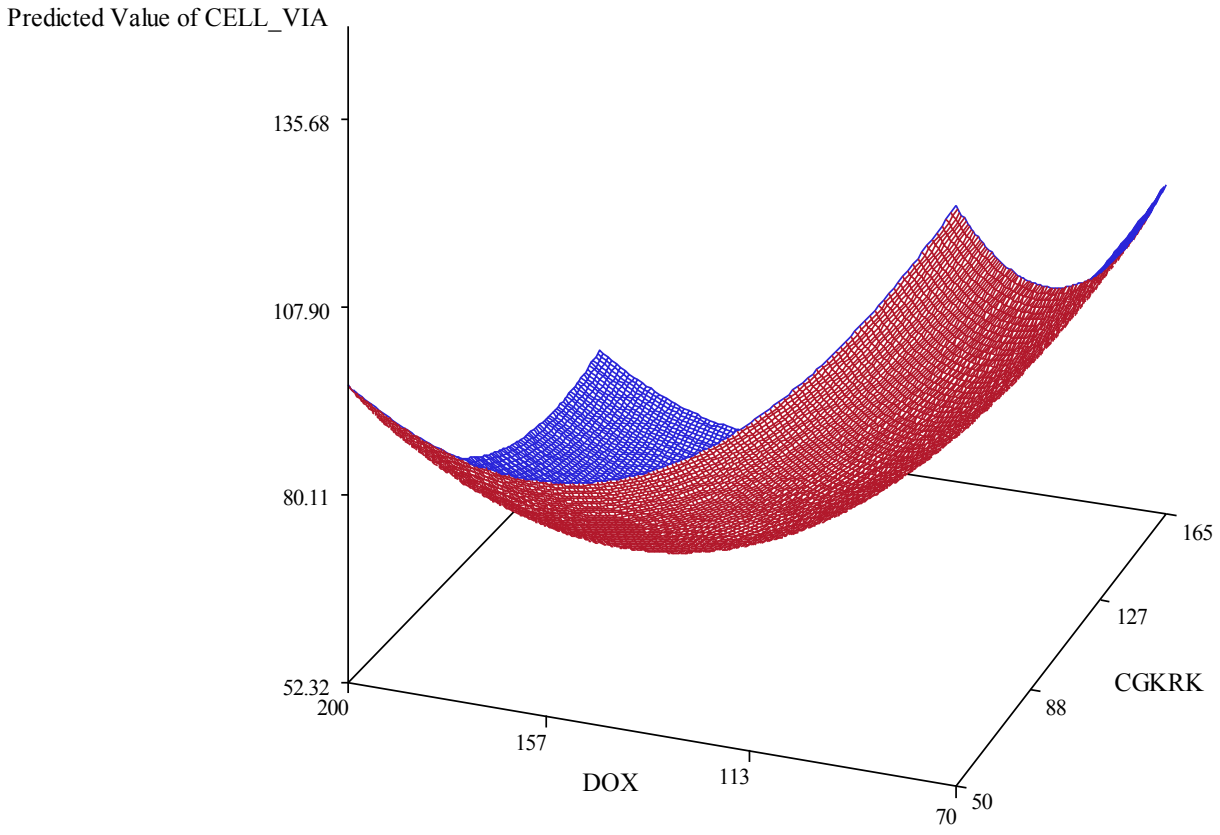

Figure 5.8 Quadratic response surface for the cell viability with respect to CGKRK and doxorubicin at nanoparticle concentration of 10 µg/ml for extended matrices

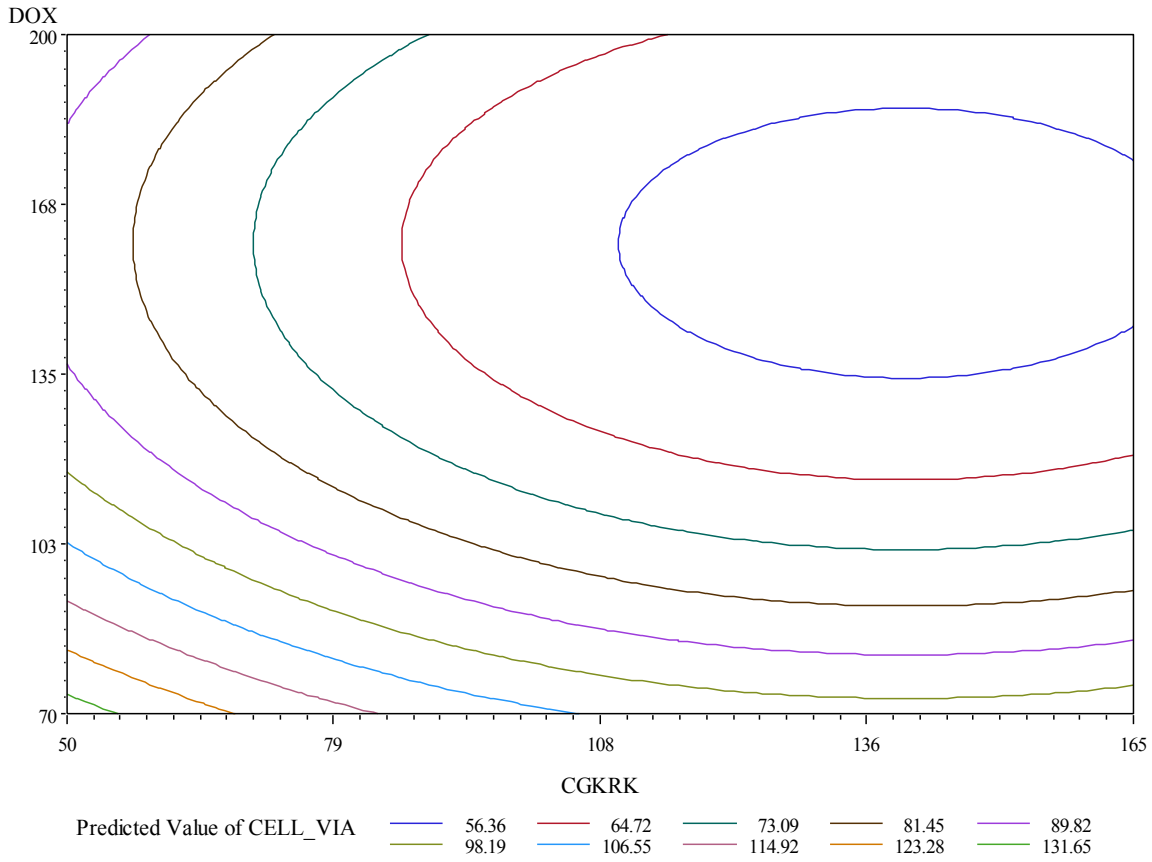

Figure 5.9 Contour plot of the cell viability with respect to CGKRK and doxorubicin at nanoparticle concentration of 50 µg/ml for extended matrices

The response surface for the percentage cell viability with respect to doxorubicin and CGKRK at 50 µg/ml concentration is a minimum, as expected and predicted in the preliminary calculations. The minimum cell viability that can be obtained using the nanoparticle at this concentration is 52.3% and the composition of the nanoparticle system should be maintained at **158<DOX<160** and **138 < CGKRK < 143**. Compared to the 10 µg/ml, the reduced model for 50 µg/ml is highly significant with a P value = 0.0049 , a larger R^2 value and a lower cell viability as well.

5.1.2.3 Percentage Cell Viability of 100 µg/ml Nanoparticle Concentration

For the 100 µg/ml cell viability data, the same experimental procedure has been carried out. Initially, the full quadratic model was fitted to check the presence of any outliers. No outliers were observed. Then the regression analysis and lack of fit tests were performed to determine the fitness of the model to the experimental data. According to the regression analysis data, the overall model was not significant with a very high P value (0.3790) for the model. The lack of fit test was conducted at α=0.05 and gave very low P value which is 0.0436. Therefore, the model is not adequate to conduct further analysis. It is also found that none of the terms in the model was significant. (P value> 0.05).

Backward elimination process was used to exclude the non-significant terms in model. DOX was the only significant factor with a P value=0.03. Therefore, the model is unable to produce a minimum or maximum for the iron/iron oxide nanoparticle concentration of 100 µg/ml. The reduced model for this concentration can be written as,

$$cell\ via = \beta_0 + \beta_1 DOX + +\varepsilon \quad (5)$$

In the preliminary analysis of the 100 µg/ml concentration, the minimum cell viability was obtained even though it is not statistically significant for both doxorubicin and CGKRK. When the nanoparticle composition is changed during the extended matrices, the experimental domain that is of interest has been moved away from the original region. Therefore, it can be assumed that the active experimental domain for the 100 µg/ml concentration may not lie within the extended matrix. The nanoparticle composition that gives the minimum cell viability was in the predicted value range, as mentioned in Table 5.7. In addition, the cell cytotoxicity obtained

for this concentration may be due to the high iron nanoparticle concentrations, rather than due to the cytotoxic activity of doxorubicin or CGKRK.

5.2 Discussion

Based on the statistical analysis carried out for both preliminary and extended matrices. it is clear that application of response surface methodology is a very suited to discover the proper composition of doxorubicin and CGKRK at the surface of the Fe/Fe_3O_4 carrier nanoparticles. Using Doehlert methodology, we were successful in developing an promising candidate for an anticancer agent for treatment of pancreatic cancer. Based on the preliminary analysis, we predicted that the initial Doehlert matrices should be extended to higher values of doxorubicin, where the number of doxorubicin molecules per nanoparticle should be higher than 120. Since the CGKRK was statistically insignificant in the model in the initial calculations CGKRK any CGKRK amounts can be used but the cell viability is comparatively to with number of CGKRK molecules are higher than 85. But CGKRK should be presence on the nanoparticles for the observed cell cytotoxicity. Extending the cell viability studies with newly synthesized iron/iron oxide nanoparticle systems with new doxorubicin and CGKRK compositions according to the preliminary data gave very good cytotoxicity activity, as predicted. Moreover, it is observed that the cell cytotoxicity of the nanoparticle systems was reduced when the doxorubicin amount was increased after 160 doxorubicin molecules per nanoparticle. Based on our analysis, both 10 μg/ml and 50 μg/ml gave very good statistical data assuming quadratic response surfaces. Minima at 156-160 doxorubicin molecules per nanoparticle for the percentage cell viability of Pan02 cells were found. From the two concentrations, 50 μg/ml gave the best results with a very low P value of 0.0049. 10 μg/ml resulted in acceptable results with a P value of 0.06. In both cases, the reduced models successfully represented the experimental data obtained from the MTT

assays. Therefore, the constructed mathematical models were fitted to the experimental region. Proper iron/iron oxide nanoparticle compositions are obtainable from this analysis, which ensure maximal therapeutic effects on Pan02 cells. Based on the data at both concentrations, very similar nanoparticle compositions were calculated: the number of doxorubicin molecules should be varied around 156 – 160 and CGKRK molecules around 125-140. Since CGKRK parameters give marginal statistical significances in both cases, further studies should be carried out in order to determine whether CGKRK truly contribute to the synergistic activity with doxorubicin or whether CGKRK can be removed from the system. It is also noteworthy that the predicted iron oxide nanoparticle compositions with required doxorubicin and CGRKR composition does show very minimum toxicity in the non-cancerous STO cells during the MTT assays.

5.3 Conclusion

Statistical analysis using response surface methodology was successfully applied in optimizing the composition of an iron / iron oxide nanoparticle based drug delivery system for doxorubicin. Statistical analysis shows that more than 50% of the cancerous Pan02 cells can be killed within 24 and 48 hours using low iron/iron oxide nanoparticle concentrations. Response surface methodology is a very promising strategy in developing potent therapeutic agents for treating pancreatic cancer. Iron / iron oxide nanoparticles proved to be suitable carriers of doxorubicin, potentiating the pharmacological action of this well-known topoisomerase II inhibitor. Further experiments need to be carried out to explore the relevance of the tumor-homing peptide sequence CGKRK in the system and to further maximize the therapeutic activity of the nanoparticle system.

Appendix A - Spectral Data

a.

Iron/iron oxide nanoparticle sample	Fe(II) concentration (mg/L)
1	68
3	64
5	70
6	68
7	70

b.

Iron/iron oxide nanoparticle sample	CGKRK concentration (mg/g)
1	23.56
3	24.6
5	21.24
6	22.56
7	23.76

Table A-1 a) Fe(II) concentration and b) CGKRK concentration present on each iron/iron oxide samples determined from ICP-OES measurements

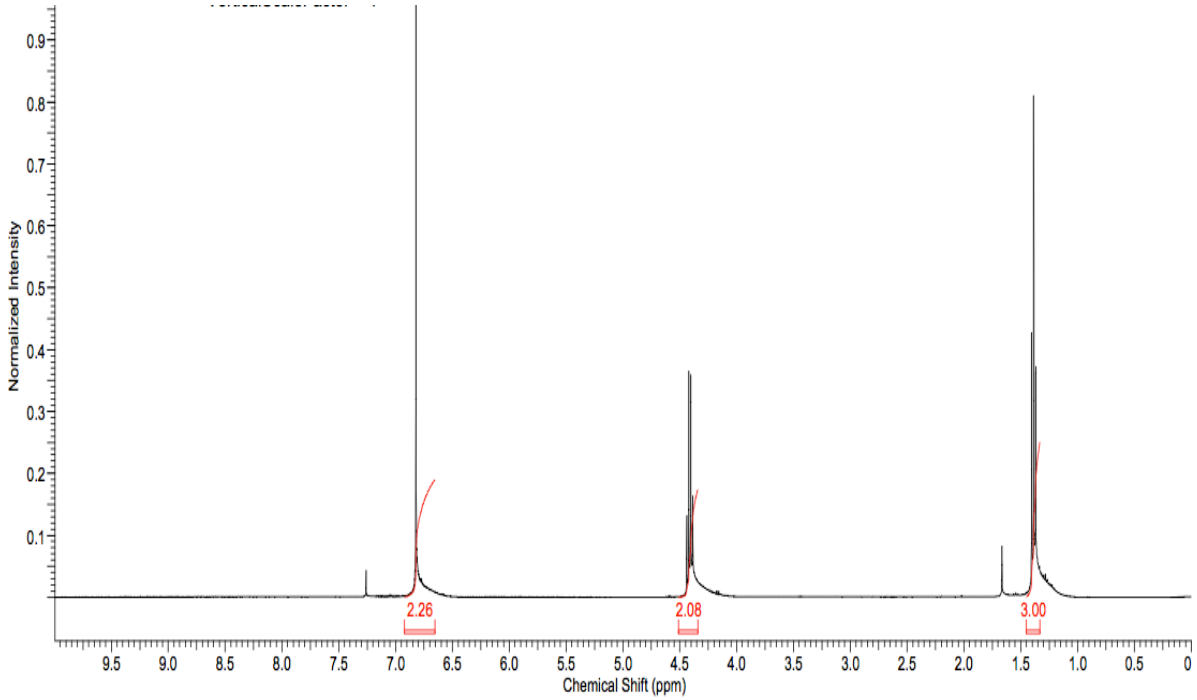

Figure A.1 ^{1}H NMR of the intermediate product of dopamine ligand 3.5

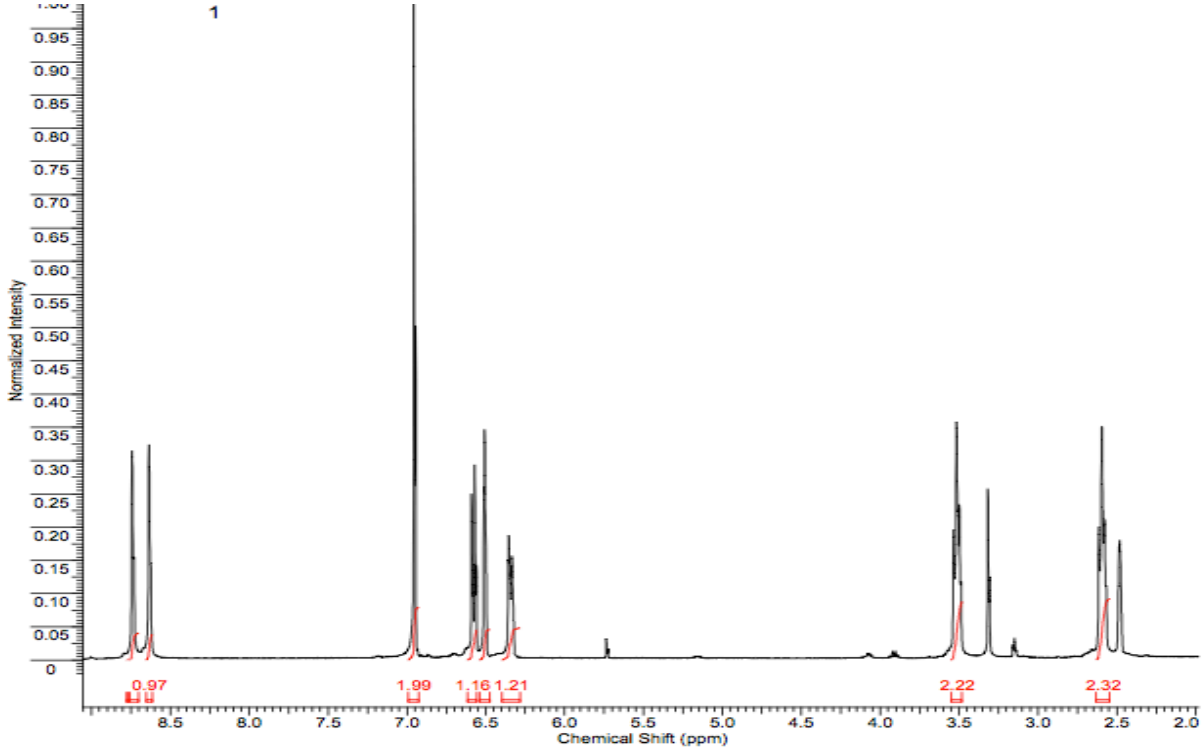

Figure A.2 ^{1}H NMR of the ligand 3.5 in DMSO

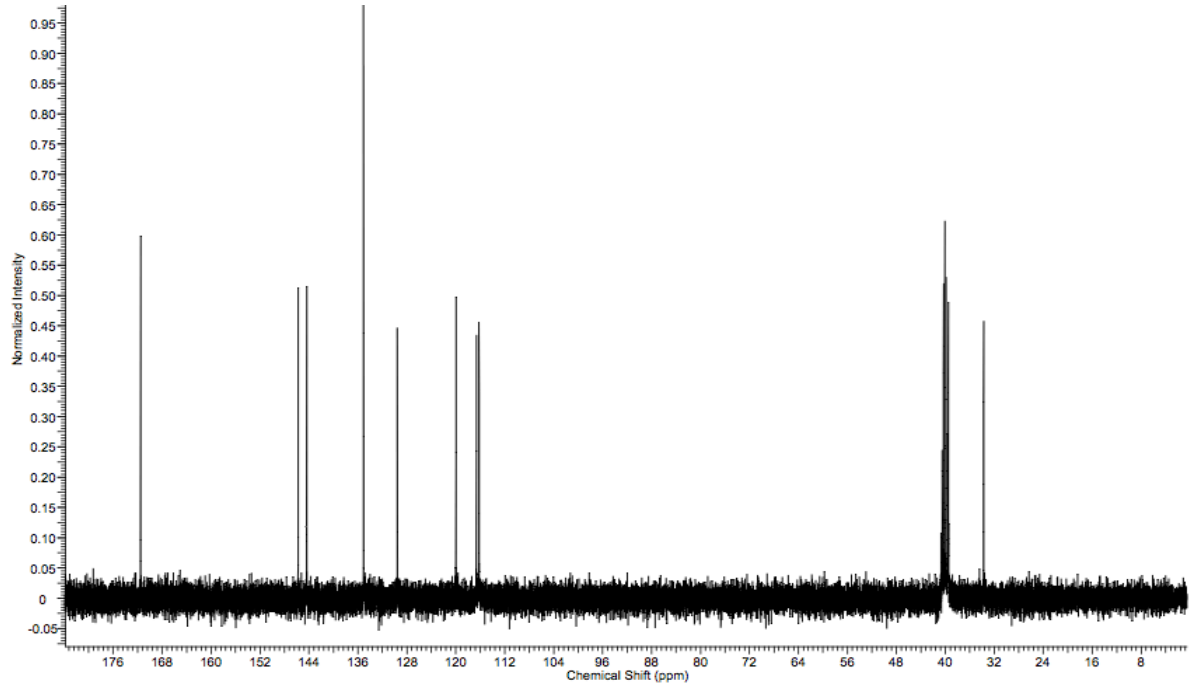

Figure A.3 ^{13}C NMR of the ligand 3.5 in DMSO

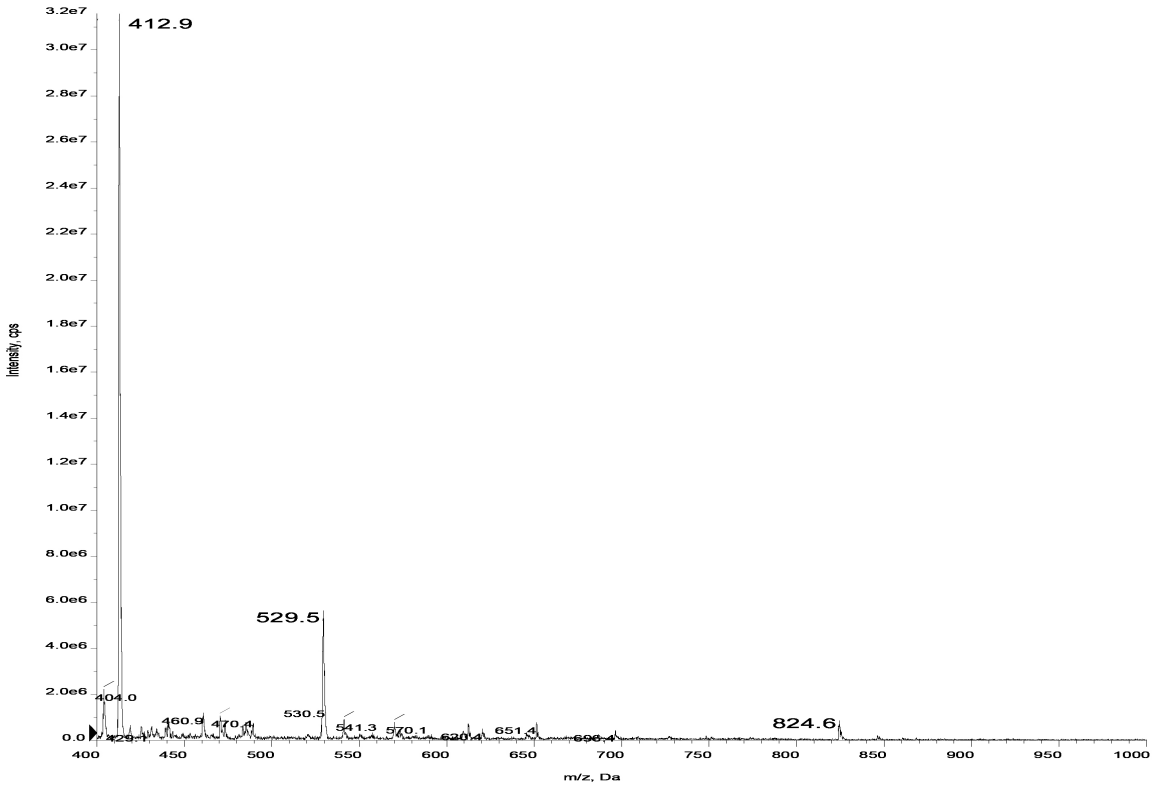

Figure A.4 MS-API of coupling product 3.9

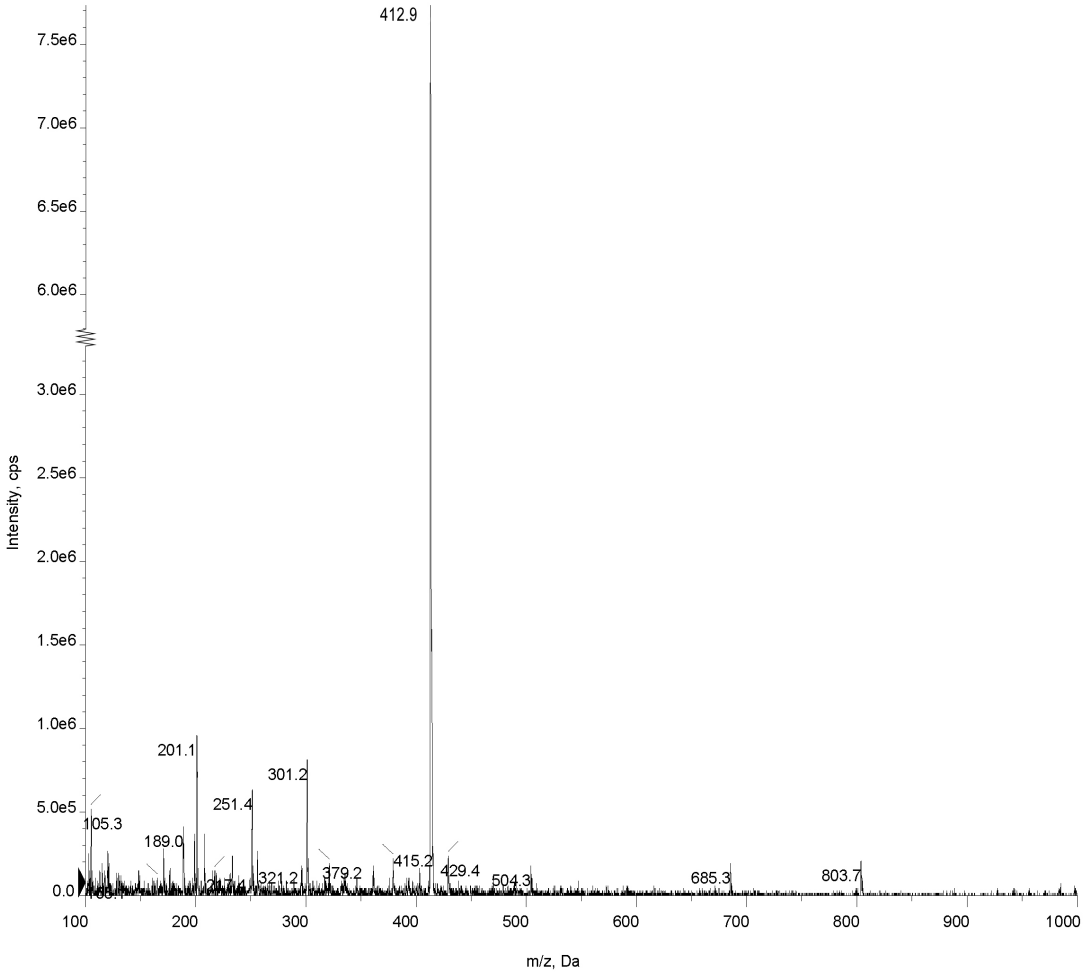

Figure A.5 MS-API of coupling product 3.10

Appendix B - Statistical Data

Calculated data for section 5.1.1.1

Analysis of Variance					
Source	**DF**	**Sum of Squares**	**Mean Square**	**F Value**	**Pr > F**
Model	5	739.21388	147.84278	2.89	0.1141
Error	6	306.45279	51.07546		
Corrected Total	11	1045.66667			

Table B-1 Regression analysis of the full quadratic model represent in the equation 1

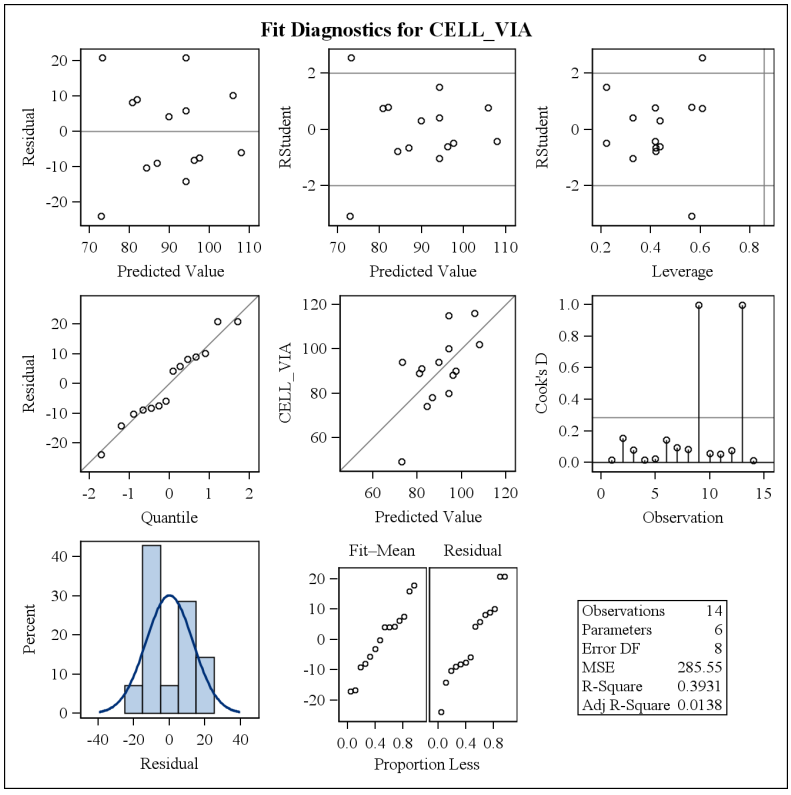

Figure B.1 Fit diagnostics for cell viability for 10 µg/ml for 24 h

Calculated data for section 5.1.1.2

Analysis of Variance					
Source	**DF**	**Sum of Squares**	**Mean Square**	**F Value**	**Pr > F**
Model	5	739.21388	147.84278	2.89	0.1141
Error	6	306.45279	51.07546		
Corrected Total	11	1045.66667			

Table B-2 Regression analysis of the full quadratic model represent in the equation 1

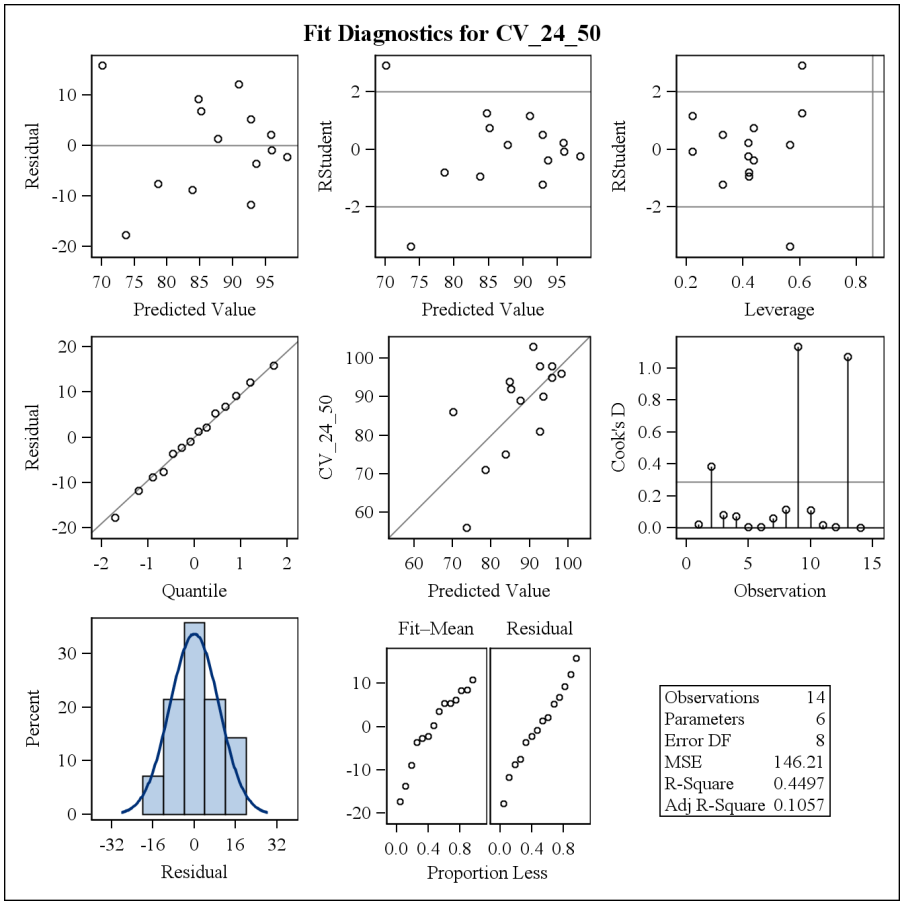

Figure B.2 Fit diagnostics for cell viability for 50 µg/ml for 24 h

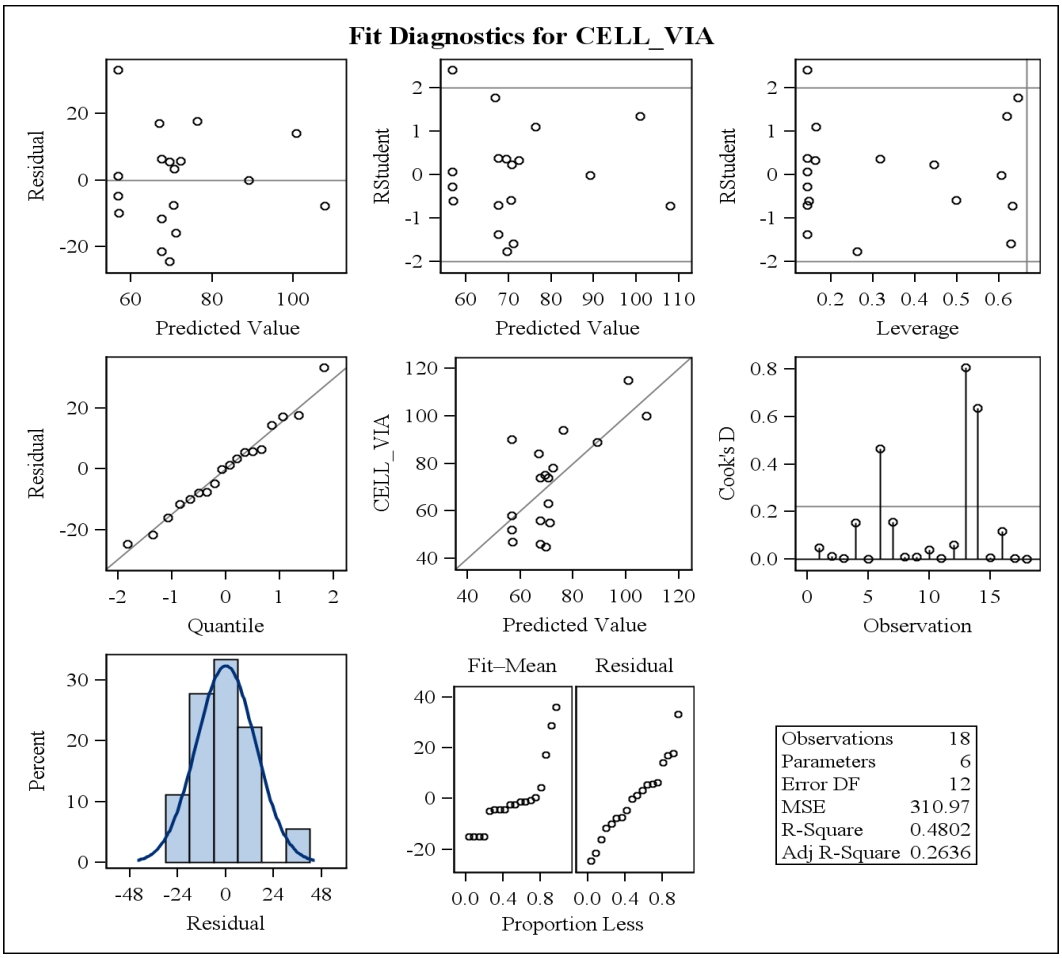

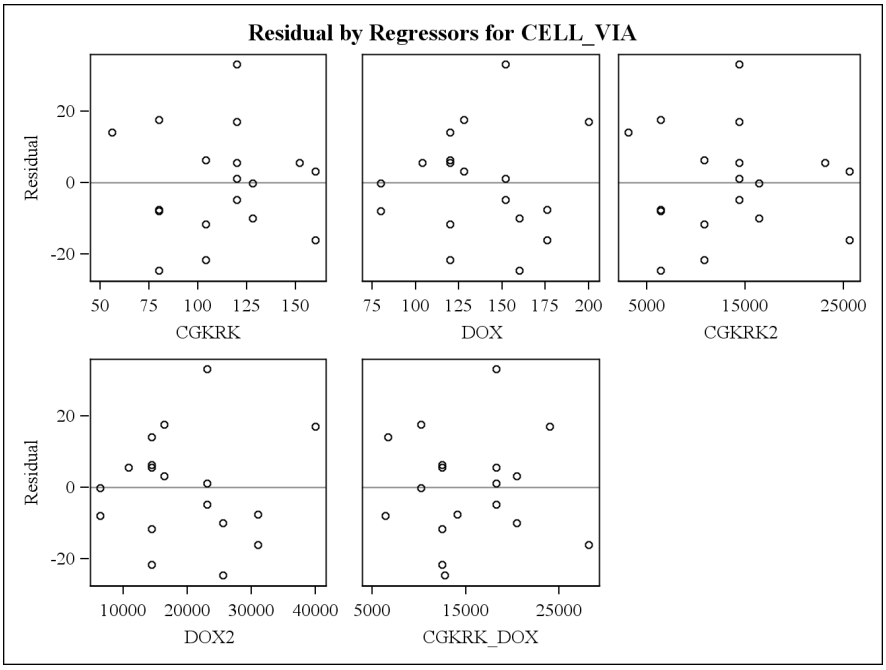

Figure B.3 Fit Diagnostics for cell viability 10 µg/ml for 24 h in section 5.1.2.1

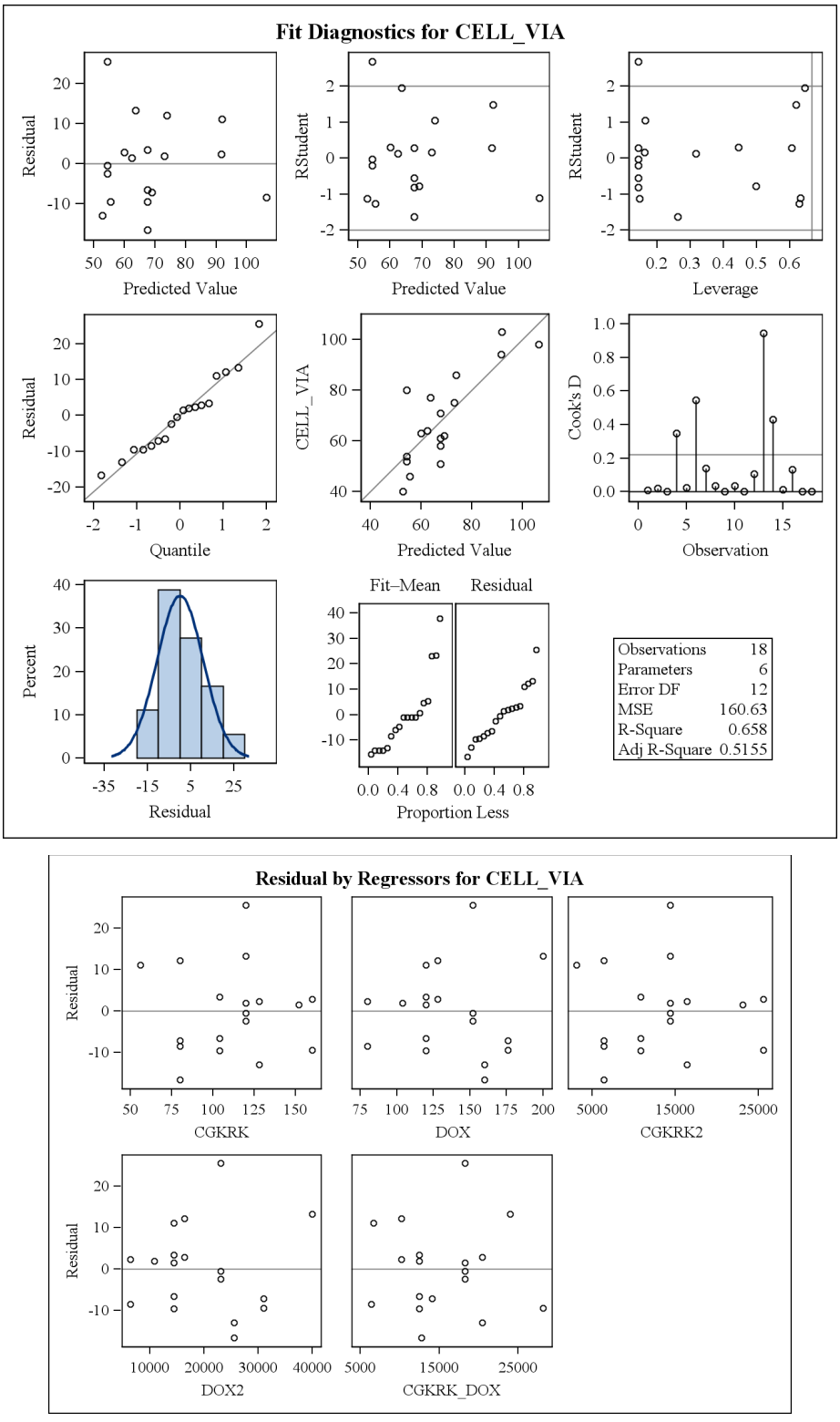

Figure B.4 Fit Diagnostics for cell viability 10 µg/ml for 24 h in section 5.1.2.2